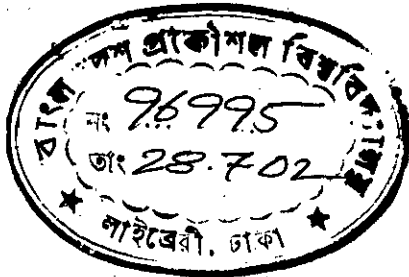# A STUDY OF WEAR OF TYRE TREADS

A thesis submitted by

Sankar Kumar Deb Nath

In partial fulfillment of the requirements for the degree of

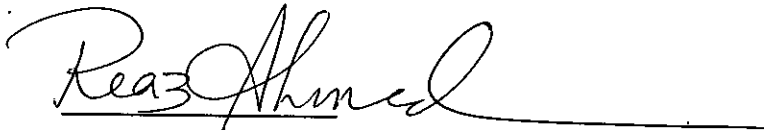## MASTER OF SCIENCE IN MECHANICAL ENGINEERING

DEPARTMENT OF MECHANICAL ENGINEERING

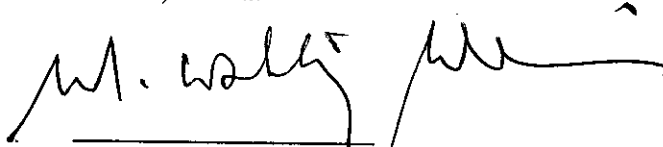BANGLADESH UNIVERSITY OF ENGINEERING & TECHNOLOGY

June, 2002

#96995#

The thesis titled 'A STUDY OF WEAR OF TYRE TREADS' Submitted by Sankar Kumar Deb Nath, Roll No. 040010011F, Session April, 2000, has been accepted as satisfactory in partial fulfillment of the requirement for the degree of **Master of Science in Mechanical Engineering** on June 01, 2002.
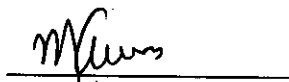
BOARD OF EXAMINARS

Dr. S. Reaz.Ahmed
Assistant Professor
Department of Mechanical Engineering
BUET, Dhaka

Chairman
(Supervisor)

Dr. Md. Wahhaj Uddin
Professor
Department of Mechanical Engineering
BUET, Dhaka

Member

Dr. Maglub Al Nur
Professor and Head
Department of Mechanical Engineering
BUET, Dhaka

Member
(Ex–officio)

Dr. Md. Fazli Ilahi
Professor
Department of Mechanical and Chemical Engineering
IUT, Gazipur, Dhaka

Member
(External)

CANDIDATE'S DECLARATION

It is hereby declared that this thesis or any part of it has not been submitted elsewhere for the award of any degree or diploma.

_____

Sankar Kumar Deb Nath

TABLE OF CONTENTS

Chapter 4: EXPERIMENTAL DETERMINATION OF MATERIAL PROPERTIES

Chapter 5 : SOLUTION OF TYRE TREAD CONTACT PROBLEM CONSIDERING FRICTIONLESS SLIPPING

Chapter 6: WEAR ANALYSIS OF TYRE TREAD SECTIONS CONSIDERING FRICTIONAL SLIPPING

ACKNOWLEDGEMENT

List of Tables

List of Figures

LIST OF SYMBOLS

Notation	Definition
x, y	rectangular coordinate
h	mesh length in x-direction
k	mesh length in y- direction
E_t	modulus of elasticity in tension
E_c	modulus of elasticity in compression
ϕ	Airy's stress functiom
ψ	displacement potential function
l, m	direction cosines of the normal at any physical boundary
μ	Poisson's ratio
u_x	displacement component in x-direction
u_y	displacement component in y-direction
σ_x	normal stress component in x-direction
σ_y	normal stress component in y-direction
σ_{xy}	shear stress component in xy-plane
u_n	displacement component normal to the boundary
u_t	displacement component tangential to the boundary
σ_n	stress component normal to the boundary
σ_t	stress component tangential to the boundary
$\bar{\sigma}_n$	σ_n / E
$\bar{\sigma}_t$	σ_t / E
a	tread contact length
b	skid depth of the tyre tread
a/b	aspect ratio
i	variable subscript corresponding to x-axis
j	variable subscript corresponding to y-axis

ABSTRACT

Wear of vehicular tyre treads is an important practical issue. Since the service life of a tyre is primarily affected by the wear of treads, a useful study of tyre treads is of great practical importance for the optimum design and thus improved life of tyres. The present thesis describes a new investigation for the identification of the causes responsible for the tyre wear and a method to provide a useful guideline for reducing the wear of tyre-treads through an extensive analysis of the mixed boundary-value contact problem of tyre-tread.

Earlier, no serious attempt was made to provide a reasonable guideline for the optimum tread sections that would ensure no wear of the treads. Actually, it has not been successful in the past mainly because of the inability of simulating the contact problem through an appropriate mathematical modeling where all the boundary conditions would be satisfied justifiably.

An ideal mathematical model for the practical stress problems, namely, the displacement potential function formulation has been used in conjunction with the finite-difference method of solution for the present analysis. For the present computational investigation all the necessary material properties of tyre are obtained experimentally. For the purpose of wear analysis, first, the contact surface of the tyre tread is assumed to be free from frictional force, and the corresponding solution of the problem is obtained where the contact boundary is only subjected to a uniform normal compressive loading from the road surface. The results of this frictionless analysis however give the basis for realizing the fact that the continuous lateral slipping action of the tread contact surface on the road plays the most important role in shortening the life of tyres as far as the wear is concerned.

Secondly, the solution of the problem is obtained by restricting the tangential displacement of the contact boundary, which is subjected to a uniform compressive stress from the road surface. From the resulting distribution of the shearing stress along the contact boundary, a relationship between the maximum shearing stress developed and the aspect ratio of the tread section is established under different contact pressures. Finally, the maximum calculated coefficient of friction obtained from the maximum shearing stress, are analyzed in the perspective of tread aspect ratio, where the dimensions of the tread section are varied in both the normal and lateral directions. From the comparison of the calculated friction coefficient with the friction coefficient available from the road, an optimum value of the aspect ratio is determined, which ensures no wear of tyre tread due to the lateral slipping of the contact surface on the road. In addition to the effects of dimensional parameters, the wear of the contact surface is analyzed for different tyre materials and also for different inflation pressures. Moreover, attempt is made to investigate the distributions of different stress components along the bond line region near the ply, which might be responsible for the separation of the tread from the ply.

Chapter-1

INTRODUCTION

1.1 General

Rubber tyres are considered as one of the indispensable components of almost all categories of automotive vehicles. They provide the required traction that enables the vehicles to accelerate, brake and make turns on the road without skidding. In order to provide good traction, sufficient friction between tyre treads and the road surface is desirable, which however, in general, has no relation with the wear of the tyre treads. Among the common reasons of rapid tyre wear, quick starting and stopping, heavy braking, high speed running, taking corners too fast, etc., are noticeable. Wear due to these reasons is basically occasional phenomenon and can be controlled, to some extent, by avoiding them. It should be noted that the friction in the direction of motion (referred to as longitudinal direction of the tyre) could hardly produce wear of the treads as far as the rotary motion of the wheel is concerned. However, it is important to note that when a tread section comes in contact with the road, the contact surface will tend to slide along the lateral direction of the tread, under the action of normal compressive stress from the road as illustrated in Fig1.1. This continuous lateral slipping action of the tread contact surface plays the most important role in shortening the life of tyres as far as the wear is concerned. It has been identified in the present research that the wear of tyre is basically caused by the lateral friction between the tread surface and the road surface. Since the service life of a tyre is affected primarily by the wear of the treads, a careful study of wear of tyre treads is of great practical importance for their optimum design and improved life.

1.2   Literature Survey

Technical reporting on the analysis and design of rubber tyres for various automotive vehicles, in the literature, is quite extensive. It is interesting to note that most of the reporting in the literature describes computational schemes and numerical solution of the present problem. The application of the finite element method to the analysis of structures, made of cord-reinforced rubber composites, has gained increased popularity in recent years. Structures like tyres, belts, and domes are generally complex in their internal and external geometry, boundary conditions, material properties and mode of operation. The structures do not render themselves to closed form type of solutions. Tabbador and Stafford [1] reported that finite element analysis has been considered to be the only viable analytical technique which can be applied without having to make numerous simplifying assumptions.

A finite-element contact formulation and the equations for the effective material properties of rubber composites have been developed and applied to the inflation and contact problem of a reinforced tyre by Huh and Kwak [2]. The equations for the effective material properties take the bending effect of reinforced cords into consideration, laying emphasis on the bending effect during shear deformation of elements. Their results indicated the stress concentration between reinforced layers as an interpretation of the separation of steel-belted layers in tyres. Their finite element results also showed the reason for wear around the corner by showing the increase in the contact pressure near the edge and the increase of the contact surface when the load is heavier than normal.

Quite recently, Wang, Daniel and Huang [3] reported an experimental stress-strain analysis by means of the Moire method in the area of the shoulder region of a retreaded tyre section and a comparison with results obtained by the finite element analysis method. The specimen for the experiment was a

cross-sectional slice of a Bandag T4100 retread on a 295/75R22-truck tyre casing approximately 25 mm thick. A loading fixture was designed to support the tyre section and to load it in a manner simulating service loading and allowing for Moire measurements. The specimen was loaded by imposing a uniform fixed deflection on the tread surface and increasing the internal pressure in steps. For the finite element comparison a 2-D quarter tyre model was created to best simulate the experimental conditions. The tyre section was modeled using three and four-noded plane stress elements. Rubber elements were modeled with isotropic, linear elastic, nearly incompressible properties. To simulate the conditions of the Moire test as closely as possible, the model was loaded in two steps. The first step was the application of a normal displacement and the second was the introduction of inflation pressure. The authors have reported that although the FEM results were in substantial agreement with the corresponding experimental results, the discrepancies were primarily because of the fact that the boundary conditions in the FEM were not exactly matched with those of the experiment. It was also reported that the FEM results were found to be very sensitive to boundary conditions, as slight changes in the boundary and loading conditions had a significant effect especially on the displacement conditions imposed around the shoulder region.

A number of authors have focussed, specially, on the stress analysis of reinforced tyres by using the finite element method [1-4]. Some of the papers [3-4] considered the static tyre contact problem for obtaining the deformed shape and stress state in the cross section without giving attention to the bending effect of the reinforced cords. In rubber composite structures the cords as well as rubbers exhibit viscoelastic characteristic under loading [5]. Some authors have discussed that the finite element method can predict mode shapes and natural frequencies [6], inflated shapes of tyres [7-9], loaded tyre shapes [10-11], tyre cord loads [12] and force/wear in conveyor belts [13-14].

The definition of the finite element model for such a tyre is complicated, if the details of the belt, bed, plies, overhead, fillers, tread, etc., are required to be included. At present most manufacturers use proprietary software to model such complexities of construction [15-16]. Numerous papers have dealt with contact problems which involve static rolling or impact events [17-23]. Padovan and Pardilok [24] have given attention detailing the influence of viscoelasticity on the development of transient and steady rolling contact at varying rolling speeds. As noted recently by Padovan [25], the hierarchy of frequency eigenvalues associated with the tyre can be determined as various of the standing waves are excited at different load speeds. A contact formulation is added by some authors [26-27] to the finite element formulation to calculate the stress state of tyres in contact with a flat, rigid road under the load due to the self-weight of a vehicle.

The lack of analytical tyre design tools has been recognized within the United States tyre industry and research has been underway for sometime to develop the techniques necessary to model the response of the tyre to its operational environment. A summary of these modeling efforts is presented in Ref.[28]. A number of survey papers have been written on computational models for tyres in Refs.[29-31] and go beyond the cited reference in detailing the recent and projected advances in finite element technology, computational algorithms, and new computing systems and their potential in tyre modeling and analysis. A typical tyre usually contains a variety of rubber compositions in order to achieve a balance of properties for a particular type of tyre service. Table 2.1 (which is based on Ref.[32]) lists some of the major requirements on the rubber compounds used for the different components of the tyre.

Although the strength and stiffness of the constituent cord and rubber components of the pneumatic tyre have been the subject of many investigations by the tyre industry, relatively little work has been done on the

cord-rubber composites. Most of the work on strength and stiffness characterization of cord rubber composites has been based on adaption of the techniques and theories developed for laminated fibrous composites [33-35]. Cord-network models are sometimes referred to as netting analysis, wherein inflation pressure is assumed to be carried exclusively by the cords Ref.[36]. These models have the limitation of neglecting both the bending of the tyre and the stiffness effects of the rubber surrounding the cords. Two-dimensional axisymmetric models are limited to axisymmetric loading. Applications of these models to the study of the tyre response to cord-shrink forces and inflation pressure are given in Refs.[37-38]. The first approach is based on using semianalytic techniques to reduce the dimensionality of the problem [37]. Two-dimensional thin and thick shell models have been proposed [39-40]. Thin shell models are based on Kirchhoff-Love shell theories which neglect transverse shear deformation and their use for modeling tyres is therefore questionable. Anisotropy results in increasing the size of the analysis model and consequently many investigators neglect its effect by using an orthotropic model.

A number of efficient algorithms have been developed for solving contact problems involving sticking, frictional sliding and separation between two bodies [41-43]. In most of these algorithms Coulomb's law of friction is used in the evaluation of the tangential traction from the normal traction. However in some of the recent studies a local friction law is presented [44]. The contact algorithm presented in Refs.[41-44] appear to be useful for analysing tyre stresses and deformation due to footprint loading. More recently, reduction methods have been used in conjunction with symmetry concepts to reduce the analysis region of a structure subjected to unsymmetrical loading [45]. Reduction methods have high potential for use in predicting the structural and thermal responses of tyres subjected to non-axisymmetric mechanical and thermal loading. Noor and Tanner [46] focus on a number of aspects of tyre

modeling and analysis including: tyre materials and their characterization; evolution of tyre models; characteristics of effective finite element models for analysing tyres; analysis needs for tyres; and impact of the advances made in finite element technology, computational algorithoms, and new computing systems on tyre modeling and analysis.

However, no serious attempt was reported so far in the literature that can provide a useful investigation on the wearing effect of treads for suggesting an effective guideline to minimize the wear of tyres. This has not been successful in the past mainly because of the inability of simulating the actual tyre contact problem by an appropriate mathematical modeling, where the wearing stress on the contact plane of the tread section would be obtained by satisfying the real boundary conditions, justifiably.

1.3   Objective of the Present Research

The central objective of the present research is to obtain the numerical solution of the tyre contact problem in such a fashion that the wear of the tread section can be analysed in an effective manner. In addition, based on the analysis, the optimum size of the tread section can be determined which will ensure minimum wear of the treads and thus improve life of tyres. Thus the objectives can be listed sequentially as follows:

(a) Mathematical simulation of the tyre-tread contact problem considering it as a two-dimensional mixed boundary value elastic problem, using displacement potential function, ψ.

(b) Development of suitable numerical scheme for the treatment of the mixed-mode of the boundary conditions associated with the tread contact problem and to obtain the corresponding numerical solution for the relevant stress and displacement components.

(c) Development of scheme for the experimental determination of elastic behaviour of different types of tyre materials including natural rubber, at different strain levels, and to determine the necessary material properties of the tyre rubbers.

(d) Analysis of the deformation pattern for the inflated tread section under the action of uniform normal compressive stress from the road, for the case of frictionless slipping of the contact surface.

(e) Determination of frictional stress required to ensure the no-slip condition of tread contact surface on the road (i.e., no displacement of the tread contact surface in the lateral direction).

(f) Development of a scheme to predict the optimum tread section, which will ensure minimum wear of the tyre treads.

(g) Investigations of the influence of tyre material on the prediction of optimum tread section for minimum wear.

(h) Analysis of different stress as well as displacement components for an optimum tyre treads section in contact with the road.

1.4 Outline of Solution Methodology

Among the existing mathematical models for the solution of two-dimensional boundary-value elastic problems, the stress function (ϕ-formulation) [47] and the two displacement functions approach Ref. [48] are noticeable. But the difficulties involved in trying to solve practical stress problem using either of the approaches are clearly pointed out in Refs. [49-50]. Dow et al. [51] have however introduced a new boundary modeling approach for finite difference applications of displacement formulation of solid mechanics. While comparing the merit of their numerical method with today's popular FEM method, they reported that the accuracy of the finite difference method in

reproducing the state of stresses along the boundary was much higher than that of FEM method. However, they have added that the computational effort of their finite difference analysis, under the new boundary modeling, is somewhat greater than that of FEM analysis.

Taking into account the respective merits and demerits of the existing approaches, recently a new method of solution has been developed for the analysis of two-dimensional boundary-value elastic problems, where an ideal mathematical formulation, called displacement potential function formulation (ψ-formulation [48]), has been used in conjunction with finite difference technique. In this approach, the whole problem is formulated using a single displacement potential function, ψ, which is defined in terms of the two displacement components - u_x and u_y. Using this formulation, a number of elementary problems, like in plane loaded plates, deep beams, etc., are solved both analytically [49] and numerically [50]. Results found from the ψ-formulation are observed to be very close to the classical solutions, which show that the ψ-formulation is a very reliable and efficient tool to handle practical stress problems. The ψ-formulation is capable of handling mixed boundary effects very efficiently where the classical ϕ-formulation is very weak. The accuracy and reliability of the numerical model of ψ- formulation has been verified repeatedly through the numerical solutions of a number of mixed boundary-value stress problems of both regular [52-56] and curved shaped bodies [57-58].

The displacement potential function formulation has been used to formulate the present tyre contact problem. Finite difference technique is used to descritize the governing bi-harmonic partial differential equation and also the differential equations associated with the boundary conditions. The discrete values of the function at the mesh points of the domain concerned are obtained by solving the system of linear algebraic equations resulting from

the discretization of the governing equation and the associated boundary conditions. An imaginary boundary, exterior to the physical boundary of the tread section is included for the discritization of the domain using a uniform rectangular mesh network.

In order to analyse the displacement components as well as the inflated shape of the tread section, the tyre tread contact problem is first solved for the case of frictionless slipping of the tread surface in contact under the action of uniform normal compressive stress from the road. The results of this analysis are considered as the basis for developing the numerical scheme for the analysis of wear of the tread surface. Secondly, the tyre tread contact problem is solved for the case of frictional slipping of the tread under the action of uniform normal compressive stress from the road, and finally, the frictional stress required to ensure the no-slip condition of the tread surface is obtained. The calculated coefficient of friction corresponding to the no-slip condition is compared with that available for the tyre and road surface, in order to determine the optimum tread section which will ensure no wear of tyre surface in contact with the road.

The use of appropriate material properties for the solution of the tyre contact problem is of utmost importance for employing the obtained results to practical design purposes. Since the elastic properties of tyre materials are not readily available in literature, an attempt is made here to determine all the necessary material constants experimentally. The stress-strain curves for natural rubber, retreaded rubber and also for the truck tyre rubber are obtained for both the conditions of tension and compression to predict the elastic modulus of the materials at different strain levels. Therefore, all the numerical solutions are obtained here by using appropriate elastic properties of the tyre rubber which are determined experimentally.

1.5   Choice of Solution Method

Solutions of structural problems can be obtained by either one of the two basic approaches – i) experimental and ii) theoretical. Experimental investigations are not of much help in solving these types of problem as they are confined to limited applications. Results obtained from a particular experiment set up can be used only for that particular shape and boundary conditions of the body.

Again the theoretical method of solution can broadly be classified into two categories - analytical and numerical approach. Analytical approach is again very limited because general solution can be obtained only for very ideal cases. Most of the practical problems of elasticity are of mixed boundary-value type and these mixed boundary-value problems are normally beyond the scope of any 'closed form' analytical solution. Of course, there are attempts to solve some stress problems analytically where the problems are of very regular-shaped body with uniform boundary conditions, that is, the boundary conditions are prescribed either in terms of stresses only or in terms of displacements only. In addition, the results are invariably approximate as they include various approximations. Therefore, there are no alternatives except the numerical methods of solution for critical stress problems like tyre tread contact problem. Further, among the numerical methods, the finite–element and finite difference methods are the two most widely used methods in almost all the branches of engineering.

In the case of finite element method, the body is divided into a finite number of elements, where the elements are connected to each other only at the nodes. Any parameter like stress, temperature, density, displacement varies within the element according to a given simple relation like linear, parabolic, etc., along length, breadth, etc, and the values of the parameters are evaluated only

at the nodes satisfying the conditions of continuity conservation, equilibrium, etc.

In the finite difference method, the problem is formulated in terms of differential equations, and the differential equations are expressed in terms of algebraic equations using finite-difference forms of the differential derivatives. In this case, the body is in one piece but the parameters are evaluated only at some selected points, called nodes, within the body. The values of the parameters at the nodal points are based on continuity conservation, equilibrium, etc.

Ultimately, both the methods involve evaluating certain parameters of structures namely, either the force parameters or the displacement parameters at the nodal points representing the whole domain of the body. Both the methods involve solution of a large set of algebraic equations. The number of equations to be solved is determined by the number of unknowns at each nodal point and also by the total number of nodal points required to represent the whole domain of the structural body.

Usually, the unknown parameters at the nodal points are the displacement components of each nodal point. Thus, in case of FEM, the number of unknowns at each nodal point is three (u_x, u_y, u_z) or two (u_x, u_y) depending on whether it's a 3-D or a 2-D problem. As a result, the total number of unknowns to be solved in FEM is much more than that in FDM. Thus the computational time is more in FEM, and eventually the solution is cruder.

On the other hand, the finite-difference technique in conjunction with the potential displacement function formulation permits reduction of parameters to be evaluated at the nodal points to one. Hence, it does not only provide more accurate results than that of finite element solution but also the computational work is less. The present problem is thus solved by the FD method.

Chapter-2

GEOMETRY OF TYRE SECTION AND DEFINITIONS OF PARAMETERS

2.1 Purpose of Tyres

Tyres have two basic functions. First, they are air-filled cushions that absorb most of the shocks caused by road irregularities. The tyres flex, or give in, as they meet these irregularities. Therefore they reduce the effect of the shocks on the passengers in the car. Second, the tyres grip the road to provide good traction. Good traction enables the car to accelerate, brake, and make turns without skidding.

2.2 Tyre Configurations and Materials

Commercially successful tyres are now built as series of layers of flexible high-modulus cords, encased in a low-modulus rubber or rubber-like material, resulting in laminated (or layered) construction. In addition to the cord-rubber plies, a tyre has tread and sidewall rubbers, innerlinear, bead filler, and inserts.

(a) Tyre Configurations

There are three typical configuration for modern tyres, namely, (a) bias-ply construction (b) bias-belted construction and (c) radial-belted construction. In the bias-ply construction the body cords make a rather large angle with the tread centerline, and there are no tread plies. Bias-belted tyres have, in addition to the body plies, two or more belt plies between the tread rubber and the tyre body. Cords in the belt plies are more nearly circumferential than

those in the body plies. In radial belted tyres the body cords are perpendicular to the tread centerline (i.e. they lie in meridional planes of the tyre). The belt constrains both the width and circumference of the tread area thereby restricting the inflated tyre profile and reducing tread movement in the footprint. In radial-belted tyres the reduction of the tread movement in the footprint is further amplified by the flexibility of the sidewall, which can act independent of the belt. The ply rating is usually 2-4 for passenger car tyres and 20 or more for commercial and military aircraft tyres.

(b) Tyre Materials and their Characterization

Modern pneumatic tyres are made from cord-rubber materials. The low modulus, high elongation rubber contains the air and provides abrasion resistance and road grip. The high-modulus, low elongation cords provide reinforcement for the rubber and carry most of the loads applied to the tyre in service.

A typical tyre usually contains a variety of rubber compositions in order to achieve a balance of properties for a particular type of tyre service. Table 2.1 lists some of the major requirements on the rubber compounds used for the different components of the tyre. There is no general agreement within the tyre industry as to how many different rubber compounds to use, or what their composition should be. In addition to material variations, the tyre designer has many options available for modifying the properties. Perhaps the most powerful is that of changing cord angles in either the body or tread plies [46].

A variety of cord materials are currently in use including nylon, polyester, steel, fiberglass, and Kevlar. In the past, cotton and rayon cords were used. Different rubber compounds for different tyre components are given in Table 2.1.

2.3 Construction of Tyres

The construction of a tyre has many material and geometric discontinuities that causes stress and strain concentrations that could potentially lead to fatigue-related tyre failures. Retreading is an effective means of renewing the tyre and extending its life since the casing has a much longer fatigue life than the tread. Both the reliability and durability of a retreated tyre depend critically on the state of stress and the adhesion strength in the tread / cushion / casing region. A tyre consists of the following parts which have their respective importance in the tyre structure :(1) Tread (2) Carcass (3) Cushion (4) Reinforcement fabric (5) Bead wires (6) Abrasion strips or breaker (7) Side wall. A typical schematic diagram of the tyre cross section with its different components is illustrated in Fig. 2.1[3]. Figure 2.2 describes the geometry of a single tread section along with its boundary conditions to be considered for the present problem. The tread and sidewall (constituting the covering airable outside of the tyre) are composed of rubber compounds to withstand wear and friction. Generally both are composed of same compound but the sidewall is thinner as it does not come in contact with road surface. Tread designs are plain or non-skid type. The cushion is placed under the breaker strips composed of an woven fabric. The breaker takes the Shocks and effect of pressure from the outside of the tyre and distributes evenly over the carcass through cushion. The cushion acts as a binder or flux between tread or breaker and the carcass has the responsibility of the real strength of the tyre. Cushion is made of a typical rubber compound which gives jerk resistance to fabric plies, whereas carcass is composed of layers of fabrics or cable cords built up to the shape and size of tyre. Bead rings are high carbon steel coated with brass to give good adhesion. Bead core forms the basis of the outer cover providing rigidity, non-extensibility and means for attachment to rims.

There are two general types of tyres, those with inner tubes and those without inner tubes, called tubeless tyres. On the inner tube type, both the tube and the tyre casing are mounted on the wheel rim. The tube is a hollow rubber doughnut. It is inflated with air after it is installed inside the tyre and the tyre is put on the wheel rim. This inflation causes the tyre to resist any change of shape. Tubes are used in truck tyres and in motorcycle tyres. Tubes are not always used in passenger-car tyres today. The tubeless tyre does not use an inner tube. Instead, tubeless tyre is mounted on the wheel rim so that the air is retained between the rim and the tyre.

The amount of air pressure used in the tyre depends on the type of tyre and the operation. Passenger tyres are inflated to about 22 to 36 psi . Heavy-duty tyres with trucks or busses may be inflated to 100 psi. Tyre casings and tubeless tyres are made in about the same way. Layers of cord, called plies, are shaped on a form and impregnated with rubber. The rubber sidewalls and treads are then applied. They are vulcanized into place to form the completed tyre. The term vulcanizing means heating the rubber under pressure. This process molds the rubber into the desired form and gives it the proper wear characteristics and flexibility. The number of layers of cord or plies varies according to the intended use of the tyre. Passenger-car tyres have 2, 4 or 6 plies. Tyres for heavy-duty service, such as earthmoving machinery, may have up to 32 plies.

2.4 Tyre Size and Marking

Tyre size is marked on the sidewall of the tyre. An older tyre might be marked 7.75-14. This means that the tyre fits on a wheel that is 14 inches in diameter at the rim where the tyre bed rests. The 7.75 means the tyre itself is about 7.75 inches wide when it is properly inflated. Tyres carry several marking on the sidewall. The marking include a letter code to designate the type of car the tyre is designated for. D means a lightweight car. F means intermediate, G

means a standard car and H, T and L are for large luxury cars and high-performance vehicles. For example, some cars use a G78-14 tyre. The 14 means .a rim diameter of 14 inches [356mm], the 78 indicates the ratio between tyre height and width. The ratio between the height and the width is called the aspect ratio or the profile ratio. The lower the number, the wider the tyre looks. The addition to the side wall marking, such as GR 78-14 indicates that the tyre is a radial. Also, if a tyre is a radial, the word radial must be molded into the sidewall. Some radials are marked in the metric system. For example, a tyre marked 175R13 is a radial tyre, which measures 175 mm wide. It mounts on a wheel with a rim diameter of 13 inches.

2.5 Description of Tyre Tread

The tread is the part of the tyre that rests on the road. There are many different tread designs. Snow tyres have large rubber cleats molded into the tread. The cleats cut through snow to improve traction. Some tyres have steel studs that stick out through the tread. Studs help the tyres to get better traction on ice and snow. However, some people claim studded tyres shorten the life of the road surface. For this reason, studded tyres are banned in some localities. Tread should have following properties:

(a)   Good scorch resistance, (b) Flat cure rate, (c) Optimum plasticity, (d) Abrasive resistance, (e) Tear resistance, (f) Flex resistance and (g) Age resistance

2.6   Compounding of Tread Compounds

Tread consists of (1) Polymer, (2) Fillers, and (3) Plasticisers.

(a) Polymers: For this, polybutadiene rubber, natural rubber, SBR or blends of these rubbers with or without reclaim rubber can be used. Natural rubber

vulcanizates have good abrasion resistance and excellent tear resistance. Styrene butadiene rubber (SBR) vulcanizates have a better abrasion resistance than corresponding natural rubber vulcanizates. These compounds do not lose their physical properties or age resistance if they are over cured. The only disadvantage of these rubber is that compounds have low green tack and low green strength. These processing disadvantages can be overcome by use of natural rubber/SBR blends or by use of natural rubber cements over the green tread. One of the advantages of SBR or Buna CB rubber is that these rubber can accept higher quantities of oil and thus more economic compounds can be made without loss in abrasion resistance. Reclaim rubbers give adverse effects regarding the abrasion resistance or tear resistance of vulcanizates. However the requirements of abrasion resistance and tear resistance in cycle tyre treads are not so very stringent as in the case of auto tyres and therefore reclaim rubber can be used in cycle tyre tread compounds. The prime advantages of reclaim rubber are the economy better control of dimension during extrusion calendering of the green tread, low thermoplastic nature of the compounds, good reversion resistance, and good flex resistance of the vulcanizates.

(b) Fillers: To improve the wear and the tear properties it is essential to use some quantities of reinforcing fillers even in natural rubber compounds. In synthetic rubbers, SBR or Buna CB, use of reinforcing fillers is a must. Carbon blacks are the prime reinforcing fillers. Carbon black of the type of HAF (High-abrasion furnace) or even FEF (Fast-extrusion furnace) can be used.

China clay is a semi reinforcing filler and can be used along with carbon blacks for improvement in the wear and tear resistance of the compounds. In compounds containing synthetic rubbers hard China clay should be preferred. In natural rubber compounds soft clays or even whiting can be used as

extender. One of the disadvantages of these mineral filler clays and whiting is their high specific gravity and when used above certain levels the vulcanizate properties deteriorate.

(c) Plasticisers: Pine tar and aromatic mineral oils are to be preferred for black compounds. If tread crumb, is used, it is preferable to use some mineral rubber (blown bitumen) in the compounds to give a better bond between the tread crumb and the compound.

2.7 Tyre Inflation and Tyre Wears

Rapid tyre wear results from quick starts and stops, heavy breaking, high speed, taking corners too fast, and striking or rubbing curbs. Too little air in the tyre can cause hard steering, front wheel shimmy, steering kickback and tyre squeal on turns. A tyre with too little air will wear on the shoulders and not in the center of the tread. If the tyre strikes a rut or stone or bumps a curb too hard, it flexes so much that it is pinched against the rim. Any of these kinds of damage can lead to early tyre failure. Different kinds of tyre wear are as follows:

(a)   Toe-in or Toe-out Tyre Wear

Excessive toe-in or toe-out on turn causes the tyre to be dragged sideways as it moves forward. For example, a tyre on a front wheel that toes in 1 inch [25.4 mm] from straight ahead will be dragged sideways about 150 feet [46 m] every mile [1.6 km]. This sideways drag scrapes off rubber. If both sides show this type of wear, the toe is incorrect. If only one tyre shows this type of wear, a steering arm probably is bent. This causes one wheel to toe in or out more than the other.

(b) Camber Wear

If a wheel has excessive camber, the tyre runs more on one shoulder than on the other shoulder. The tread wears excessively on that side.

(c) Cornering Wear

Cornering is caused by taking curves at excessive speeds. The tyre skids and tends to roll, producing the diagonal type of wear. This is one of the more common causes of tyre wear.

(d) Uneven Tyre Wear

Uneven tyre wear, with the tread unevenly or spottily worn. These include miss aligned wheels, unbalanced wheels, uneven or "grabby" brakes, over inflated tyres, and out- of-round brake drums.

(e) High Speed Wear

Tyres wear more rapidly at high speed than at low speed. Tyres driven consistently at 70 to 80 mph [113 to 129km/h] will give less than half the life of tyres driven at 30 mph [48 km/h]

2.8 Tyre Retreading

Tyre retreading or 'recapping' is a specialized process that involves applying new tread material to the old casing and vulcanizing it into place. Only Casings that are in good condition should be recapped. Recapping cannot repair a casing with broken or separated plies or other damage. Recapping requires special equipment. If a tyre is in sound condition and only its tread is worn or cut, it will be accepted for retreading.

Various Steps in Retreading Process

(a) **Inspection**-Used tyre is mounted on a pneumatically operated machine for close inspection of the inside of casing and wounds or cuts on the tread to judge whether the tyre is acceptable for retreading or it should be rejected.

(b) Removal of Tread- The old tread is removed by pulling of the top layer to a very close limits on a special machine and outer layer of the remaining tyre buffed. In practice, it is very important to buff or otherwise roughen all surfaces to which new materials are to be added. Both cleanliness and roughness are essential for retreading.

(c) Solutioning - The outer buffed layer of tyre casing is given a coat of solution to obtain a foundation for retreading.

(d) Application of Material and Curing - When solution is dry, new tread is built on the old casing as usual. In orbitread process, a ribbon of tread is extruded directly on the buffed cemented casing and wound helically. The complete tyre is then fitted into a mould and mounted on a curing table where steam, heat and pressure are applied for curing. After curing the new tyre with the old casing is as good as a new tyre. A retread compounds (camelback or slab) should have a long storage life and should be abrasion and wear resistant, flux resistant, wet skid resistant and silent running. Synaprene 1712 and EBR-OE are preferred in camelback compounds. For passenger retreads EBR-OE is blended with S-1712, while for truck treads EBR-OE is blended with NR to minimize heat build up during use. Insoluble sulphur is used in retread compounds to reduce blooming and to increase storage life of the products. SBR compounds exhibit lower building tack compared to NR compounds. But the use of NR cushion gum eliminates building up difficulties and fusion of retread with the casing is excellent.

Chapter 3

MATHEMATICAL FORMULATION AND NUMERICAL SOLUTION

3.1 Introduction

Almost all engineering materials posses to a certain extent the property of elasticity. If the external forces producing deformation do not exceed a certain limit, the deformation disappears with the removal of forces. Throughout this thesis it will be assumed that the bodies undergoing the action of external forces are perfectly elastic, that is, that they resume their initial form completely after removal of forces. Atomic structure will not be considered here. It will be assumed that the matter of an elastic body is homogeneous and continuously distributed over its volume so that the smallest element cut from the body possesses the same specific physical properties as that of the body. To simplify the discussion it will also be assumed that, for the most part, the tread section is isotropic, that is, the elastic properties are the same in all directions.

3.2 General Formulation for Elastic Problems

There are two kinds of external forces, which may act on bodies. Forces applied over the surface of the body are known as surface forces and that distributed over the volume of a body are called body forces. In the analysis of stress in almost all-engineering problems, the effect of body forces compared to those of surface forces are very small. Thus, the effect of body force may be neglected and that is why, in the present work, only the influence of surface forces is considered. The surface force per unit area will resolve into three components parallel to cartesian coordinates x, y, z. The

normal stress components are represented by σ_x, σ_y and σ_z in the x-, y-and z-directions, respectively, while the components σ_{xy}, σ_{yz}, σ_{zx} are the components of shear stress in xy-, yz- and zx- planes respectively. The normal stress, σ_x is taken positive when it produces tension and negative for compression. For shearing stress, σ_t (tangential stress) on external surface, the sign is positive when acting clockwise and negative for anticlockwise.

In discussing the deformation of an elastic body it is assumed that there are constraints to prevent the body from moving as a rigid body so that no displacements of particles of the body are possible without a deformation of it. The displacements of particles of deformed body are first resolved into components $-u_x$, u_y, u_z parallel to the co-ordinates x, y, z, respectively. It is also assumed that these displacement components are very small quantities, varying continuously over the volume of the body.

By definition, the normal and shear strains in an elastic body are [47],

$$\varepsilon_x = \frac{\partial u_x}{\partial x}, \quad \varepsilon_y = \frac{\partial u_y}{\partial y}, \quad \varepsilon_z = \frac{\partial u_z}{\partial x}$$

$$\gamma_{xy} = \frac{\partial u_x}{\partial y} + \frac{\partial u_y}{\partial x}, \quad \gamma_{yz} = \frac{\partial u_y}{\partial z} + \frac{\partial u_z}{\partial y}, \quad \gamma_{zx} = \frac{\partial u_z}{\partial x} + \frac{\partial u_x}{\partial z} \tag{3.1}$$

where ε_x, ε_y, ε_z are the strain components parallel to the co-ordinate axes and γ_{xy}, γ_{yz}, γ_{zx} are shear strains in the xy-, yz- and zx-planes, respectively.

The stresses are related to strains through the elastic constants, according to the Hook's law. The relations are as follows:

$$\varepsilon_x = \frac{1}{E}\left[\sigma_x - \mu(\sigma_y + \sigma_z)\right]$$

$$\varepsilon_y = \frac{1}{E}\left[\sigma_y - \mu(\sigma_x + \sigma_z)\right] \tag{3.2}$$

$$\varepsilon_z = \frac{1}{E}\left[\sigma_z - \mu(\sigma_y + \sigma_x)\right]$$

The six quantities σ_x, σ_y, σ_z, σ_{xy}, σ_{yz}, σ_{zx} are sufficient to describe the state of stress at a point within the body [45]. If a cubic block element, cut-off from a solid body with its sides parallel to the co-ordinate axes is in equilibrium under the action of continuous functions σ_x, σ_y, σ_z, σ_{xy}, σ_{yz}, σ_{zx}, then equations of equilibrium for general 3-D problem, in absence of body forces, are

$$\frac{\partial \sigma_x}{\partial x} + \frac{\partial \sigma_{xy}}{\partial y} + \frac{\partial \sigma_{zx}}{\partial z} = 0$$

$$\frac{\partial \sigma_y}{\partial y} + \frac{\partial \sigma_{xy}}{\partial x} + \frac{\partial \sigma_{yz}}{\partial z} = 0 \qquad (3.3)$$

$$\frac{\partial \sigma_z}{\partial z} + \frac{\partial \sigma_{zx}}{\partial x} + \frac{\partial \sigma_{yz}}{\partial y} = 0$$

In the theory of elasticity, determination of the state of stress in a body submitted to the action of given forces is a fundamental problem. In a 3-D problem, it is necessary to solve the differential equations of equilibrium (3.3), and the solution must be such as to satisfy the boundary conditions imposed on the boundary surface. The stress components vary within the body and, on the boundary, they must be such as to be in equilibrium with the external forces on the boundary. Thus the external forces may be regarded as a continuation of the internal forces in the body. The equilibrium equations (3.3), derived by application of the equations of statics and containing six stress components are not sufficient for the determination of six unknowns - σ_x, σ_y, σ_z, σ_{xy}, σ_{yz}, σ_{zx}. The problem is a statically indeterminate one, and in order to obtain the solution, the elastic deformation of the body must be considered. The additional equations ensure continuity of deformation in the

body and known as compatibility equations. In fact, they ensure compatibility of displacement u_x, u_y and u_z. The three compatibility equations in terms of strain components are as follows:

$$\frac{\partial^2 \varepsilon_y}{\partial x^2} + \frac{\partial^2 \varepsilon_x}{\partial y^2} = \frac{\partial^2 \gamma_{xy}}{\partial x \partial y}$$

$$\frac{\partial^2 \varepsilon_y}{\partial z^2} + \frac{\partial^2 \varepsilon_z}{\partial y^2} = \frac{\partial^2 \gamma_{yz}}{\partial y \partial z} \tag{3.4}$$

$$\frac{\partial^2 \varepsilon_z}{\partial x^2} + \frac{\partial^2 \varepsilon_x}{\partial z^2} = \frac{\partial^2 \gamma_{zx}}{\partial z \partial x}$$

3.3 Two-Dimensionalization of the Problem

Although a body is always three dimensional, most of the practical problems of stress analysis can be reduced to a two-dimensional one under two simplifying assumptions. The first of these two assumptions is that the loading on the body is confined in a plane and the dimension of the body in the direction perpendicular to its plane is relatively small compared to the other two. In such cases, the stresses in the body perpendicular to the plane of loading is usually very small and thus can be neglected. As a result, these problems become two-dimensional, usually referred to as plane stress problems. The second simplifying assumption holds for bodies whose one of the three dimensions is relatively large or straining of the body in a particular direction is restrained. Under such circumstances, the problem of stress analysis becomes two-dimensional, referred to as plane strain problem.

In case of plane problems, only the stress components σ_x, σ_y, σ_{xy} and displacement components u_x and u_y are to be determined as a function of x and y. Knowing the stress components σ_x, σ_y, σ_{xy} at any point of a plane in a condition of plane stress or plane strain, the stress acting on any plane passing

through this point and inclined to the x- and y-axes can be calculated from the equations of statics.

With reference to a rectangular coordinate system (x, y), the differential equations of equilibrium for the case of two-dimensional problems, in the absence of body forces, are as follows:

$$\frac{\partial \sigma_x}{\partial x} + \frac{\partial \sigma_{xy}}{\partial y} = 0$$

$$\frac{\partial \sigma_y}{\partial y} + \frac{\partial \sigma_{xy}}{\partial x} = 0$$

(3.5)

Equation (3.5) must be satisfied at all points within the body. The condition of compatibility for the two dimensional case becomes,

$$\frac{\partial^2 \varepsilon_x}{\partial y^2} + \frac{\partial^2 \varepsilon_y}{\partial x^2} = \frac{\partial^2 \gamma_{xy}}{\partial x \partial y}$$

(3.6)

Elimination of strains in terms of stresses from equation (3.6) gives

$$\left(\frac{\partial^2}{\partial x^2} + \frac{\partial^2}{\partial y^2} \right) (\sigma_x + \sigma_y) = 0$$

(3.7)

It is mentioned here that the compatibility equation (3.7) in terms of stress components holds for both the cases of plane stress and plane strain problems in the absence of body forces.

The normal and shear stress components σ_n and σ_t on a plane where normal has the direction cosines (l,m) are given by

$$\sigma_n = l^2 \sigma_x + m^2 \sigma_y + 2lm \sigma_{xy}$$

$$\sigma_t = lm(\sigma_y - \sigma_x) + (l^2 - m^2)\sigma_{xy}$$

(3.8)

Similarly, if u_n and u_t are the normal and tangential components of displacement, respectively, on a plane whose normal has the direction cosines l and m, then it can be shown that

$$u_n = lu_x + mu_y$$
$$u_t = lu_y - mu_x$$

(3.9)

Here σ_n and u_n are taken positive when directed normally outward on the boundary and tangential components (σ_t, u_t) are taken positive if they act anti-clockwise on the body, but u_x, u_y are taken positive in the direction of positive x and y axes for both the body and the boundary.

3.4 Displacement Potential Function Formulation

In order to formulate the two dimensional elastic problems in terms of displacement potential function, ψ, both the equilibrium equations and the boundary conditions are required to be expressed in terms of the displacement components u_x and u_y. In absence of body forces, the equilibrium equations for two-dimensional elastic problems in terms of displacement components are,

$$\frac{\partial^2 u_x}{\partial x^2} + \left(\frac{1-\mu}{2}\right)\frac{\partial^2 u_x}{\partial y^2} + \left(\frac{1+\mu}{2}\right)\frac{\partial^2 u_y}{\partial x \partial y} = 0$$

$$\frac{\partial^2 u_y}{\partial y^2} + \left(\frac{1-\mu}{2}\right)\frac{\partial^2 u_y}{\partial x^2} + \left(\frac{1+\mu}{2}\right)\frac{\partial^2 u_x}{\partial x \partial y} = 0$$

(3.10)

Where u_x and u_y are the displacement components of a point in the x and y directions, respectively. These two homogeneous elliptical partial differential equations with the appropriate boundary conditions should be sufficient for the evaluation of the two functions u_x and u_y, and the knowledge of these functions over the region concerned will uniquely determine the stress components.

Although the above two differential equations are sufficient to solve mixed boundary-value elastic problems, but in reality, it is difficult to solve for two functions simultaneously. So, to overcome this difficulty, equations (3.10) are converted into a single equation, using a potential function. If a function is defined in terms of the displacement components u_x and u_y, then the determination of that function uniquely determines the stress functions sought for.

The present potential function approach involves investigation of the existence of a function defined in terms of the displacement components. In this approach, as in the case of Airy's stress function, the problem is reduced to the determination of a single variable. The potential function ψ (x,y) is defined in terms of displacement components as,

$$u_x = \frac{\partial^2 \psi}{\partial x \partial y}$$

$$u_y = -\left[\left(\frac{1-\mu}{1+\mu}\right)\frac{\partial^2 \psi}{\partial x^2} + \left(\frac{2}{1+\mu}\right)\frac{\partial^2 \psi}{\partial x^2}\right] \tag{3.11}$$

With this definition of ψ (x, y), the first of the two equations (3.10) is automatically satisfied. Therefore, ψ has only to satisfy the second equation. Expressing this equation in terms ψ, the condition that ψ has to satisfy becomes,.

$$\frac{\partial^4 \psi}{\partial x^4} + 2\frac{\partial^4 \psi}{\partial x^2 \partial y^2} + \frac{\partial^4 \psi}{\partial y^4} = 0 \tag{3.12}$$

Therefore the problem is reduced to the evaluation of a single variable ψ (x,y) from the bi-harmonic partial differential equation (3.12).

In order to solve the problem in terms of the potential function ψ of the bi-harmonic equation (3.12), the boundary conditions should also be expressed in terms of ψ. The boundary conditions are prescribed as known restraints and loadings, that is, known values of components of stresses and displacements on the boundary. The relations between the known functions on the boundary and the function ψ (x,y) are

$$u_x = \frac{\partial^2 \psi}{\partial x \partial y}$$

$$u_y = -\left[\left(\frac{1-\mu}{1+\mu}\right)\frac{\partial^2 \psi}{\partial y^2} + \left(\frac{2}{1+\mu}\right)\frac{\partial^2 \psi}{\partial x^2}\right]$$

$$\sigma_x = \left(\frac{E}{1-\mu^2}\right)\left(\frac{\partial u}{\partial x} + \mu\frac{\partial v}{\partial y}\right) = \frac{E}{(1+\mu)^2}\left[\frac{\partial^3 \psi}{\partial x^2 \partial y} - \mu\frac{\partial^3 \psi}{\partial y^3}\right] \qquad (3.13)$$

$$\sigma_y = \left(\frac{E}{1-\mu^2}\right)\left(\frac{\partial u_y}{\partial y} + \mu\frac{\partial u_x}{\partial x}\right) = \frac{E}{(1+\mu)^2}\left[\frac{\partial^3 \psi}{\partial x^2 \partial y} + (\mu+2)\frac{\partial^3 \psi}{\partial x^2 \partial y}\right]$$

$$\sigma_{xy} = \frac{E}{2(1+\mu)}\left(\frac{\partial u_x}{\partial y} + \mu\frac{\partial u_y}{\partial x}\right) = \frac{E}{(1+\mu)^2}\left[\mu\frac{\partial^3 \psi}{\partial x \partial y^2} - \frac{\partial^3 \psi}{\partial x^3}\right]$$

From these expressions it is found that, as far as boundary conditions are concerned, either known restraints or known stresses or any combination of these, can readily be converted to finite difference expressions in terms of ψ on the boundary.

To analyze the state of stress for two-dimensional regular/irregular-shaped bodies with mixed boundary condition, the 4th order-partial differential equation (3.12) together with the stress and displacement components given by the Eq. (3.13) are considered as the governing equations. The expressions for stress and displacement components [Eq. 3.13] are valid for points within

the body as well as on the boundary. But for the case of practical problems, the boundary conditions are known in terms of their normal and tangential components on the boundary. Thus the boundary equations for the known conditions on the boundary having arbitrary shape are,

$$u_n(x,y) = u_x.l + u_y.m$$

$$= -\frac{2m}{1+\mu}\frac{\partial^2\psi}{\partial x^2} - \frac{m(1-\mu)}{1+\mu}\frac{\partial^2\psi}{\partial y^2} + l\frac{\partial^2\psi}{\partial x\partial y}$$

$$u_t(x,y) = u_y.l - u_x.m$$

$$= -\frac{2l}{1+\mu}\frac{\partial^2\psi}{\partial x^2} - \frac{l(1-\mu)}{1+\mu}\frac{\partial^2\psi}{\partial y^2} - m\frac{\partial^2\psi}{\partial x\partial y} \qquad (3.14)$$

$$\sigma_n(x,y) = l^2\sigma_x + 2lm.\sigma_{xy} + m^2\sigma_y$$

$$= \frac{.E}{(1+\mu)^2}\left[-2lm\frac{\partial^3\psi}{\partial x^3} + (l^2 - 2m^2 - \mu m^2)\frac{\partial^3\psi}{\partial x^2\partial y} + 2lm\mu\frac{\partial^3\psi}{\partial x\partial y^2} - (\mu l^2 + m^2)\frac{\partial^3\psi}{\partial y^3}\right]$$

$$\sigma_t(x,y) = (l^2 - m^2)\sigma_{xy} + lm(\sigma_y - \sigma_x)$$

$$= \frac{E}{(1+\mu)^2}\left[-(l^2 - m^2)\frac{\partial^3\psi}{\partial x^3} - lm(\mu+3)\frac{\partial^3\psi}{\partial x^2\partial y} + \mu(l^2 - m^2)\frac{\partial^3\psi}{\partial x\partial y^2} + lm(\mu-1)\frac{\partial^3\psi}{\partial y^3}\right]$$

By knowing the proper boundary conditions (u_n, u_t, σ_n, σ_t) the function Ψ would be solved by using equation (3.12) and equation (3.14). Then stress or strain components within the body as well as on the boundary would be determined by the equations (3.14). The computational work in solving any problem remains the same in the present case as it was in the case of ϕ-formulation, since both of them have to satisfy the same bi-harmonic equation. But the ψ-formulation is free from the inability of the ϕ-formulation in handling the mixed boundary conditions.

3.5 Finite Difference Modeling of the Problem

Finite-difference method is the oldest numerical technique, which is particularly suitable for the solution of differential equations. In the present approach, the governing differential equation and the boundary conditions are replaced by their corresponding finite-difference algebraic equations. The general approach of finite difference solution assumes that the function can be represented in a prescribed range with a sufficient degree of accuracy by Taylor series with origin at the successive pivotal points of the range. For the solution of our present problem, the pivotal points are taken as the regular mesh points of the domain of dependence of the functions, obtained by dividing the domain by lines parallel to the co-ordinate axes.

3.5.1 Solution Procedure

Method of Solution

The mixed boundary value problem is unquestionably beyond the scope of pure analytical methods of solutions. Thus numerical solution for this class of problems is the only plausible approach. Here, finite difference technique is used to discretize the bi-harmonic partial differential equation and also the differential equations associated with the boundary conditions. The discrete values of the displacement potential function $\psi(x,y)$, at the mesh points of the domain (Fig.3.1) concerned, is solved from the system of linear algebraic equations resulting from the discretization of the bi-harmonic equation and the associated boundary conditions.

Discretization of the Domain

According to the usual practice, the region in which a dependent function is to be evaluated is divided into a desirable number of mesh points and the values

of the function are sought only at these mesh points. The present program is to solve a function within a stepped rectangular region, which is divided into meshes with lines parallel to rectangular co-ordinate axes. As a result, the boundary may not always pass through the mesh points of rectangular networks. But the physical problems are associated with the known boundary conditions at the boundary points of arbitrary shaped bodies. It requires a further treatment to relate the values on the boundary with the field grid points.

The governing bi-harmonic equation, which is used to evaluate the function ψ at the internal mesh points, is expressed in its corresponding difference equation using central difference operators. When all the derivatives present in the bi-harmonic equation are replaced by their respective central difference formulae, the complete finite difference expression for biharmonic equation becomes

$$
\begin{aligned}
R^4 & \{\psi(i-2,j) - 4\psi(i-1,j) + 6\psi(i,j) - 4\psi(i+1,j) + \psi(i+2,j)\} \\
& + 2R^2 \{\psi(i+1,j+1) + \psi(i+1,j-1) + \psi(i-1,j+1) + \psi(i-1,j-1) + 4\psi(i,j) \\
& - 2\psi(i+1,j) - 2\psi(i,j+1) - 2\psi(i,j-1) - 2\psi(i-1,j)\} + \{\psi(i,j-2) \\
& - 4\psi(i,j-1) + 6\psi(i,j) - 4\psi(i,j+1) + \psi(i,j+2)\}
\end{aligned}
\tag{3.15}
$$

The grid structure of the governing equation at any internal mesh point (i,j) is shown in Figs 3.1 and 3.2. The pivotal point (i, j) in the grid structure is the point of application of the governing equation. For the case of any interior mesh point, the finite-difference equation (3.15) contains the discretized variable of the thirteen neighboring mesh points, and when the point of application (i, j) becomes an immediate neighbor of the physical boundary, the equation will involve mesh points both interior and exterior to the physical boundary as shown in Fig. 3.2.

3.5.2 Management of Boundary Conditions

Normally, the boundary conditions are specified either in terms of loadings or of restraints or of some combination of two. Each mesh point on the physical boundary of the domain always entertains two of the four possible boundary conditions at a time namely, (1) normal stress and shear stress; (2) normal stress and tangential displacement; (3) shear stress and normal displacement; (4) normal displacement and tangential displacement. The computer program is organized here in such a fashion that, out of these two conditions, one is used for evaluation of ψ at the concerned boundary point and the other one for the corresponding point on the exterior false boundary. Thus, when the boundary conditions are expressed by their appropriate difference equations, every mesh point of the domain will have a single linear algebraic equation tagged to it for its evaluation.

As the differential equations associated with the boundary conditions contain second and third order derivatives of the function ψ, the application of the central difference expression is not practical as, most of the time, it leads to the inclusion of the points exterior to the false boundary. The derivatives of the boundary expressions are thus replaced by their corresponding backward or forward difference formulae, keeping the order of local truncation error the same.

The boundary of the tread section is divided into four segments, namely, (a) the top-left, (b) the bottom left, (c) the bottom right, and (d) the top right. Four different sets of boundary expressions are used for the four segments.
The finite difference expressions of the boundary conditions for four different segments are as follows.

Finite diffrence expressions of different boundary conditions for bottom left boundary segment:

$$u_n(i,j) = u_x(i,j).l + u_y(i,j)$$
$$= (9.s1.l - m.s2).\psi(i,j) + zk7.s2.m.\psi(i-1,j) + zk6.m.s2.\psi(i,j-1)$$
$$+ (zk6.m.s2 - 12.s1.l)\psi(i,j+1) + 3.s1.l.\psi(i,j+2) + 16.s1.l.\psi(i+1,j+1)$$
$$+ (zk7.m.s2. - 12.s1.l).\psi(i+1,j) - 4.s1.l.\psi(i+1,j+2) + 3.s1.l.\psi(i+2,j)$$
$$- 4.s1.l.s.\psi(i+2,j+1) + s1.l.\psi(i+2,j+2)$$

(3.16)

$$u_t(i,j) = u_y(i,j).l + u_x(i,j).m$$
$$= (-9.s1.m - l.s2).\psi(i,j) + zk7.s2.l.\psi(i-1,j) + zk6.l.s2.\psi(i,j-1)$$
$$+ (zk6.l.s2 + 12.s1.m)\psi(i,j+1) - 3.s1.m.\psi(i,j+2) - 16.s1.m.\psi(i+1,j+1)$$
$$+ (zk7.l.s2. + 12.s1.m)\psi(i+1,j) + 4.s1.m.\psi(i+1,j+2) - 3.s1.m.\psi(i+2,j)$$
$$+ 4.s1.m.\psi(i+2,j+1) - s1.m.\psi(i+2,j+2)$$

(3.17)

$$\sigma_n(i,j) = \sigma_x(i,j).l^2 + 2lm.\sigma_{xy}(i,j) + m^2.\sigma_y(i,j)$$
$$= \psi(i-1,j).\{6.zk9.R.s3.lm - 3zk9.s3.l^2 - 3zk10.s4.m^2\}$$
$$+ \psi(i-1,j+1).\{4.zk9.R.s3.l^2 + zk10.s4.m^2 + \psi(i-1,j+2)\{-zk9.s3.l^2 -$$
$$zk10.s4.m^2\} + \psi(i,j-1)\{1.5(s3.l^2 - s4.m^2 - 2lm.R.s3)\} + \psi(i,j)\{s4.m^2$$
$$(5 + 6.zk10) + s3.l^2\{(6.zk9 - 5) + 2R.s3.lm(3 - 10zk9)\} + \psi(i,j+1)\{s3.l^2(6$$
$$- 8.zk9) - 3.R.s3.lm - s4.m^2(6 + 8.zk10)\} + \psi(i,j+2)\{s4.m^2(3 + 2.zk10)$$
$$s3.l^2(2.zk9 - 3)\} + \psi(i,j+3)\{0.5(s3.l^2 - s4.m^2)\} + \psi(i+1,j-1).4.R.s3.lm$$
$$\psi(i+1,j)\{2R.s3.lm(12.zk9 - 4) - 3(zk9.s3.l^2 + zk10.s4.m^2)\}$$
$$\psi(i+1,j+1)\{4(R.s3.lm + zk9.s3.l^2 + zk10.s4.m^2)\}$$
$$\psi(i+1,j+2)(-zk9.s3.l^2 - zk10.s4.m^2) + \psi(i+2,j-1)(-R.s3.lm)$$
$$\psi(i+2,j)\{2R.s3.lm(1 - 6.zk9)\} + \psi(i+2,j+1)(-R.s3.lm)$$
$$\psi(i+3,j)(2zk9.R.s3.lm)$$

(3.18)

$$\sigma_t(i,j) = (l^2 - m^2)\sigma_{xy}(i,j) + lm\{\sigma_y(i,j) - \sigma_x(i,j)\}$$
$$= \psi(i-1,j)\{3.lm(-zk10.s4 + zk9.s3) - 3.zk9.R.s3(m^2 - l^2)\}$$
$$+ \psi(i-1,j+1)\{-4lm(zk9.s3.l^2 - zk10.s4)\}m^2 + \psi(i-1,j+2)\{-lm(zk10.s4 -$$
$$zk9.s3\} + \psi(i,j-1)\{-1.5lm(s3 + s4) + 1.5R.s3(m^2 - l^2)\}$$
$$+ \psi(i,j)[lm\{-s4(5 + 6.zk10) + s3(6.zk9 - 5)\} + R.s3(m^2 - l^2)(3 - 10.zk9)]$$
$$- \psi(i,j+1)[lm\{s4(6 + 8.zk10) + s3(6 - 8.zk9)\} - R.s3(m^2 - l^2)(1.5)]$$
$$- \psi(i,j+2)[lm\{s3(2.zk9 - 3) - s4(3 + 2.zk10)\}] - \psi(i,j+3)\{0.5lm\{s3 + s4\}\}$$
$$- \psi(i+1,j-1)\{2.R.s3(m^2 - l^2)\} - \psi(i+1,j)[3lm(s4.zk10 - s3.zk9)$$

$$+(12.zk9-4)R.s3(m^2-l^2)]-\psi(i+1,j+1)[4lm(s3.zk9-s4.zk10+$$

$$2.R.s3(m^2-l^2)]-\psi(i+1,j+2)\{lm(s4.zk10-s3.zk9)\}-\psi(i+2,j-1)$$

$$\{-0.5R.s3(m^2-l^2)\}-\psi(i+2,j)\{1-6.zk9)R.s3(m^2-l^2)\}-\psi(i+2,j+1)$$

$$\{-0.5R.s3(m^2-l^2)\}-\psi(i+3,j)\{zk9.R.s3(m^2-l^2)\}$$

$$(3.19$$

Finite difference equations of different boundary conditions for bottom right boundary segment:

$$u_n(i,j)=u_x(i,j).l+u_y(i,j).m$$

$$=(-9.s1.l-m.s2).\psi(i,j)+zk7.s2.m.\psi(i+1,j)+zk6.m.s2.\psi(i,j-1)$$

$$+(zk6.m.s2+12.s1.l)\psi(i,j+1)-3.s1.l.\psi(i,j+2)-16.s1.l.\psi(i-1,j+1)$$

$$+(zk7.m.s2.+12.s1.l)\psi(i-1,j)+4.s1.l.\psi(i-1,j+2)-3.s1.l.\psi(i-2,j)$$

$$+4.s1.l.s.\psi(i-2,j+1)-s1.l.\psi(i-2,j+2)$$

$$(3.20)$$

$$u_t(i,j)=u_y(i,j).l+u_x(i,j).m$$

$$=(9.s1.m-l.s2)\psi(i,j)+zk7.s2.l.\psi(i+1,j)+zk6.l.s2.\psi(i,j-1)$$

$$+(zk6.l.s2-12.s1.m)\psi(i,j+1)+3.s1.m.\psi(i,j+2)+16.s1.m.\psi(i-1,j+1)$$

$$+(zk7.l.s2.-12.s1.m).\psi(i-1,j)-4.s1.m.\psi(i-1,j+2)+3.s1.m.\psi(i-2,j)$$

$$-4.s1.m.s.\psi(i-2,j+1)+s1.m.\psi(i-2,j+2)$$

$$(3.21)$$

$$\sigma_n(i,j)=\sigma_x(i,j).l^2+2lm.\sigma_{xy}(i,j)+m^2.\sigma_y(i,j)$$

$$=\psi(i+1,j).\{-6.zk9.R.s3.lm-3zk9.s3.l^2-3zk10.s4.m^2\}$$

$$+\psi(i+1,j+1).\{4(zk9.s3.l^2+zk10.s4.m^2\}+\psi(i+1,j+2)\{-zk9.s3.l^2-$$

$$zk10.s4.m^2\}+\psi(i,j-1)\{1.5(s3.l^2-s4.m^2+2lm.R.s3)\}+\psi(i,j)\{s4.m^2$$

$$(5+6.zk10)+s3.l^2\{(6.zk9-5)-2R.s3.lm(3-10zk9)\}+\psi(i,j+1)\{s3.l^2(6$$

$$-8.zk9)+3.R.s3.lm-s4.m^2(6+8.zk10)\}+\psi(i,j+2)\{s4.m^2(3+2.zk10)$$

$$s3.l^2(2.zk9-3)\}+\psi(i,j+3)\{0.5(s3.l^2-s4.m^2)\}-\psi(i-1,j-1).4.R.s3.lm$$

$$+\psi(i-1,j)\{-2R.s3.lm(12.zk9-4)-3(zk9.s3.l^2+zk10.s4.m^2)\}$$

$$\psi(i-1,j+1)\{4(-R.s3.lm+zk9.s3.l^2+zk10.s4.m^2)\}$$

$$\psi(i-1,j+2)(-zk9.s3.l^2-zk10.s4.m^2)+\psi(i-2,j-1)(R.s3.lm)$$

$$-\psi(i-2,j)\{-2R.s3.lm(1-6.zk9)\}+\psi(i-2,j+1)(R.s3.lm)$$

$$\psi(i-3,j)(2zk9.R.s3.lm)$$

$$(3.22)$$

$$\sigma_t(i,j) = (l^2 - m^2)\sigma_{xy}(i,j) + lm\{\sigma_y(i,j) - \sigma_x(i,j)\}$$

$$= \psi(i+1,j)\{3.lm(-zk10.s4 + zk9.s3) - 3.zk9.R.s3(m^2 - l^2)\}$$

$$+ \psi(i+1,j+1)\{4.zk9.s3.l^2 + zk10.s4.m^2 + \psi(i+1,j+2)\{-lm(zk10.s4 - zk9.s3\} + \psi(i,j-1)\{-1.5lm(s3+s4) - 1.5R.s3(m^2 - l^2)\}$$

$$+ \psi(i,j)[lm\{-s4(5 + 6.zk10) + s3(6.zk9 - 5)\} - R.s3(m^2 - l^2)(3 - 10.zk9)]$$

$$- \psi(i,j+1)[lm\{s4(6 + 8.zk10) + s3(6 - 8.zk9)\} + R.s3(m^2 - l^2)(1.5)]$$

$$- \psi(i,j+2)[lm\{s3(2.zk9 - 3) - s4(3 + 2.zk10)\}] - \psi(i,j+3)\{0.5lm\{s3+s4\}$$

$$+ \psi(i-1,j-1)\{2.R.s3(m^2 - l^2)\} - \psi(i-1,j)[3lm(s4.zk10 - s3.zk9)$$

$$- (12.zk9 - 4)R.s3(m^2 - l^2)] - \psi(i-1,j+1)[4lm(s3.zk9 - s4.zk10 -$$

$$2.R.s3(m^2 - l^2)] - \psi(i-1,j+2)\{lm(s4.zk10 - s3.zk9)\} - \psi(i-2,j-1)$$

$$\{0.5R.s3(m^2 - l^2)\} + \psi(i+2,j)\{1 - 6.zk9)R.s3(m^2 - l^2)\} - \psi(i-2,j+1)$$

$$\{0.5R.s3(m^2 - l^2)\} + \psi(i-3,j)\{zk9.R.s3(m^2 - l^2)\}$$

$$(3.23)$$

Finite difference equations of different boundary conditions for top right boundary segment:

$$u_n(i,j) = u_x(i,j).l + u_y(i,j)$$

$$= (9.s1.l - m.s2)\psi(i,j) + zk7.s2.m.\psi(i+1,j) + zk6.m.s2.\psi(i,j+1)$$

$$+ (zk6.m.s2 + 12.s1.l)\psi(i,j-1) + 3.s1.l.\psi(i,j-2) + 16.s1.l.\psi(i-1,j-1)$$

$$+ (zk7.m.s2. - 12.s1.l)\psi(i-1,j) + 4.s1.l.\psi(i-1,j-2) + 3.s1.l.\psi(i-2,j)$$

$$- 4.s1.l.\psi(i-2,j-1) + s1.l.\psi(i-2,j-2)$$

$$(3.24)$$

$$u_t(i,j) = u_y(i,j).l + u_x(i,j).m$$

$$= (-9.s1.m - l.s2)\psi(i,j) + zk7.s2.l.\psi(i+1,j) + zk6.l.s2.\psi(i,j+1)$$

$$+ (zk6.l.s2 + 12.s1.m)\psi(i,j-1) - 3.s1.m.\psi(i,j-2) - 16.s1.m.\psi(i-1,j-1)$$

$$+ (zk7.l.s2. + 12.s1.m)\psi(i-1,j) + 4.s1.m.\psi(i-1,j-2) - 3.s1.m.\psi(i-2,j)$$

$$+ 4.s1.m.s.\psi(i-2,j-1) - s1.m.\psi(i-2,j-2)$$

$$(3.25)$$

$$\sigma_n(i,j) = \sigma_x(i,j).l^2 + 2lm.\sigma_{xy}(i,j) + m^2\sigma_y(i,j)$$

$$= \psi(i+1,j).\{-6.zk9.R.s3.lm + 3zk9.s3.l^2 + 3zk10.s4.m^2\}$$

$$-\psi(i+1,j-1).\{4.zk9.R.s3.l^2 + zk10.s4.m^2 + \psi(i+1,j-2)\{zk9.s3.l^2 +$$

$$zk10.s4.m^2\} - \psi(i,j+1)\{1.5(s3.l^2 - s4.m^2 - 2lm.R.s3)\} - \psi(i,j)\{s4.m^2$$

$$(5 + 6.zk10) + s3.l^2\{(6.zk9-5) + 2R.s3.lm(3-10zk9)\} - \psi(i,j-1)\{s3.l^2(6$$

$$-8.zk9) - 3.R.s3.lm - s4.m^2(6+8.zk10)\} - \psi(i,j-2)\{s4.m^2(3+2.zk10)$$

$$+s3.l^2(2.zk9-3)\} - \psi(i,j-3)\{0.5(s3.l^2 - s4.m^2)\} - \psi(i-1,j+1).4.R.s3.lm$$

$$-\psi(i-1,j)\{2R.s3.lm(12.zk9-4) - 3(zk9.s3.l^2 + zk10.s4.m^2)\}$$

$$-\psi(i-1,j-1)\{4(R.s3.lm + zk9.s3.l^2 + zk10.s4.m^2)\}$$

$$\psi(i-1,j-2)(zk9.s3.l^2 + zk10.s4.m^2) + \psi(i-2,j+1)(R.s3.lm)$$

$$-\psi(i-2,j)\{2R.s3.lm(1-6.zk9)\} + \psi(i-2,j-1)(R.s3.lm)$$

$$-\psi(i-3,j)(2zk9.R.s3.lm)$$

(3.26)

$$\sigma_t(i,j) = (l^2 - m^2)\sigma_{xy}(i,j) + lm\{\sigma_y(i,j) - \sigma_x(i,j)\}$$

$$= \psi(i+1,j)\{3.lm(zk10.s4 - zk9.s3) + 3.zk9.R.s3(m^2 - l^2)\}$$

$$+ \psi(i+1,j-1)\{4lm(zk9.s3 - zk10.s4)\} + \psi(i+1,j-2)\{lm(zk10.s4 -$$

$$zk9.s3\} - \psi(i,j+1)\{-1.5lm(s3+s4) + 1.5R.s3(m^2 - l^2)\}$$

$$+ \psi(i,j)[lm\{-s4(5+6.zk10) + s3(6.zk9-5)\} + R.s3(m^2 - l^2)(3-10.zk9)]$$

$$+\psi(i,j-1)[lm\{s4(6+8.zk10) + s3(6-8.zk9)\} - R.s3(m^2 - l^2)(1.5)]$$

$$+ \psi(i,j-2)[lm\{s3(2.zk9-3) - s4(3+2.zk10)\}] + \psi(i,j-3)\{0.5lm\{s3+s4\}\}$$

$$+\psi(i-1,j+1)\{2.R.s3(m^2 - l^2)\} + \psi(i-1,j)[3lm(s4.zk10 - s3.zk9)$$

$$+(12.zk9-4)R.s3(m^2 - l^2)] + \psi(i-1,j-1)[4lm(s3.zk9 - s4.zk10 +$$

$$2.R.s3(m^2 - l^2)] + \psi(i-1,j-2)\{lm(s4.zk10 - s3.zk9)\} - \psi(i-2,j+1)$$

$$\{0.5R.s3(m^2 - l^2)\} + \psi(i-2,j)\{1-6.zk9)R.s3(m^2 - l^2)\} - \psi(i-2,j-1)$$

$$\{0.5R.s3(m^2 - l^2)\} + \psi(i-3,j)\{zk9.R.s3(m^2 - l^2)\}$$

(3.27)

Finite difference equations of different boundary conditions for top left boundary segment:

$$u_n(i,j) = u_x(i,j).l + u_y(i,j)$$

$$= (-9.s1.l - m.s2)\psi(i,j) + zk7.s2.m.\psi(i-1,j) + zk6.m.s2.\psi(i,j+1)$$

$$+ (zk6.m.s2 + 12.s1.l)\psi(i,j-1) - 3.s1.l.\psi(i,j-2) - 16.s1.l.\psi(i+1,j-1)$$

$$+ (zk7.m.s2. + 12.s1.l)\psi(i+1,j) + 4.s1.l.\psi(i+1,j-2) - 3.s1.l.\psi(i+2,j)$$

$$+ 4.s1.l\psi(i+2,j-1) - s1.l.\psi(i+2,j-2)$$

$$(3.28)$$

$$u_t(i,j) = u_y(i,j).l + u_x(i,j).m$$

$$= (9.s1.m - l.s2)\psi(i,j) + zk7.s2.l.\psi(i-1,j) + zk6.l.s2.\psi(i,j+1)$$

$$+ (zk6.l.s2 - 12.s1.m)\psi(i,j-1) + 3.s1.m.\psi(i,j-2) + 16.s1.m.\psi(i+1,j-1)$$

$$+ (zk7.l.s2. - 12.s1.m)\psi(i+1,j) - 4.s1.m..\psi(i+1,j-2) + 3.s1.m.\psi(i+2,j)$$

$$- 4.s1.m.s.\psi(i+2,j-1) + s1.m.\psi(i+2,j-2)$$

$$(3.29)$$

$$\sigma_n(i,j) = \sigma_x(i,j).l^2 + 2lm.\sigma_{xy}(i,j) + m^2\sigma_y(i,j)$$

$$= \psi(i-1,j).\{6.zk9.R.s3.lm + 3zk9.s3.l^2 + 3zk10.s4.m^2\}$$

$$- \psi(i-1,j-1).\{4.(zk9.R.s3.l^2 + zk10.s4.m^2)\} + \psi(i-1,j-2)\{zk9.s3.l^2 +$$

$$zk10.s4.m^2\} + \psi(i,j+1)\{1.5(-s3.l^2 + s4.m^2 - 2lm.R.s3)\} - \psi(i,j)\{s4.m^2$$

$$(5 + 6.zk10) + s3.l^2\{(6.zk9 - 5) - 2R.s3.lm(3 - 10zk9)\} - \psi(i,j-1)\{s3.l^2(6$$

$$- 8.zk9) + 3.R.s3.lm - s4.m^2(6 + 8.zk10)\} - \psi(i,j-2)\{s4.m^2(3 + 2.zk10)$$

$$+ s3.l^2(2.zk9 - 3)\} - \psi(i,j-3)\{0.5(s3.l^2 - s4.m^2)\} + \psi(i+1,j+1).4.R.s3.lm$$

$$+ \psi(i+1,j)\{2R.s3.lm(12.zk9 - 4) + 3(zk9.s3.l^2 + zk10.s4.m^2)\}$$

$$+ \psi(i+1,j-1)\{4(R.s3.lm - zk9.s3.l^2 - zk10.s4.m^2)\}$$

$$+ \psi(i+1,j-2)(zk9.s3.l^2 + zk10.s4.m^2) + \psi(i+2,j+1)(-R.s3.lm)$$

$$+ \psi(i+2,j)\{2R.s3.lm(1 - 6.zk9)\} + \psi(i+2,j-1)(-R.s3.lm)$$

$$\psi(i+3,j)(2zk9.R.s3.lm)$$

$$(3.30)$$

$$\sigma_t(i,j) = (l^2 - m^2)\sigma_{xy}(i,j) + lm\{\sigma_y(i,j) - \sigma_x(i,j)\}$$

$$= \psi(i-1,j)\{3.lm(zk10.s4 - zk9.s3) - 3.zk9.R.s3(m^2 - l^2)\}$$
$$+ \psi(i-1,j-1)\{4lm(zk9.s3 - zk10.s4) - \psi(i-1,j-2)\{-lm(zk10.s4 - zk9.s3\} + \psi(i,j+1)\{1.5lm(s3+s4) + 1.5R.s3(m^2 - l^2)\}$$
$$- \psi(i,j)[lm\{s4(5+6.zk10) - s3(6.zk9 - 5)\} + R.s3(m^2 - l^2)(3 - 10.zk9)]$$
$$+ \psi(i,j-1)[lm\{s4(6+8.zk10) + s3(6 - 8.zk9)\} + R.s3(m^2 - l^2)(1.5)]$$
$$+ \psi(i,j-2)[lm\{s3(2.zk9 - 3) - s4(3 + 2.zk10)\}] + \psi(i,j-3)\{0.5lm\{s3+s4\}\}$$
$$- \psi(i+1,j+1)\{2.R.s3(m^2 - l^2)\} + \psi(i+1,j)[3lm(s4.zk10 - s3.zk9)$$
$$- (12.zk9 - 4)R.s3(m^2 - l^2)] + \psi(i+1,j-1)[4lm(s3.zk9 - s4.zk10 - 2.R.s3(m^2 - l^2)] + \psi(i+1,j-2)\{lm(s4.zk10 - s3.zk9)\} - \psi(i+2,j+1)$$
$$\{-0.5R.s3(m^2 - l^2)\} - \psi(i+2,j)\{1 - 6.zk9)R.s3(m^2 - l^2)\} - \psi(i+2,j-1)$$
$$\{-0.5R.s3(m^2 - l^2)\} - \psi(i+3,j)\{zk9.R.s3(m^2 - l^2)\}$$

$$(3.31)$$

The definition of the coefficients used in the above expressions are given below:

$$zk6 = \frac{1-\mu}{2(1-\mu+2R^2)} \qquad zk7 = \frac{R^2}{2(1-\mu+2R^2)}$$

$$zk9 = \frac{R^2}{2\mu} \qquad zk10 = \frac{R^2(2+\mu)}{2}$$

$$s1 = \frac{1}{4Rh^2} \qquad s2 = -\frac{1}{zk8}$$

$$zk8 = \frac{(1-\mu)R^2h^2}{2(1-\mu+2R^2)} \qquad P2 = \frac{(1+\mu)^2 R^3 h^3}{\mu}$$

$$s3 = -\frac{E}{P2} \qquad s4 = -\frac{E}{\mu P2}$$

3.5.3 Tagging of Boundary Conditions to Mesh Points and Evaluation of Parameters of Interest

Since there are two conditions to be satisfied at an arbitrary point on the physical boundary of the tire tread, the finite difference expressions of the differential equations associated with the boundary conditions are applied to the same point on the boundary. It should be noted that two linear algebraic equations are assigned to a single point on the boundary. Out of these two equations, one is used to evaluate the function ψ at point on the physical boundary and the other one for the corresponding point on the false boundary.

Therefore, every mesh point of the domain has a single linear algebraic equation tagged to it. The discrete values of the potential function, $\psi(x, y)$, at mesh points are solved from the system of linear algebraic equations resulting from the discretization of the governing equation and the associated boundary conditions. There are numerous existing methods of solving a system of algebraic equations. In the present problem, the number of unknowns in the system of equations is extremely large but only a few in each individual equation. Under this condition, the iterative method may be preferable. But the problem of solving the difference equations by the iterative method has certain shortcomings. Although this method works very well for certain boundary conditions, it fails to produce any solution for other complex boundary conditions. In certain cases, the rate of convergence of iteration is extremely slow, which makes it impractical. As the iterative method has the limitation of not always converging to a solution and sometimes converging but very slowly, the present problem is solved by the use of the triangular decomposition method which ensures better reliability as well as better accuracy of solution in a shorter period of time.

Finally, the same difference equations are organized for the evaluation of all the parameters of interest in the solution of tire tread, namely the components of stress and displacement at every interior and boundary points from the ψ values at mesh points of the body, as all the components of stress and displacement are expressed in terms of derivatives of the function, ψ.

A tire tread along with a portion of the tread-bed in which the tire tread is embedded has been considered as the stress field as shown in Figs.3.4 and 3.5. The portion of the boundary of the stressed tread within the tread-bed, marked with dotted lines, is considered as rigidly fixed. However, the boundaries DE and GF are assumed to be free from shearing stress, but at the same time, they allow no displacement in the direction perpendicular to the boundaries. The remaining boundary is considered free from external stress except the boundary in contact with the road, where two different cases of boundary conditions are considered as illustrated in Figs. 3.4 and 3.5.

Chapter 4

EXPERIMENTAL DETERMINATION OF TYRE MATERIAL PROPERTIES

4.1 Introduction

Tyre tread is one of the major parts or components of tyres. Tyre tread is made of rubbers, binders, colors and other filler materials. The mechanical properties of tyre materials are not readily available in the literature. For the present research work, elastic properties of rubber, for example, modulus of elasticity, Poisson's ratio, etc. are required for appropriate analysis of wear of treads. These properties are obtained by direct experiment. Different tyre manufacturing companies make tyre tread of rubber materials with different properties of constituents, which eventually leads to different mechanical properties. So it is difficult to specify unique properties for tyre tread materials. In the present analysis, attempts have been made to determine experimentally all the important mechanical properties, such as, modulus of elasticity, hardness, Poisson's ratio of natural rubber, retreading tyre rubber, original truck tyre rubber. The modulus of elasticity has been determined for both cases of compression and tension and the results are compared to each other. The ultimate strength (fracture) of different tyre materials has been determined by tension test.

Tyre rubber consists of different materials including air. Under load it absorbs strain energy, however after releasing load it does not give-up the total strain energy. As a whole a little amount of energy is absorbed by the tyre tread as a result of loading. If the properties of creeping and hysteresis could be decreased, it is possible to find out yield point. In order to obtain accurate result, all the experiments have been repeated 4-5 times or even

more, and the results were averaged. Tyre tread is not exactly homogenous or isotropic because tyre tread rubber does not have binders, additives at the same ratio. That is why the results were found to vary, to some extent, from specimen to specimen. The complete stress-strain behavior of all the rubber materials were analyzed under both the conditions of tension and compression. The compression modulus of the tyre material has been used throughout the whole calculation, as in service, the tyre tread is subjected to compressive loading. The compression modulus of tyre tread materials has been determined in three different strain range such as low strain range, medium strain range and high strain range. The tension modulus has been determined for the low strain range. The original truck tyre used is specified as extra heavy tread Nylon. Single maximum load is 2550 kg at 795 kpa and Dual maximum load is 2325 kg at 725 kpa. The commercial name of the tyre is DUNLOP R.T.M SUPREME, made in India.

4.2 Experimental Apparatus and Procedure for Compression Test

The apparatus used for the compression test are (a) Universal testing machine (b) digital slide calipers (c) dial gauge (d) compression block (Specimen) (e) white marker (f) sharp knife (g) small grinding machine. Maximum range of digital slide calipers was 300 mm. Maximum loading capacity of universal testing machine was 20 ton. Type of grinding machine used was Bench grinder (Model SIST-150). It's of speed 2800 rev/min. Safe linear velocity is 35 m/s.

Procedure: First, tyre tread sections were cut by sharp knife for preparing compression block for compression test. Then the surfaces of the compression blocks were made smooth by grinding machine. Compression blocks were prepared from three different materials of tyres, namely, natural rubber, retreaded rubber and truck tyre rubber. For measuring the overall dimensions

of the block, each dimension is measured 8 times and the average values were taken as the accurate one. The compression block was fixed between the jaws of Universal testing machine, and the jaws were under the contact of two surfaces of the block. After setting the specimen, the ram was lift about 20mm to confirm the '0' position of pointer before testing. Afterwards load was increased slowly and the corresponding deformation of the block was read from the dial gauge scale, and the load was increased at the same rate up to a total deformation of 50% of the initial block. For compression test, more than three compression blocks of each tyre material, such as, natural rubber, retreaded tyre rubber, truck tyre rubber were tested.

Dimension of the Specimen made out of the truck tyre were as follows:

For specimen #1

Breadth = 3.90cm, Width = 2.82cm and Height = 2.63 cm

Contact surface area = 11.02cm^2

For specimen #2

Breadth = 3.77cm, Width = 2.92cm and Height = 2.51cm

Contact surface area = 11.01cm^2

For specimen #3

Breadth = 3.99cm, Width = 2.77cm and Height = 2.45cm

Contact surface area = 11.09cm^2

4.3 Experimental Apparatus and Procedure for Tension Test

For the tension test, the apparatus consisted of (a) a Universal testing machine (b) a digital slide calipers (c) a sharp knife (d) tensile specimens (e) white marker and small grinding machine.

Procedure: First, more than three pieces each of the three tyre materials were taken and tensile specimens were prepared by a sharp knife, and then the surfaces of the specimen were smoothened by the help of grinding machine.

The length, width, thickness and gage length of each specimen were measured by the digital slide calipers. Then the specimens were increasingly loaded at a constant slow rate and extensions were measured by digital slide calipers, and the corresponding load was read from the dial gauge.

During preparation of the tension specimen fillet radius was controlled. The load was increased up to the limit at which the specimen broke, and the corresponding load and extension at break were recorded.

Dimensions of the tensile specimens of the truck -tyre tread were as follows:

For specimen #1

Gage length = 26.68mm, Breadth = 9.04mm and Thickness = 7.90mm

Cross sectional area = $0.71416cm^2$

For specimen #2

Gage length= 27.76mm, Breadth = 9.06mm and Thickness = 5.40mm

Cross sectional area = $0.4886cm^2$

4.4 Experimental Apparatus and Procedure for Hardness Test

The apparatus used are (a) Hardness meter (Shore-A-Durometer) and (b) blocks of different tyre tread material.

The range of the hardness tester is (0-100). The hardness of any substance which has hardness number below 100 can be measured by the present tester.

Procedure: At first, the hardness meter was pressed by fingers on the surface of the specimens in different places, and the corresponding hardness numbers were recorded and their average value is calculated. Following same procedure, the hardness of natural rubber, retreading tyre rubber, Neoprene rubber and Truck tyre rubber was measured.

4.5 Determination of Elastic Modulus of Tyre Materials

Figure 4.1(a) shows the stress-strain relationship for the truck rubber under compression. From the figure, it is seen that the strain increases with the increase of stress, but not any constant rate. It is thus very difficult to identify a unique proportional limit, which is, in general, necessary for determining elastic modulus. In order to determine the elastic modulus, the stress-strain relation is assumed to be composed of three segments. First portion of the curve of Figure 4.1(a) is fitted with a straight line which is shown in Figure 4.1(b). Three strain ranges are identified to represents these segments of the curve namely, low strain range (0-21%), medium strain range (22-38%) and high strain range (38-51%). The measured relations in each strain range are approximated by the corresponding best fitted straight lines. The equation of best fitted straight line of Figure 4.1.(a) is given in Figure 4.1(b). Following the same procedure, the elastic modulus of different types of rubbers for different strain ranges are obtained from the measured relation of stress and strains (Figure 4.2-4.3). The stress-strain relationships under tension for different rubber materials are shown in Figs. 4.4-4.7. For these tension tests, data were taken upto the breaking point of the specimens. The truck tyre rubber was found to break at a strain of 479%. For the strain range, 0-130%, the relation was nearly linear and the corresponding modulus of elasticity was obtained in a similar fashion as that of the compression test, as shown in Fig. 4.4 (b). For determining the elastic modulus of different tyre rubbers, two or three specimens for each material were tested under tension and compression. The final values of the elastic modulus were obtained by averaging the data obtained for each specimen. The modulus of elasticity under compression and tension and also the ultimate strength of the materials are listed in Tables 4.1 and 4.2, respectively.

4.6 Determination of Poisson's Ratio and Hardness Number

Poisson's ratio is defined as the ratio of lateral strain to longitudinal strain. It is expressed mathematically as μ = Lateral strain/Longitudinal strain. Poisson's ratio is obtained from the tension test of different tyre material. For obtaining Poisson's ratio, four tensile specimens were prepared. The specimens were found to extend longitudinally and contract laterally when they were subjected to tensile loading. For obtaining Poisson's ratio, 3 / 4 specimens were prepared each of the materials. The Poisson's ratio for the three different materials along with the corresponding lateral and longitudinal strains is listed in Table 4.3. From the results it is seen that the Poisson's ratio for the truck tyre rubber is in between those of natural rubber and retreaded rubber. For measuring the hardness of different tyre materials, five specimens of each material were prepared. The measured hardness were arranged in descending order and third hardness value is taken as the average hardness of the material. The Shore-A-Durometer hardness values are given in Table 4.4. From the measured results it is seen that natural rubber has the lowest hardness and the retreading rubber the highest. The hardness of truck tyre rubber lies in between those of natural rubber and retreading rubber.

The percentage elongation of different kinds of rubber materials at break is shown in Table 4.5. It is seen that the rubber of truck tyre has the highest elongation at break and natural rubber has the lowest.

4.7 Results and Discussion

If the modulus of elasticity for different tyre materials obtained under the condition of tension and compression is compared with each other, it is observed that the two modulus are quite different. Elastic modulus of all the tyre materials are higher than in compression than that in tension. Therefore, for the appropriate analysis of wear of tyre-treads the compression modulus

cannot be replaced by the tension modulus. Further, experimental investigation shows that both the ultimate strength and percentage elongation of truck tyre rubber are higher than those of natural rubber. Hardness and the Poisson's ratio of truck tyre rubber are in between the values obtained for natural rubber and retreading rubber.

Therefore the present experimental investigation reveals that the mechanical properties of tyre rubbers vary significantly from those of natural rubber and thus determination of appropriate material properties is of utmost importance for reliable prediction of stress and strains in tyre treads.

Chapter 5

SOLUTION OF TYRE TREAD CONTACT PROBLEM CONSIDERING FRICTIONLESS SLIPPING

5.1 Introduction

In this chapter, the tyre tread contact problem is analyzed mainly in the perspective of deformation pattern. Actually, the deformation pattern, or in other words, the deformed shape of the tyre tread section subjected to normal compressive stress from the road surface, is analyzed in an attempt to identify the displacement component responsible for the tyre wear. In this chapter, the solution of the tread contact problem is obtained considering frictionless slipping of the tread surface in contact, i.e., the tread contact plane will be allowed to deform both normally and laterally. Here, it is allowed to deform both normally and laterally. However it will experience no frictional force (i.e., stress) from the road that will tend to oppose the displacement in the lateral direction. It is important to mention here that, in the present study of wear, the deformation pattern of the tread sections for the case of frictionless slipping gives the basis for analyzing the wear of tyre treads.

5.2 Numerical Modeling and the Solution

First, attempt is made to solve the tyre tread stress problem in terms of the normal uniform pressure at the contact boundary. The normal loading at the contact boundary is considered as the uniformly distributed normal compressive stress from the road surface, which just balances the internal tyre inflation pressure. The relevant boundary conditions which have been satisfied by the different segments of the tyre tread section are illustrated in

Table 5.1. Since the tread section of a truck tyre is considered here, the inflation pressure inside the tyre is likewise assumed to be 690 kPa. Table 5.2 illustrates the scheme for treating the corner boundary points, which are, in general, the points of singularity. For example, the corner points of the contact boundary share the conditions of boundary in contact and of a free boundary, simultaneously. Figure 5.1 shows the deformed shape of the tyre tread section obtained satisfying the conditions mentioned above.

From the result it is seen that the normal displacement, u_y is not constant over the whole contact boundary of the tread section, rather, the displacement is lower in the corner regions of the boundary, which ultimately leads to an impractical deformation pattern of the tread section. In an attempt to get rid of the problem, a large number of trial and error have been made and finally it has been observed that the problem can be eliminated if the applied normal pressure on the contact boundary can be replaced by its equivalent normal displacement. The boundary conditions of the corner mesh points are satisfied in accordance with those shown in Tables 5.3 and 5.4. The deformed shape of the same tyre tread section obtained by satisfying the conditions as mentioned in Tables 5.3 and 5.4, is shown in Fig 5.2. As appears from the figure, it satisfies almost all the physical requirements and also, the overall accuracy of the solution is found better than that obtained with the applied normal stress. It has also been verified that the same normal compressive stress is reproduced along the boundary if the problem is solved in terms of its equivalent normal displacement component.

5.3 Influence of Dimensional Parameters (a and b) on the Deformation of the Tread Section

In this Section, the obtained solutions are analyzed mainly in the perspective of the tread aspect ratio. First, the influence of the tread contact length, a is

investigated when skid depth, b is kept constant, and secondly, the influence of the skid depth is investigated keeping length, a constant.

Figure 5.3 describes the influence of skid depth, b on the normal displacement of the tread contact boundary. The result is presented as a function of tread aspect ratio a/b, where b is varied and the contact length a is kept fixed as 8.31 unit. It is seen that with the increase of the skid depth, the normal displacement of the contact boundary increases for the constant normal loading from the road surface. In other words, it can be said that at higher aspect ratio, the rate of change of normal displacement is very low. Since all the problems are solved with the equivalent normal displacement of the contact boundary, instead of using the inflation pressure, it is important to know the equivalent normal displacement corresponding to every aspect ratio of the tread section under the constant inflation pressure. Fig. 5.3 can easily serve the purpose of providing the equivalent normal displacement for various aspect ratios ranging from 0 to 5.5, under different inflation pressure from 517.5 kPa to 828 kPa.

Figure 5.5 illustrates the influence of skid depth, b on the tangential displacement component for contact boundary under the inflation pressure of 690 kPa. In this figure, the distribution of tangential displacement component is plotted along the contact boundary of the tread section for different aspect ratio. In this case, as before, while changing the value of b, a is kept fixed. From the general trend of the curves it is seen that the tangential displacement at both the ends takes the maximum positive and negative values, leaving the central point undisturbed. Another conclusion is that with the increase of aspect ratio, the maximum tangential displacement decreases. In other words, for a constant contact length of the tread section and also for the same inflation pressure of the tyre, increase of skid depth increases the tangential deformation of the tread contact boundary.

Figures 5.6 to 5.8 illustrate the corresponding influence of contact length, a, on the various displacement components obtained for the tread section when the skid depth is kept constant. From Fig 5.6 it is seen that the normal displacement of the contact boundary decreases as the contact length is increased keeping the skid depth constant. The corresponding influence on the deformed shape is illustrated in Fig. 5.7. The influence of length of the contact boundary, a on the tangential displacement is described in Fig. 5.8. Here the contact length a is varied while the skid depth is kept constant. From the figure it is concluded that with the increase of aspect ratio, the tangential displacement is increased. Also the nonlinearity of the distribution of the tangential displacement component is found to increase with the increase of aspect ratio. Therefore, with the increase of contact length of the tread section, the tangential displacement of the contact boundary increases when the skid depth is kept constant. With the increase of aspect ratio of the tyre tread section, the tangential displacement increases upto a certain limit of aspect ratio, and then the tangential displacement becomes saturated, i.e., no further change in the tangential displacement component is observed with the increase of contact length (aspect ratio). It is the critical value of aspect ratio, which permits maximum tangential displacement under a particular contact pressure. From this analysis it is clear that wear does not occur at middle portion of the contact surface because the middle portion of the contact surface is basically free from tangential displacement under any situation.

5.4 Effect of Normal Contact Pressure (Inflation Pressure) on the Deformation of the Tread Section

In order to investigate the influence of contact pressure on the tyre tread contact boundary, on the individual displacement components and also on the deformed shape, a particular tyre tread section has been analyzed with varying normal contact pressure, (i.e., inflation pressure) ranging from 100 to 900 kPa. Figure 5.9 represents the relation between the normal displacement and

normal contact pressure on the contact boundary for an aspect ratio of 1.51. It is clear from the figure that a linear relationship exists between the normal displacement and contact pressure. That is, with the increase of contact pressure, the normal displacement of the contact boundary increases linearly. Figure 5.10 illustrates the influence on the tangential displacement component; it is seen that the displacement is zero at the middle and it increases as we move towards the corner of the tread, and ultimately maximum tangential displacement occurs at the corners. But these maximum displacements at the two corners are of opposite nature. In general, it is revealed from the figure that the tangential displacement component increases with the increase of inflation pressure inside the tyre. Moreover, the non-linearity of the distribution is observed to increase with the increase of the contact pressure on the tread boundary. The influence of the contact pressure on the overall inflation of the tread section is shown in Figure 5.11. As seen in the figure, the inflation of the tread section increases significantly when the contact pressure is increased. on the contact boundary of the tread section.

Chapter 6

WEAR ANALYSIS OF TYRE TREAD SECTIONS CONSIDERING FRICTIONAL SLIPPING

6.1   Introduction

In this section, the same tyre tread contact problem of chapter 5 is solved taking the frictional slipping of the tread contact surface into account. It has been verified in chapter 5 that when the tread section is subjected to uniform contact pressure/displacemt from the road, the contact boundary tends to slip laterally on the road due to its tangential component of the displacement. If there is no friction between the tyre surface and the road, the magnitude of lateral slipping on the road will be maximum. However, if the frictional slipping is taken into account, the tangential displacement of the contact boundary under the normal compressive stress/displacement from the road, is opposed by the frictional force, that is, stress developed from the road. The frictional stress due to the road surface is a function of normal contact pressure σ_n, and thus, for a constant inflation pressure of the tyre, the frictional stress remains constant for all tyre treads of same material. It should be made clear that this frictional stress may, however, vary for different tyre materials because of the fact that the friction coefficient between the road and different tyre materials is different.

The essential feature of the present method of wear analysis is that, here the mixed boundary value contact problem of tyre tread is solved to obtain the corresponding amount of shearing stress (frictional stress due to the road) which will completely stop the lateral slipping of the tread contact surface

over the road. It is noted here that this shearing stress on the tread contact boundary is a function of skid depth, contact length on the road, inflation pressure and also of the tyre material. After determining the no-slip shearing stress on the contact boundary, it is compared with the frictional stress available from the road.

If the calculated maximum frictional stress for a tread section is found to be equal or lower than that available from the road, then no wear of the tyre tread occurs on that particular tread section. This is because of the fact that the frictional stress available from the road is there just equal or even higher than that required to deform the tread section under the action of normal compressive stress from the road, keeping the contact boundary free from any lateral displacement.

6.2 Solution of Tyre Tread Contact Problem under No-Slip Condition of the Contact Boundary

First, attempt is first made to solve the tyre tread contact problem in terms of normal uniform contact pressure on the contact boundary. The normal loading on the contact boundary is considered as the uniformly distributed compressive stress from the road surface, which is just balancing the tyre inflation pressure. The relevant boundary conditions which on the different segments of the tread sections are given in Table 6.1. Since the tread sections of the truck tyre are considered here, the inflation pressure inside the tyre is likewise assumed to be 690 kPa. Table 6.2 illustrates the scheme for modeling the boundary conditions at the corner points, usually, the points of singularity. For example, the corner points of the contact boundary share the conditions of a loaded boundary and a free boundary. For obtaining accurate results of different stresses which would be developed at the contact surface of the tyre tread, the uniform normal stress acting on the contact boundary can be replaced by its equivalent normal displacement; and the management of the

boundary conditions for the boundary segments and corner points are done in accordance with those shown in Table 6.3 and 6.4, respectively.

Figure 6.1 shows the influence of skid depth, b on the normal displacement of the contact boundary. The result is presented as a function of tread aspect ratio a/b, where b is varied and the contact length a is kept fixed as 8.31 unit. It is seen that with the increase of skid depth, the normal displacement of the contact boundary is increased for the constant normal loading from the road surface. More specifically, it can be said that at higher aspect ratios, the rate of change of the normal displacement is very low. Since all the problems are solved with the equivalent normal displacement of the contact boundary instead of using the direct inflation pressure, it is important to know the equivalent normal displacement corresponding to every aspect ratio of the tread section under different inflation pressures. From Fig. 6.2 normal displacement of the contact surface is found to be uniform along the skid surface. With the decrease of aspect ratio normal displacement of the contact boundary increases. Tangential displacement of the contact surface is zero, which is verified from Fig. 6.2.

Figures 6.3 and 6.4 illustrate the influence of contact length, a on the two displacement components and the overal deformation pattern the tread section when the skid depth, b, is kept constant. From Fig. 6.3, it shows that the normal displacement of the contact boundary decreases as the contact length is increased at constant skid depth. From Fig. 6.4 it is observed that with the increase of contact length, normal displacement of the middle portion of the skid surface decreases. The tread sections are found to be inflated under the action of normal uniform displacement applied at the contact boundary, leaving the contact boundary free from any lateral displacement.

6.3 Analysis of Shearing Stress on the Contact Boundary of the Tread Section

In Figure 2.2, AB is the contact surface of the tread with the road. In order to predict the shearing stress along the contact boundary, the problem is solved in such a fashion that the contact boundary experiences a uniform normal displacement, equivalent to an inflation pressure inside the tyre. Keeping all the boundary conditions of the contact surface of the tread section constant, attempt is made to solve the problem by managing the boundary conditions of the two corner points of the contact boundary in two different ways (case-A and case-B), the corresponding boundary conditions along with their points of application are illustrated in Tables 6.5 and 6.6. These two solutions (case-A&B) show that the obtained stress and displacement components for the whole tread domain are exactly same except at the two corner points of the contact boundary; case-A gives an extremely high value of the shear stress at the corner points while case-B gives zero shearing stress, which is quite likely as these points are in general, the points of stress singularity. Figure 6.5 illustrates the two different solutions of shearing stress along the contact boundary. The solutions differ mainly at the corner points. In order to obtain a justified value of the shear stress at the corner points of the contact boundary, stresses are predicted by extrapolation keeping the slope of the curve near the corner the same. This extrapolated curve along with the two other solutions are presented in Fig 6.5.

Figure 6.6 describes the shear stress distribution along the contact surface of the tyre tread at different aspect ratios, when skid depth, b is varied keeping the contact length same under contact pressure of 690 kPa. At the middle portion of the contact surface, shear stress is completely for all the sizes of treads. Away from the middle portion of the contact surface shear stress increases upto the corner point of the contact surface, and thus maximum shear stresses are developed at the two extreme points on the contact

boundary with equal in magnitudes but opposite in sign for all the tread sections. Figure 6.7 shows the distribution of the shear stress along the contact surface under a contact pressure of 690 kPa when contact length of the tyre tread is varied, keeping the skid depth constant. From the figure, it is clear that when contact length increases, shear stress increases. It is interesting to note that shearing stress at the contact boundary increases up to a certain limit with the increase of contact length, but beyond this value of a , it is found to remain the same, i.e., no change of shearing stress with the increase of a.

6.4 Determination of Optimum Tread Section for Minimum Wear

It is necessary to investigate the maximum shear stress at the contact surface for the analysis of wear of tyre treads. Figure 6.8 shows the relationship between maximum shear stress and aspect ratio under a contact pressure of 690 kPa. For higher aspect ratios, maximum shear stress increases with nearly a linear rate with the decrease of aspect ratio and then remains nearly constant for the lower range of aspect ratio, when the contact length is kept fixed but the skid depth is varied. The magnitude of maximum shear stress even at the very low aspect ratio is less than half of the inflation pressure and at a very high aspect ratio, the contact pressure is more than eight times of maximum shear stress developed at the corner of the contact boundary. Figure 6.9 describes the distribution of coefficient of friction of the contact surface at different aspect ratio under a contact pressure of 690 kPa. Here the calculated coefficient of friction is obtained by dividing the shearing stress developed on the contact surface of the tread by the normal contact pressure. At the middle portion of the contact surface the coefficient of friction is zero which means there would be no friction at the mid point, and beyond the middle portion of the contact surface coefficient of friction increases up to the corner point of the contact surface. When the aspect ratio is increased keeping the contact

length fixed, coefficient of friction decreases. Figure 6.10 shows the relationship between the calculated maximum coefficient of friction and aspect ratio of tyre tread when the size of the tread is kept fixed in tangential direction and that in normal direction is varied. For example, at a very high aspect ratio maximum calculated coefficient friction is found 0.12 and at very low aspect it is 0.33. Figure 6.10 is divided into two regions, such as, wear zone and no wear zone. It is also necessary to investigate the maximum shear stress distribution of the contact surface of the tyre tread at a definite contact pressure when the size of the tyre tread is varied in tangential direction keeping the skid depth constant. Figure 6.11 shows the relationship between maximum shear stress and aspect ratio under a contact pressure of 690 kPa. Maximum shear stress increases nearly at a linear rate and then the rate of increasing maximum shear stress decreases and this rate is zero for higher aspect ratio. Figure 6.12 shows the relationship between maximum coefficient of friction and aspect ratio where the skid depth is kept constant and the size of the tread in tangential direction is varied. When the aspect ratio is increased, the calculated maximum coefficient of friction increases and then the rate decreases to zero with the increase of aspect ratio.

Table 6.7 shows actual coefficient of friction for different kinds of tyre with the road surface at different speed and for different conditions. A value of actual coefficient of friction between the road and the contact surface of truck tyre, for example, 0.28, divides Figs. 6.10 and 6.12 into two zones, such as, wear zone and no wear zone. At this coefficient of friction in Figs. 6.10 and 6.12, a horizontal line is drawn which cuts the curves of Figs. 6.10 and 6.12 separately at a point and the vertical line drawn at this point ultimately divides the curve into wear and no wear zones.. In Fig 6.10 the left portion of the line is identified as wear zone and right part is no wear zone when the size of tyre tread is varied in normal direction, keeping the contact length constant. Figure 6.12 also shows the left portion of curve as no wear zone and right portion as

wear zone, when the size of tyre tread is varied in tangential direction, keeping the skid depth constant. For designing an optimum size of tyre tread any size of the tyre tread from the no wear zone can be taken as a safe one which allows no wear of the tyre tread at any inflation pressure.

6.5 Influence of Inflation Pressure on the Analysis of Wear of Tyre Treads

Figure 6.13 describes the relationship between the normal displacement of the tyre tread contact surface and the contact pressure. From the figure, normal displacement is found to increase linearly with the increase of contact pressure. This relation can be used to determine the corresponding normal displacement of the tread contact surface, subjected to various normal contact pressures. Figure 6.14 shows the deformed shapes of a truck tyre tread of a/b=1.51 under different contact pressures. From the Figure, it is clear that all the treads are inflated under the action of uniform normal displacement on the contact surface, however, as desired, the contact boundary was completely free from the lateral displacement for all the cases considered. Moreover, the inflation of the tread increases with the increase of normal contact pressure. From the distribution of shear stress along the contact surface of the tread section under different contact pressure, as shown in Fig. 6.15, it is seen that at the middle portion of the contact surface shear stress is always zero, no matter what value of normal pressure is used away from the middle portion of the contact surface, the shear stress increases when the contact pressure is increased. Therefore it is said that when contact pressure is increased shear stress distribution along the contact surface increases. For all cases maximum shear stress is less than half of the normal contact pressure. For the analysis of wear of tyre tread, it is very important to know the shear stress distribution along the contact surface. The portion of the contact surface, for which magnitude of shear stress is less than the frictional stress due to coefficient of

friction, wear will not occur at that portion of the tyre tread. Figure 6.16 shows the maximum shear stress obtained for different contact pressure (for the tread of a/b=1.51). As appears from the figure, maximum shear stress increases linearly with the increase of contact pressure. The maximum coefficient of friction obtained from the maximum shearing stress developed at the corners of tread contact boundary is again presented as a function of normal contact pressure in Fig. 6.17. It is seen from the figure, calculated maximum coefficient of friction remains the same when the contact pressure is increased or decreased. Calculated maximum coefficient of friction is thus found to be independent of the normal contact pressure. Since the relationship between the maximum shearing stress and the normal contact pressure is linear (Fig. 6.16), the maximum coefficient of friction, which is basically the slope of the straight line relation, is found to remain constant when analysed in the perspective of normal contact pressure (Fig. 6.17). If the coefficient of friction of the road surface with the tyre tread contact surface is greater or even equal than the calculated maximum coefficient of friction, tyre tread does not wear, because in that case the lateral displacement of the contact surface will not occur even with the increase of contact pressure. However, if the coefficient of friction is lower than the calculated one, the wear of tyre tread increases with the increase of contact pressure because with the increase of normal contact pressure lateral tangential displacement of the contact boundary will be increased, which is responsible for the wear of tyre treads.

Chapter 7

INFLUENCE OF TYRE MATERIAL ON THE PREDICTION OF OPTIMUM TYRE TREAD SECTIONS

7.1 Introduction

This chapter is on the analysis of the influence of tyre material on the determination of optimum tyre tread section for minimum wear. Three different materials, namely, natural rubber, truck tyre rubber and retreaded tyre rubber are considered for the present analysis. All the necessary properties of the three rubber materials have been determined experimentally and presented in Chapter 4. Using these material properties, a number of tyre tread contact problems are solved with an inflation pressure of 690 kPa. Both the problems of frictionless slipping and frictional slipping are considered for better comprehention of the analysis.

7.2 Frictionless Slipping of Tyre Treads of Different Materials

In an attempt to investigate the influence of different tyre materials on the deformation of the tyre tread under uniform contact pressure, three different tyre materials are considered as the tread material, and then solutions are compared with each other. Figure 7.1 shows the relationship between normal displacement and aspect ratio (a/b) of different tyre materials. This relationship is obtained for the direct normal contact pressure of 690 kPa. In this figure, it is seen that the normal displacement increases for all the materials of interest if the skid depth is increased, keeping the contact length constant, for the constant uniform contact pressure. Further, for a given aspect ratio, normal displacement is found to be maximum for natural rubber, minimum for retreading rubber and in-between for truck tyre. At higher

aspect ratio (a>b), the difference in the magnitude of the normal displacement among the three tyre materials is not that high as in the case of low aspect ratio. From this figure, it is possible to find the corresponding normal displacement for a particular size of tyre tread for three different tyre materials under a particular contact pressure of 690 kPa . Figure 7.2 shows the original shape and the corresponding deformed shape of tyre tread section (a/b=2.1) of different tyre materials under contact pressure of 690 kPa , considering frictionless sleeping of the tread contact surface. From the figure, it is clear that the inflation of the natural rubber is highest and that of retreading rubber is lowest. Since the material properties of truck tyre lies in between those of natural rubber and retreading tyre, inflation of the truck tyre under the same contact pressure is found in between them. Here it is observed that the bond line of tyre tread in contact with the ply and the interior side boundaries of tyre tread do not displace from it's own position.

Lateral displacement of the contact boundary for the tyre treads are shown in Figure 7.3 as a function of grid points along the contact boundary. The nonlinear distribution of the tangential displacement component conforms to the deformed shapes of the treads (Figure 7.2), as the tangential displacement is highest for the case of natural rubber and lowest for the retreading tyre. The truck tyre remains in between those of natural rubber and retreading rubber. A quantitative analysis of the tangential displacement shows that, maximum tangential displacement for the case of natural rubber is twice than that of the retreading tyre rubber. Since this displacement component is mainly responsible for the tread wear, the present analysis shows that wear due to the lateral slipping will be higher for the same contact pressure if a soft material like natural rubber is used as the tyre tread material and the same will be lower for the present retreading tyre rubber.

7.3 Frictional Slipping of the Treads of Different Materials

For the comparative analysis, firstly, the size of the tyre tread is varied in normal direction keeping the contact length fixed and secondly the size of the tyre tread is varied in tangential direction keeping the skid depth constant. In the present work, the normal displacement of the tyre tread of different tyre materials such as natural rubber, truck tyre and retreading rubber and their deformed shapes under a constant contact pressure of 690 kPa are observed. It is necessary to investigate the shear stress distribution along the contact surface of the tyre tread and then the maximum shear stress and the corresponding maximum coefficient of friction of the contact boundary with the road surface under the same contact pressure of 690 kPa.

Figure 7.4 shows the effect of size on the normal displacement of the contact surface of different tyre materials under the same contact pressure when the dimension of the tyre tread is varied in normal direction keeping the contact length constant. In this figure, the normal displacement is highest for the tyre treads of natural rubber and lowest for retreading tyre rubber and the normal displacement for truck tyre tread remains in between natural rubber and retreading rubber. With the increase of aspect ratio, normal displacement decreases when the dimension of the tyre tread is varied in normal direction. The deformed shape of tyre tread of three different tyre materials are shown in Fig 7.5. It is clear from the figure that tangential displacement of the contact surface is zero for the three different tyre treads. The inflation of the side surfaces is maximum for tyre tread of natural rubber and minimum for retreading rubber and the same for the truck tyre tread remains in between those of natural rubber and retreading rubber.

As is shown in Fig.7.6, for a definite contact pressure of 690 kPa shear stress is zero at the middle portion of the contact surface of the tyre treads (a/b=2.1) and this shear stress increases up to the corner points of the contact boundary

for all the tyre tread of three different tyre materials. Beyond the middle portion of the contact surface, the slope of curve of retreading rubber is lowest and the slope of natural rubber is highest and the slope of truck tyre remains between the two materials. Therefore, it is said that the amount of shear stress developed under no slip condition of the contact surface for natural rubber is maximum and is minimum for retreading tyre tread and the shear stress of truck tyre remains in between the two tyre materials except middle portion of the contact surface. Figure 7.7 describes the effect of tread size on the maximum shear stress developed at the corners of the contact surface of tyre tread of three different tyre materials under a uniform contact pressure of 690 kPa, where the horizontal dimension, a is kept constant. From the variation of the stresses it is revealed that, with the decrease of aspect ratio, maximum shear stress for all the three different tyre tread contact surfaces increase linearly up to a certain limit and then become nearly constant. From this relationship, it is clear that the maximum shear stress for a particular aspect ratio is highest for the tyre tread of natural rubber and lowest for retreading tyre tread. Results of Fig.7.7 is again represented in a more useful form in Fig.7.8, which shows the maximum coefficient of friction required to ensure the no slip condition of the contact surfaces as a function of aspect ratio. From this relationship, it is clear that maximum coefficient of friction is highest for tyre tread of natural rubber and is lowest for the tyre tread of retreading rubber and that for the truck tyre remains in between the two materials. If a horizontal line corresponding to the available coefficient of friction (for example, 0.28 in Fig.7.8) for the tyres is drawn, it will intersect three curves for three different materials at three points. The corresponding aspect ratios of the tread section of the point of intersections are considered as the optimum tread section, and the values higher than the optimum one will experience no wear due to lateral slipping over the road.

Figure 7.9 describes the variation of normal displacement of the tyre treads of different tyre materials under a uniform contact pressure of 690 kPa, with respect to tread aspect ratio where the skid depth is kept fixed. From this figure, it is observed that the normal displacement for a particular aspect ratio is highest for natural rubber and is lowest for retreading rubber and the normal displacement of truck tyre tread lies between other two. Figure 7.10 shows the relationship between maximum shearing stress and aspect ratio under the uniform contact pressure 690 kPa when the length of the contact boundary is varied. Figure 7.11 describes the corresponding relationship of Fig. 7.8, i.e., the relationship between the maximum coefficient of friction and the tread aspect ratio, where the length of the contact boundary is varied while the skid depth is kept constant. It is seen that maximum coefficient of friction of tyre tread of any size is highest for the tyre tread of natural rubber and lowest for the tyre tread of retreading tyre rubber with truck tyre tread between the two. This analysis is of great importance for the selection of tyre material, which will minimize the wearing effect of the tyres due to the lateral slipping of the tread surface on the road. It is possible to design the appropriate size of tyre tread of different tyre materials by comparing the available coefficient of friction of the road with the calculated maximum coefficient of friction. For removing or minimizing the wearing effect of tyre tread the available coefficient of friction should be greater or equal to the maximum coefficient of friction obtained for tyre treads of different tyre materials. If the available coefficient of friction of the road is found to be close to the maximum calculated coefficient of friction with the variation of size and material of tyre tread, wearing effect of tyre tread can be removed.

Chapter 8

STRESS ANALYSIS OF TYRE TREAD SECTIONS

8.1 Introduction

In this chapter, attempt is made to investigate the state of stresses, especially at the bond line region of the tyre. Bond line is situated between the tread and ply of tyre. Life of tyre depends on the strength of the bond line material. Bond line is defined by an imaginary line which separates the tyre tread from the tyre plies. For the case of weak bonding of tyre tread with the ply, tyre tread and ply may separate from each other due to the developed shear stress at the bond line region. In the present analysis, contact portion of the tyre tread is assumed to be loaded with a uniform normal displacement which is corresponds to an inflation pressure inside the tyre. Firstly, the bond line stresses are obtained for various inflation / contact pressures. Further, for a particular contact pressure, the variation of stresses is investigated at the bond line for various sizes of the tyre tread. Besides, the stresses in the whole tread domain are analysed through stress contours. The normal and tangential displacement at different sections of tyre tread are obtained under a particular contact pressures. From this analysis, the critical region of stress concentrations is identified. Retreading is basically the process of making the old tyre into new one by attaching new tyre tread by the process of vulcanizing. For improving the life of retreading tyre, it is necessary to investigate the bond line stress. The stress distribution of the whole field of tyre tread has been observed by different contour plots which indicates stress concentration at different sections of tyre tread.

8.2 Stresses at the Bond Line Region of the Tread for Various Contact Pressures

Figure 8.1 shows the relationship of normal stress σ_x along x-direction for different contact pressure. From this relationship, it is clear that at the middle portion of the contact surface, this stress is maximum for any contact pressure. Beyond the middle portion of the contact surface, this stress decreases gradually and tends to about zero at the bond line region of tyre tread. With the increasing contact pressure, this stress increases in all grid positions. From this relation, maximum stress is less than half of each contact pressure. Figure 8.2 presents the relationship of normal stress σ_y in the y-direction with grid position at various contact pressures. The shape of curves is similar to Fig. 8.2. Maximum stress is seen in this figure at the middle portion of the bond line region and minimum stress is seen at last portion of the bond line. Maximum bond line stress is very close to the normal contact pressure. At low pressure the rate of change of stress distribution is very low.

Figure 8.3 describes the distribution of another relationship between shear stress as a function of grid position in the x-direction different contact pressure. At the middle portion of the bond line contact surface, the shear stress is zero and this stress increases towards the curve half-positive and half-negative in the same manner. This shear stress increases up to a certain limit and then decreases. The main reason of failure of tyre tread bond with the ply is the shear stress concentration. With the increase of contact pressure, shear stress increases at the bond line region.

8.3 Stresses at the Bond Line Region of Tyre Treads of Different Sizes

Figure 8.4 illustrates the relationship of normal stress σ_y with the Grid position along x-direction at various sizes of tyre tread. Here, a is kept fixed

and b is varied. At the middle portion of the bond line this stress increases with the increasing aspect ratio (a/b). In this figure stress distribution is seen for three different tyre tread size. Beyond the middle portion of the bond line, this stress decreases up to a certain limit. The rate of decreasing stress remains constant for all the treads.

Shear stress distribution along the bond line section also depends on the size of the tread section, as shown in Fig.8.5. At the middle portion of the contact surface, shear stress remains zero and then increases up to a certain limit and then decreases. After increasing upto a certain limit of tread size, the shear stress increase and remains constant.

Shear stress distribution along the bond line increases with the increasing tread aspect ratio when a is varied and b is kept fixed. This type of stress distribution is seen in Fig.8.6. Shear stress is zero at the middle portion of bond line.

8.4 Stress Distribution in the Whole Tyre Tread Section

Here different kinds of stresses, such as σ_x, σ_y and σ_{xy} for a definite size of tyre tread (a/b=1.51) are studied. In Figure 8.7 normal stress σ_x is shown at different section. At the contact surface, σ_x is same everywhere except at the two corner point. Shape of the curve at the section, y/k=5, is quite different from all other curves in this figure. The magnitude of the stress is almost same for the mid portion of the section but increases towards the inner corner points (H and C, Fig. 8.7.a) and finally decreases to zero at the outer corner point G and D. At sections, y/k = 1 & 9, the nature of the variation is found to be similar. The stress at the bond line (y/k=1) is more than the stress at the section (y/k=9). At the contact surface (y/k=1) the rate of increasing and decreasing stress is slower than section (y/k=9). There is given different sections of a tyre tread in Fig. 8.7.a.

Normal stresses (σ_y) at different sections of a definite size of tyre tread (a/b=1.51) is shown in Figure 8. 8. At the middle portion, normal stress (σ_y) is almost same for all the sections except that of y/k=5.. At the last portion of the skid depth of section (y/k=5) the normal stress (σ_y) concentrates at sharp edge region.

Figure 8.9 illustrates the distribution of shear stress at different section of tyre tread. Shear stress concentrates at the sharp edge of the tyre tread at the section (y/k=5). At the section (y/k=5), the shear stress is zero at the middle portion of the contact surface and then increases at a certain rate up to a certain limit and the maximum shear stress occurs at the sharp edge. Shear stress is zero at the middle portion of each section of tyre tread and then increases positively and negatively. At the bond line of sharp edge the shear stress is maximum and then decreases.

Figure 8.10 is a contour plot (σ_x) for the whole field of tyre tread. In this figure, the stress distribution is observed to be similar in left and right portion of the graph. Stress concentrates at the sharp edge of the tyre tread. Stresses are plotted here as normalised form (σ_x/E). In some regions dimensionless stress is zero. At some region this stress is maximum. From this figure we clearly understand the stress distribution and it's overall concentration in deferent regions of tyre tread.

Figure 8.11 shows the contour plot of the normalised stress in y-direction (σ_y/E). But the stress (σ_y/E) concentrates at the sharp edge but remains almost same for the contact boundary. From this stress contour it is clear that the stress is lower at the skid boundary, and for the interior points the stress is found to be almost same. At the bond line outside the sharp edge (σ_y/E) decreases to zero. Dimensionless shear stress distribution is presented in figure 8.12. The shear stress distribution of the top left and top right is similar

to look at and the shear stress distribution at the bottom left and bottom right is also similar.

8.5 Normal and Tangential Displacements at Different Sections of a Tyre Tread

As appears from figure 8.13, the normal displacement is constant at the contact surface (section=16); the normal displacement is maximum at this section. Beyond the contact surface normal displacement is found to decrease as we move from top to bottom of the tread section. The shape of curves at sections 16,10 and 5 are observed to be similar. The general pattern of curves at section 5 and 3 is similar. Rate of normal displacement with grid points is near about same along the skid depth of sections 5 and 3 and then decreases to zero. The normal displacement is minimum at section 3 among these sections.

It is observed that the tangential displacement is zero at the contact surface of tyre tread in Figure 8.14. At the middle portion of the contact surface tangential displacement is zero for all the sections. With the increase of distance from the contact boundary towards the bond line, tangential displacement gradually decreases. Tangential displacement is half positive and half negative. At sections $y/k=5$ & 3, tangential displacement is zero at the middle portion as well as at the two corner points of tyre tread. At the section $y/k= 5$, tangential displacement increases from the middle portion of the contact to the sharp edge at the same rate and then decreases, increases and decreases to zero. At the section $y/k=3$, tangential displacement increases from the middle portion of the contact surface up to a certain limit at a constant rate and then decreases to zero.

Chapter 9

CONCLUSIONS AND RECOMMENDATIONS

9.1 General

The main purpose of the present research is to investigate the cause of wear of tyre tread at the contact surface under different contact pressure and then to determine the optimum condition for which the wear of tyre will be minimum, through an extensive analysis of the mixed boundary value contact problem of tyre tread. Earlier, the finite element method was the only tool for the analysis of tyre contact problem and eventually a number of authors investigated the stress and strain in tyre section using finite element method. However, no useful study was reported so far in the literature concentrating the wear of tyre treads, which can suggest an optimum section of tyre treads for minimizing the wear. The present thesis is an attempt to remove that limitation in the literature, which provides a useful guideline for improved design and thus improved life of vehecular tyres. The three dimensional problem is considered here as a two-dimensional plane problem. In the present analysis all the necessary material properties of tyre, such as, modulus of elasticity for tension and compression, Poisson's ratio, etc. are obtained by direct experimental method. For the analysis, first, the contact surface of the tyre tread is assumed to be free from frictional force and the corresponding solution of the problem is obtained for the case where the contact boundary of the tread is only subjected to a normal compressive loading from the road surface. Deformation (inflation) patterns are analysed in the perspective of dimensional parameters, loading, materials, etc. Secondly the solution is obtained for the same tyre treads section, loaded normally from the road, by restricting the lateral displacement of the contact boundary. Therefore, from

the resulting distribution of the shearing stress on the contact surface the relationship between the maximum shearing stress on the contact surface of the tyre tread and the aspect ratio has been established under different contact pressures. The relationship between the calculated maximum friction coefficient at the contact surface and aspect ratio are obtained for the analysis of wear of tyre tread contact surface. The maximum shear stress and maximum calculated coefficient of friction are analysed as a function of aspect ratio, where the dimensional parameters are varied in both the normal and lateral direction. From the comparison of the calculated friction coefficient with the friction coefficient available from the road, a suitable tread section is selected, which will minimize or even remove the wear of tyre tread contact surface due to the lateral slipping of the contact surface on the road. In addition to the effects of dimensional parameters, the wear of tyre tread contact surface has been analysed for different tyre materials. Here the property of tyre materials is defined in terms of their elastic modulus and Poisson's ratio. Further, attempt is made to investigate the shear stress distribution along the bond line region near to the ply, which is responsible for the separation of tyre tread from the ply. Shear stress distributions are investigated for varying the size of the tyre tread in both the normal and lateral directions. Attempt is also extended to investigate different kinds of stress distribution at the bond line region. In addition the stress distribution of the whole tyre tread section has been observed for a definite size of tyre tread and thus the critical zones of stress concentration are identified.

9.2 Conclusions

From the present investigation the following important conclusions are made.

(1)   In an attempt to generate useful data for the practical applications, solutions of tyre-treads are obtained here by using the actual material properties of tyre. The modulus of elasticity in tension and compression

of tyre materials are found to be different. Compression modulus of elasticity is used for the present solution. Besides, the Poisson's ratio and other mechanical properties of tyre materials are determined by experiments, which have provided a general comprehension of the materials used for vehicular tyres.

(2) In contrast to the usual method of solution of elasticity, the displacement potential function is used in conjunction with finite difference technique for solve in the present problem of tyre treads. In case of displacement potential formulation, the whole problem is formulated in terms of a single function, defined in terms of displacement components. Therefore the computational effort is drastically reduced when compared to the conventional finite element method of solution where two variables are evaluated at each node of the two dimensional domain. Therefore the present solution is claimed to be highly accurate and reliable.

(3) The problem was first solved considering frictionless slipping of the tyre tread contact surface. For a constant inflation pressure, lateral or lateral displacement of the contact surface of the tyre tread increases with the increasing of aspect ratio when the contact length is constant. If the available frictional force due to coefficient of friction between the road and the tyre is not enough to stop such lateral displacement of the contact surface with the road, wear of tyre tread will occur.

(4) Then the behaviour of the lateral displacement of the contact surface of the tyre tread is analysed for different contact length of the tread, keeping the skid depth constant. When the size of the tyre tread is increased in lateral direction, lateral displacement of the contact surface of the tyre treads increases. Similarly if the lateral displacement of the contact surface of the tyre tread is decreased by varying the size in

lateral direction, wear of the contact surface of the tyre tread will be decreased or removed.

(5) For a particular aspect ratio, the lateral displacement at the contact surface increases when the inflation pressure is increased. So it may be realised that maximum wear occurs at higher contact pressures.

(6) Secondly, the problem is solved for the case of frictional slipping of tread at the contact boundary, where it is assumed that the available friction from the road surface is such that it will allow no displacement of the contact boundary in the lateral direction. In this analysis, the distribution of the shear stress on the contact surface is obtained for different aspect ratio where the contact length of the tread is kept fixed. For the portion of the contact boundary, where the available frictional force from the road surface is greater than that obtained from the calculation, wear will not occur, however, there will be wear if the available frictional force is lower than the calculated one. Extent of wear depends on the difference between the magnitude of shearing stress developed on the contact surface and the available frictional stress from the road on the tyre tread. In general, it can be said that if the maximum calculated coefficient of friction is less than the coefficient of friction available from the road with the tyre tread, wearing of tread surface due to lateral slipping will not occur.

(7) The shear stress distribution along the contact surface is investigated as a function of aspect ratio, where the contact length is varied keeping the skid depth constant. At the middle portion of the contact surface for any given size shear stress is zero. So there is no wear at the middle of the contact length. If the calculated maximum shear stress or maximum calculated coefficient of friction is less than the available frictional force or coefficient of friction respectively, tyre tread contact surface does not

allow wear of tyre tread contact surface due to lateral slipping. By varying the size a of the tyre tread, it is possible to design optimum size of tyre tread which removes the wears of tyre tread contact surface.

(8) It has been verified that with the increase of inflation pressure, maximum shear stress increases but maximum calculated coefficient of friction remains the same. If the available coefficient of friction from the road surface is greater than the maximum calculated coefficient of friction, tyre tread contact surface will not experience any wear with the increase of contact pressure, as with the increase of contact pressure, the available frictional stress will be increased. If the coefficient of friction of the road with the tyre tread is less than the maximum calculated coefficient of friction, the wear of tyre tread contact surface increases with the increase of contact pressure.

(9) In an attempt to investigate the influence of tyre material on the analysis, solutions are obtained for different materials of interest. At a definite contact pressure and with a definite size of tyre tread, the lateral displacement of the contact surface of the tyre tread of natural rubber is maximum and that of retreading tyre rubber is minimum and the lateral displacement of the contact surface of the truck tyre remains between them. If the available lateral frictional force from the road surface is not enough to restrict the lateral displacement of the contact boundary, wear will be higher for the case of softer tyre material, like natural rubber, and will be lower for the relatively harder material, like retreaded rubber.

(10) The shear stress distribution at the bond line region with the ply is important factor for attaching the tyre tread with the ply. For a definite size middle portion of the tyre tread bond line shear stress is zero. At the bond line of the tyre tread with the ply along the sharp edge, shear stress is maximum, and this maximum shear stress increases with the increase

of contact pressure. With the decrease of aspect ratio, shear stress increases at that portion. Bond line failure may be occurred for the concentration of shear stress at this region.

(11) The stress distribution for the whole field of tyre tread section is also investigated. It is observed that and maximum normal stress in x-direction, maximum normal stress in y-direction and maximum shear stress concentrates at the sharp edge region of the tyre tread which identifies the sharp edge regions of the tyre tread section to be critical.

(12) Besides, maximum shear stress concentrates at the outer portion of the contact surface. Shear stress is zero at the mid vertical portion of the tyre tread from the bond line to contact surface and from the middle portion of one skid surface to another skid surface.

9.3 Recommendation for Future Investigation

For improving the life of tyre it is necessary to investigate the wear of shoulder regions of tyre tread. Besides it is necessary to investigate the stress and strain in rubber ply region thoroughly, where two materials are used one is rubber and other is cotton. The following recommendations are however made as the future research guide.

(1) It has been observed in our present analysis that the corner points of the tread section are the points of singularity and the solution of the tyre tread contact problem is sensitive to the boundary conditions of the points of singularity. Attention should be given to incorporate an improved treatment for the boundary conditions for the points of singularity. These singularities are encountered in combining the different groups of boundary equations coming from two different boundaries. One appropriate method of treating these singularities would

be to assume some series of ψ satisfying the local conditions, and then to use these series in truncated from for the evaluation of the functions at these points instead of using the finite difference expressions.

(2) In the present research, the wearing effect of tyre tread at the shoulder region has not been analysed. Since the shoulder region is considered as the critical in terms of wear, the present solution scheme should be extended to the analysis of wear of the contact surface of shoulder tread region of tyres.

(3) The stress analysis for the tyre tread contact problem has been performed for the condition of no-slip over the road surface. Attempt should be made to extent the stress analysis scheme to another cases of interest, for example, frictional slipping of the tread surface over the road. Further, since, the geometry of the shoulder treads has more discontinuity than the central treads, analysis of stress concentrations for the shoulder tread sections would be very interesting for the researches in the field of tyre science and technology.

(4) Attempt can be made to perform the similar analysis experimentally in the laboratory by measuring the deformation and strains for the loaded tyre blocks. Then the results obtained from the experimental results can be compared with those obtained by our present numerical method of solution.

REFERENCES

1. F. Tabaddor and J.R. Stafford, Some aspects of rubber composite finite element analysis. Computers & Structures, Vol. 21, pp. 327-339 (1985)

2. H. Huh. and Y. K. Kwak, Finite element stress analysis of the reinforced Tire contact problem. Department of mechanical Engineering, Korea Institute of Technology, Taejon, pp. 305-701, Korea.

3. Wang, T.M., Daniel, I.M, and Huang, K. Stress Analysis of Tire sections, Tire Science and Technology, Vol.24, No.4 pp. 349-366 (1996)

4. H. Rothert and R. Gall, On the three-dimensional computation of steel-belted tires. Tire Science and Technology, Vol. 14, pp. 116-124 (1986).

5. F. Tabaddor and S. K. Clark. Viscoelastic loss characteristics of cord-rubber composites, Proc. Fourth international conference on vehicle structural mechanics, pp. 233-240 (1981)

6. F. Tabaddor and J. R. Stafford, Nonlinear vibration of cord-reinforced composite shells. Computers & Structures, Vol. 13, pp. 737-743 (1981)

7. J. R. Stafford and F. Tabaddor, Load updating for pressurized structures. Nonlinear Finite element analysis and ADINA conference, MIT, Cambridge, MA, August (1979).

8. M. Durand and E. Jankovich, Nonapplicapability of linear finite element programs to stress analysis of tires. NASA Users' Colloquium, Langely Research center, Hampton. VA. pp. 11-12 (1972).

9. E. Jankovich and M. Durand, Comparative tire stress analysis study by ASKA, NASTRAN, and TITUS. NASTRAN Users' Forum, (1974).

10. M. J. Trinko. ply and rubber stresses and contact forces for a loaded tire. Tire Sci.Technol, Vol. 11, pp.20-37 (1983).

11. H. Rothert and W. Idelberger, on the contact problem for tires including friction, institute for structural analysis. University of Hannover, Germany (1984).

12. R. A. Ridha, Computation of Stresses, Strains and deformations of tires. Rubb. chem. Technol. Vol.53, pp. 849-902 (1980).

13. L. K. Nordell and Z. P. Ciozda, Transient and belt stresses during starting and stopping, Elastic response simulation by finite element methods. Bulk Solids Handling 4, pp.92-98 (1984).

14. H. Ballhaus, Stress and wear of conveyer belts by loading point impact. Bulk solid Handling 3, pp.177-184 (1983).

15. J. R. Stafford, Computer aided design of tires. Winter meeting, Akron rubber group, ACS. Akron. OH, January (1983).

16. P. S. Shoemaker, Tire engineering by finite element modeling. International congress and Exposition, Paper No. 840065, Detroit, MI (1984).

17. R. C. Bara, M. Levinson and Betz, Rubber covered rolls-thermoviscoelastic problem. A finite element solution. Int J. Numerical Methods in Engineering, Vol. 11, p. 671 (1970).

18. C. N. Bapat and R. C. Batra, Finte plain strain deformations of nonlinear viscoelastic rubber covered rolls. Int. J. Numer. Meth.Engng.

19. J. Padovan and I. Zeid, On the development of travelling load finte elements.

20. I. Zeid J. Padovan, Finite element modling of rolling contact,. Computers & Structures, Vol. 14, pp. 163-170 (1981).

21. J. Padavan , S. Tovichakchaikul and I. Zeid, Finite element analysis of steadily moving contact fields, Computers & Structures, Vol. 18, p. 191 (1984).

22. T. J. R. Hughes, R. L. Taylor, J. L. Sackman, A Curnier and W. Kanoknukulchai, Finite element formulation and solution of a class of contact-impact problems in continuum mechanics. Trans. 3rd Int. Conf. On Structural Mech. in reaction Technology, Paper no. J5/5, London (1975).

23. J. Padovan, S. Tovichakchaikul and I. Zeid, Finite element analysis of steadily moving contact fields, Computers & Structures, Vol. 18, p.191 (1984).

24. J. Padovan and O. Paramadilok, Transient and steady state viscoelasic rolling contact, Computers & Structures, Vol. 20, pp. 545-553 (1985).

25. J. Padovan and O. Paramadilok, Generalized solution of time dependent travelling load problem via moving finite element scheme, J. Sound Vibr. Vol.91, p.195 (1983).

26. J. T. Oden and N. Kikuchi, Use of variational methods for the analysis of contact problems in solid mechanics, IUTAM symp. pp.260-264 (1978).

27. S. K. Clark (Ed), Mechanics of Pneumatic tires. U. S. Department of Transport (1981).

28. J. A. Tanner, (Compiler) Tire modeling. NASA CP-2264 (1983).

29. J. D. Walter, Tire stress and Deformation. Mechanics of Pneumatic tires (Edited by S. K. clark), National Bureau of Standards Monograph No. 122, Washington, D. C, pp.406-444. (1971).

30. R. A. Ridha, Computation of stresses, strains and deformations of tires, Rubb. Chem. Technol. Vol.53, pp. 849-902 (1980).

31. R. A. Ridha and S. K. Clark, Tire stress and deformation. Mechanics of Pneumatic tires (Edited by S. K. Clark), U. S. Department of Transportation, National Highway Traffic Safety Adminstration, Washington, D.C. pp. 475-540 (1981).

32. J. R. Beatty, Physical properties of rubber Compounds. Mechanics of Pneumatic tires (Edited by S. K. Clark), U. S. Department of

Transportation, National Highway Traffic Safety Adminstration, Washington, D.C, pp. 871-885 (1981).

33. J. D. Walter, Cord-rubber tire composites: theory and applications. Rubber. Chem. Technol. Vol.51, pp.524-576 (1978).

34. J. D. Walter and H. P. Patel, Approximate expressions for the elastic constants of cord-rubber laminates. Rubb. Chem. Technol. Vol.52, pp. 710-724 (1979).

35. S. K. Clark, Theory of the elastic net applied to cord rubber composites. Rubb.Chem. Technol. Vol.56, pp.372-389 (1983).

36. F. Frank and W. Hofferberth, Mechanics of the Pneumatic tire. Rubb. Chem. Technol. Vol.40, pp.271-322 (1967).

37. R. A. Ridha, Analysis for tire mold design, Tire Sci Technol. Vol. 1, pp.195-210 (1974).

38. H. Kaga, K. Okamoto and Y. Toxawa, Internal stress analysis of the tire under vertical loads using finite element method. Tire Sci Technol. Vol. 5, pp.102-118 (1977).

39. H. K. Brewer, Stresses and deformations in multi-ply aircraft tires subject to inflation pressure loadings. Wright Patterson Air Force Base, Ohio, Techn. Rep. AFFDL-TR-70-62 (1970).

40. A. Kalnins, Analysis of Shells of revolution subjected to symmetrical and non-symmetrical loads. J. Appl. Mech. Vol. 31, pp.223 (1964).

41. K. J. Bathe and A. Chaudhary, On finite element analysis of large deformation frictional contact problems. Unification of Finite Element Methods (Edited by H. Kardestuncer), pp.123-135, North-Holland, Amsterdam (1984).

42. L. T. Campos. J. T. Oden and N. KiKuchi, A numerical analysis of a class of contact problems with friction in elastostatics. Comput. Meth. Appl. Mech. Engng, Vol. 34, pp.821-845 (1982).

43. J. T. Oden, E. B. Becker, T.L. Lin, L. Demkowicz, Formulation and finite element analysis of a general class of rolling contact problems with finite elastic deformations. Mathematics of Finite Elements with Applications, Vol. V, (Edited by J. R. Whiteman), Academic, London (1984).

44. J. T. Oden and E. B. Pires, Numerical analysis of certain contact problems in elasticity with nonclassical friction laws. Computers & Structures, Vol. 16, pp.48-485 (1983).

45. A. K. Noor. C. M. Andersen and J. A. Tanner, Mixed models and Reduction Techniques for large-rotation nonlinear analysis of shells of revolution with application to tires. NASA Technical paper TP-2343 Humpton, VA, October (1984).

46. A. K. Noor and J. A. Tanner, Advances and trends in the development of computational models for tires, Computers & Structures, Vol. 20, pp. 517-533 (1985).

47. Timoshenko, S P & Goodier, J N, Theory of Elasticity, 3rd ed., Newyork, McGraw-Hill Book Company (1970).

48. Uddin, M W, Finite Difference Solution of Two-Dimensional Elastic Problems with Mixed Boundary Conditions, M.Sc. Thesis, Carleton University, Canada (1966).

49. Idris, A. B. M., A New Approach to Solution of Mixed Boundary Value Elastic Problems, M. Sc. Thesis, Department of Mechanical Engineering, Bangladesh University of Engineering and Technology (1993).

50. Ahmed S.R., Numerical Solution of Mixed Boundary Value Elastic Problems, M. Sc. Thesis, Department of Mechanical Engineering, Bangladesh University of Engineering and Technology (1993).

51. Doe J., Jones M.S, Harwood S.A., A new approach to boundary modeling for finite difference applications in solid mechanics, International Journal for Numerical methods in Engineering, Vol. 30, pp. 99-113 (1990).

52. Idris, A.B.M, Ahmed, S.R, Uddin, M.W. Analytical solution of a 2-D elastic problem with mixed boundary conditions, Journal of the Institution of Engineers (Singapore), Vol.36, No.6, pp. 11-17 (1996).

53. Ahmed, S. R., Khan, M.R., Islam, K.M.S. and Uddin, M.W., Analysis of Stresses in deep beams using displacement potential function, Journal of Institution of Engineers (India), Vol. 77, pp.141-147 (1996).

54. Ahmed, S.R., Idris, A.B.M., Uddin, M.W., Numerical Solution of both ends fixed deep beams, Computers and Strucures, Vol.61, No.1, pp. 21-29.(1996).

55. Ahmed, S.R., Khan, M.R., Islam, K.M.S., Uddin, M.W., Investigation of Stresses at the fixed end of deep cantilever beams, Computers and Structures, Vol.69, pp.329-338 (1998).

56. Ahmed, S. R., Idris, A. B. M., Uddin, M.W., An alternative method for numerical Solution of mixed boundary- value elastic problems, Journal of Wave-Material Interaction, Vol.14, No. 1-2, pp. 12-25 (1999)

57. Akanda, M.A.S, Ahmed, S.R., Khan, M.R., Uddin, M.W., A finite difference scheme for mixed boundary-value problems of arbitrary-Shaped elastic bodies, Advances in Engineering Software, Vol. 31, No.3, pp.173-184 (2000)

58. Akanda, M.A.S., Ahmed, S.R., Uddin, M.W., Stress analysis of gear teeth using displacement potential function and finite differences, International Journal for Numerical methods in Engineering, Vol. 53, pp. 1629-1640 (2002).

59. Marks' Standard Handbook for Mechanical Engineers (Tenth Edition) Mcgraw-Hill International Editions, Mechanical Engineering Series, pp-3-24.

APPENDIX A

TABLES

Table 2.1. Requirements for rubber compounds used for different tyre components

Tyre component	Requirements
Tread compound	(a) Abrasion resistance (b) Wet and dry skid resistance (c) Crack growth resistance (d) Low hysteresis
Undertread	(a) Low hysteresis (b) Bond well to the cord-rubber composite making up the carcass or body of the tyre
Sidewall	(a) Good fatigue life (b) Resistance to oxygen and ozone attack (c) Good molding properties
Carcass Coat stock	(a) Good flow properties (b) Good addesion (c) Low hysteresis (d) Good fatigue
Bead Filler and Rubber compounds in the Bead area	(a) High modulus (b) Good adhesion
Innerliner for Tubeless Tyre	(a) Good flex resistance (b) Mold with no imperfections (c) Have low air permeability

Table 4.1 Modulus of elasticity of different kinds of rubbers under compression

Material	Strain range	Specimen number	Modulus of elasticity (kPa)	Average modulus of elasticity, E (kPa)
Truck tyre	Low (0-0.21)	1	6581.529	7030.827
		2	7032.789	
		3	7478.163	
	Medium (0.228-0.38)	1	7197.597	10101.357
		2	11252.07	
		3	11853.423	
	High (0.41-0.51)	1	27336.546	31654.908
		2	36287.190	
		3	31341.969	
Retreading tyre	Low (0-0.15)	1	8343.405	8855.487
		2	9367.569	
	Medium (0.15-0.32)	1	12264.462	11877.948
		2	11491.434	
	High (0.32-0.47)	1	46788.795	37183.824
		2	27578.853	
Natural rubber	Low (0-0.17)	1	5263.065	4853.988
		2	4444.911	
	Medium (0.17-0.41)	1	7515.441	6833.646
		2	6152.832	
	High (0.41-0.52)	1	19501.299	16139.412
		2	12777.525	

Table 4.2   Modulus of elasticity and ultimate strength of different kinds of
rubbers under tension

Material	Strain range	Modulus of Elasticity (kPa)	Ultimate Strength (kPa)	Average modulus of Elasticity (kPa)	Average Ultimate Strength (kPa)
Truck tyre	0-1.3	2869.621	31720.63	2547.755	27742.185
	0-1.2	2225.889	23763.74		
Retreading tyre	0-1.05	3165.687	12241.51	3603.998	12342.942
	0-1.01	3935.379	12555.43		
	0-1.05	3710.927	12241.51		
Neoprene rubber	0.0-0.55	2239.329	7283.827	2192.0445	6741.432
	0.0-0.43	2144.662	6199.626		
Natural rubber	0.0-1.1	11990.17	3086.815	1277.8506	3079.359
	0.0-1.1	1356.625	3071.609		

Table 4.3 Poisson's ratio of different kinds of tread rubbers

Material	Specimen number	Lateral Strain	Longitudinal Strain	Poisson's ratio	Average Poisson's ratio
Truck tyre	1	0.0866	0.2109	0.4105	0.427
	2	0.1118	0.2492	0.4486	
	3	0.0335	0.0768	0.4360	
	4	0.1164	0.2822	0.4126	
Retreading tyre	1	0.1254	0.3160	0.3968	0.39
	2	0.3370	0.8667	0.3889	
	3	0.4359	1.1333	0.3858	
Natural rubber	1	0.0492	0.0982	0.5062	0.50
	2	0.0498	0.0955	0.5120	
	3	0.0444	0.0907	0.4893	

Table 4.4 Hardness number of different kinds of rubbers

Material	Hardness number (Shore –A-Durometer)	Average Hardness Number (Shore-A-Durometer)
Truck tyre	65, 65, 64, 64, 63	64
Retreading tyre	70, 70, 70, 68, 68	70
Neoprene rubber	63, 63, 62, 62, 61	62
Natural rubber	55, 54, 53, 52, 52	53

Table 4.5 Percentage ultimate elongation of different tyre rubbers

Material	Ultimate elongation (%)	Average ultimate elongation (%)
Truck tyre	469.16	452.91
	436.66	
Retreading tyre	306.37	303.19
	300.00	
Neoprene rubber	331.02	330. 51
	330.00	
Natural rubber	267.71	263.86
	260.00	

Table 5.1 Specification of the boundary conditions (contact boundary under uniform normal pressure and free from friction)

Boundary segment	Boundary conditions	Tagging of boundary conditions	
		Mesh point on the physical boundary	Mesh point on the false boundary
AB	σ_n , σ_t	σ_n	σ_t
BC	σ_n , σ_t	σ_n	σ_t
CD	σ_n , σ_t	σ_n	σ_t
DE	u_n , σ_t	u_n	σ_t
EF	u_n , u_t	u_t	u_n
FG	u_n , σ_t	u_n	σ_t
GH	σ_n , σ_t	σ_n	σ_t
AH	σ_n , σ_t	σ_n	σ_t

Fig. A Simplified geometry of the tread Section

Table 5.2 Boundary condition modeling for the corner points of the tread
Section, corresponding to Table 5.1

Corner point	Available boundary condition	Boundary condition at the physical boundary	Boundary condition at the false boundary	Additional boundary condition on the false boundary
A	(σ_n, σ_t), (σ_n, σ_t)	σ_n (AB)	σ_t(top)	σ_t(left)
B	(σ_n, σ_t), (σ_n, σ_t)	σ_n (AB)	σ_t(top)	σ_n(right)
D	(u_n, σ_t), (σ_n, u_t)	u_n (DE)	σ_t(right)	u_t(top)
E	(u_n, u_t), (u_n, σ_t)	u_t (EF)	u_n(bottom)	σ_t(right)
F	(u_n, u_t), (u_n, σ_t)	u_t (GF)	u_n(bottom)	σ_t(left)
G	(u_n, σ_t), (σ_n, u_t)	u_n (GF)	σ_t(left)	u_t(top)

Fig. A Simplified geometry of the tread Section

Table 5.3   Specification of the boundary conditions (contact under uniform normal displacement and free from friction)

Boundary Segment	Boundary conditions	Tagging of boundary conditions	
		Mesh point on the Physical boundary	Mesh point on the false boundary
AB	u_n , σ_t	σ_t	u_n
BC	σ_n , σ_t	σ_t	σ_n
CD	σ_n , σ_t	σ_n	σ_t
DE	u_n , σ_t	u_n	σ_t
EF	u_n , u_t	u_t	u_n
FG	u_n , σ_t	u_n	σ_t
GH	σ_n , σ_t	σ_n	σ_t
AH	σ_n , σ_t	σ_t	σ_n

Fig. A Simplified geometry of the tread Section

Table 5.4   Boundary condition modeling for the corner points of the tread
Section, corresponding to Table 5.3

Corner point	Possible boundary conditions	Boundary conditions at the physical boundary	Boundary conditions at the false boundary	Additional boundary condition on the false boundary
A	(u_n, σ_t), (σ_n, σ_t)	σ_t (AB)	u_n(top)	σ_t(left)
B	(u_n, σ_t), (σ_n, σ_t)	σ_t (AB)	σ_t(right)	σ_n(right)
D	(u_n, σ_t), (σ_n, σ_t)	u_n (DE)	σ_t(right)	σ_n(top)
E	(u_n, u_t), (u_n, σ_t)	u_t (EF)	u_n(bottom)	σ_t(right)
F	(u_n, u_t), (u_n, σ_t)	u_t (EF)	u_n(bottom)	σ_t(left)
G	(u_n, σ_t), (u_n, σ_t)	u_n (GF)	σ_t(left)	σ_n(top)

Fig. A Simplified geometry of the tread Section

Table 6.1   Specification of the boundary conditions (contact boundary under uniform normal pressure and frictional slipping)

Boundary Segment	Boundary conditions	Tagging of boundary conditions	
		Mesh points on the Physical boundary	Mesh points on the false boundary
AB	u_t , σ_n	u_t	σ_n
BC	σ_n , σ_t	σ_n	σ_t
CD	σ_n , σ_t	σ_n	σ_t
DE	u_n , σ_t	u_n	σ_t
EF	u_n , u_t	u_t	u_n
FG	u_n , σ_t	u_n	σ_t
GH	σ_n , σ_t	σ_n	σ_t
AH	σ_n , σ_t	σ_n	σ_t

Fig. A Simplified geometry of the tread Section

Table 6.2 Boundary condition modeling for the corner mesh points of the tread section corresponding to Table 6.1

Corner point	Available boundary conditions	Boundary conditions at the physical boundary	Boundary conditions at the false boundary	Additional boundary condition on the false boundary
A	(u_t, σ_n) (σ_n, σ_t)	u_t (AB)	σ_n(top)	σ_t(left)
B	(u_t, σ_n) (σ_n, σ_t)	u_t (AB)	σ_n(top)	σ_t(right)
D	(u_n, σ_t) (σ_n, σ_t)	u_n (DE)	σ_t(right)	σ_t(top)
E	(u_n, σ_t) (σ_n, σ_t)	u_n (EF)	σ_t(right)	σ_t(bottom)
F	(u_n, σ_t) (σ_n, σ_t)	u_n (EF)	σ_t(left)	σ_t(bottom)
G	(u_n, σ_t) (σ_n, σ_t)	u_n (GF)	σ_t(left)	σ_t(top)

Fig. A Simplified geometry of the tread Section

Table 6.3　Specification of the boundary conditions (contact boundary under uniform normal displacement and frictional slipping)

Boundary Segment	Boundary conditions	Tagging of boundary conditions	
		Mesh points of the Physical boundary	Mesh points of the false boundary
AB	u_n , u_t	u_t	u_n
BC	σ_n , σ_t	σ_n	σ_t
CD	σ_n , σ_t	σ_n	σ_t
DE	u_n , σ_t	u_n	σ_t
EF	u_n , u_t	u_t	u_n
FG	u_n , σ_t	u_n	σ_t
GH	σ_n , σ_t	σ_n	σ_t
AH	σ_n , σ_t	σ_n	σ_t

Fig. A　Simplified geometry of the tread Section

Table 6.4 Boundary condition modeling for the corner points of the tread
section corresponding to Table 6.3

Corner point	Possible boundary conditions	Boundary conditions at the physical boundary	Boundary conditions at the false boundary	Additional boundary condition on the false boundary
A	(u_n, u_t) (σ_n, u_t)	u_t (AB)	u_n(top)	σ_n(left)
B	(u_n, u_t) (σ_n, u_t)	u_t (AB)	u_n(top)	σ_n(right)
D	(u_n, σ_t) (σ_n, σ_t)	u_n (DE)	σ_t(right)	σ_n(top)
E	(u_n, σ_t) (σ_n, σ_t)	u_n (EF)	σ_t(right)	σ_t(bottom)
F	(u_n, σ_t) (σ_n, σ_t)	u_n (EF)	σ_t(left)	σ_t(bottom)
G	(u_n, σ_t) (σ_n, σ_t)	u_n (GF)	σ_t(left)	σ_t(top)

Fig. A Simplified geometry of the tread Section

Table 6.5   Boundary condition modeling for the solution of Case-A in Fig.
6.5

Corner point	Possible boundary conditions	Boundary condition at the physical boundary	Boundary condition at the false boundary	Additional boundary condition on the false boundary
A	(u_n, u_t) (σ_n, u_t)	u_t (AB)	u_n(top)	σ_n(left)
B	(u_n, u_t) (σ_n, u_t)	u_t (AB)	u_n(top)	σ_n(right)
D	(u_n, σ_t) (σ_n, σ_t)	u_n (DE)	σ_t(right)	σ_n(top)
E	(u_n, σ_t) (σ_n, σ_t)	u_n (EF)	σ_t(right)	σ_t(bottom)
F	(u_n, σ_t) (σ_n, σ_t)	u_n (EF)	σ_t(left)	σ_t(bottom)
G	(u_n, σ_t) (σ_n, σ_t)	u_n (GF)	σ_t(left)	σ_t(top)

Fig. A Simplified geometry of the tread Section

Table 6.6 Boundary condition modeling for the solution of case-B in Fig.6.5

Corner point*	Possible boundary conditions	Boundary condition at the physical boundary	Boundary condition at the false boundary	Additional boundary condition on the false boundary
A	(u_n, u_t) (σ_n, u_t)	u_t (AB)	u_n(top)	σ_t(left)
B	(u_n, u_t) (σ_n, u_t)	u_t (AB)	u_n(top)	σ_t(right)
D	(u_n, σ_t) (σ_n, σ_t)	u_n (DE)	σ_t(right)	σ_n(top)
E	(u_n, σ_t) (σ_n, σ_t)	u_n (EF)	σ_t(right)	σ_t(bottom)
F	(u_n, σ_t) (σ_n, σ_t)	u_n (EF)	σ_t(left)	σ_t(bottom)
G	(u_n, σ_t) (σ_n, σ_t)	u_n (GF)	σ_t(left)	σ_t(top)

Fig. A Simplified geometry of the tread Section

Table 6.7   Coefficient of friction by the tests of **The Goodrich Company** on
wet pavement with tires of different treads (Ref.[59])

	Coefficient of friction			
	Static (before slipping)		Sliding (after slipping)	
Speed mile/hr	5	30	5	30
Smooth tyre	0.49	0.28	0.43	0.26
Circumferential groove	0.58	0.42	0.52	0.36
Angular grooves at 60^0	0.75	0.55	0.70	0.39
Angular grooves at 45^0	0.77	0.55	0.68	0.44

APPENDIX B

FIGURES
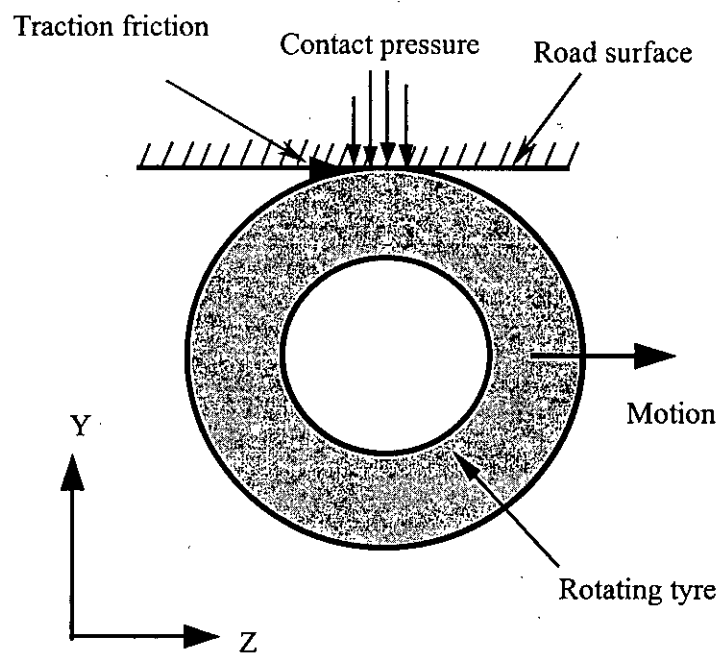
Fig. 1.1(a) Direction of motion of tyre with traction friction on tyre treads
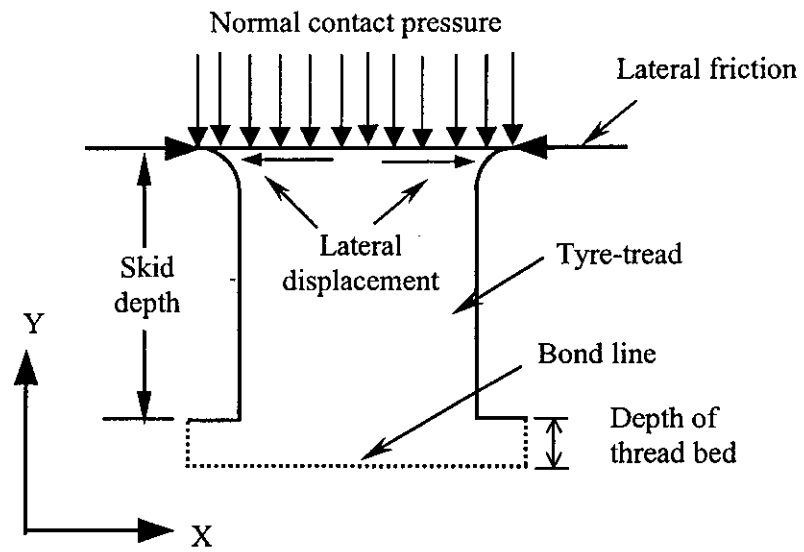
(b) Lateral friction on tyre treads opposing slippage
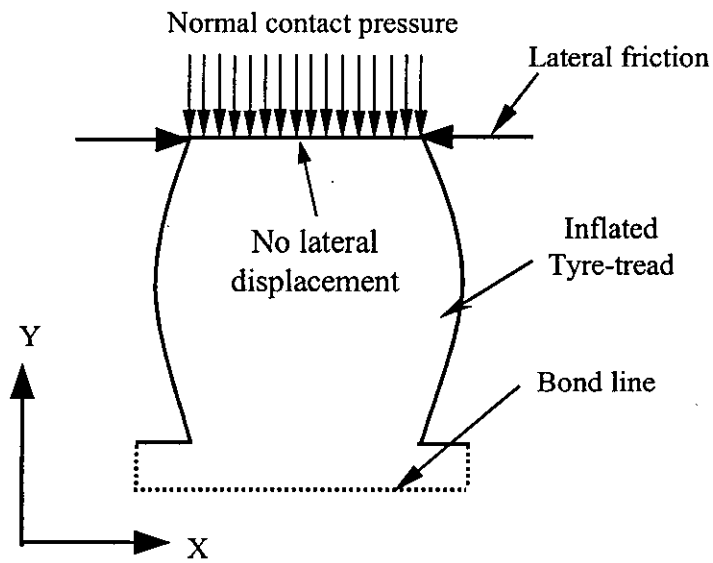
(c) No-slip condition of the tyre tread contact boundary

Figure 1.1   Direction of motion and the corresponding frictional forces on
the tyre tread
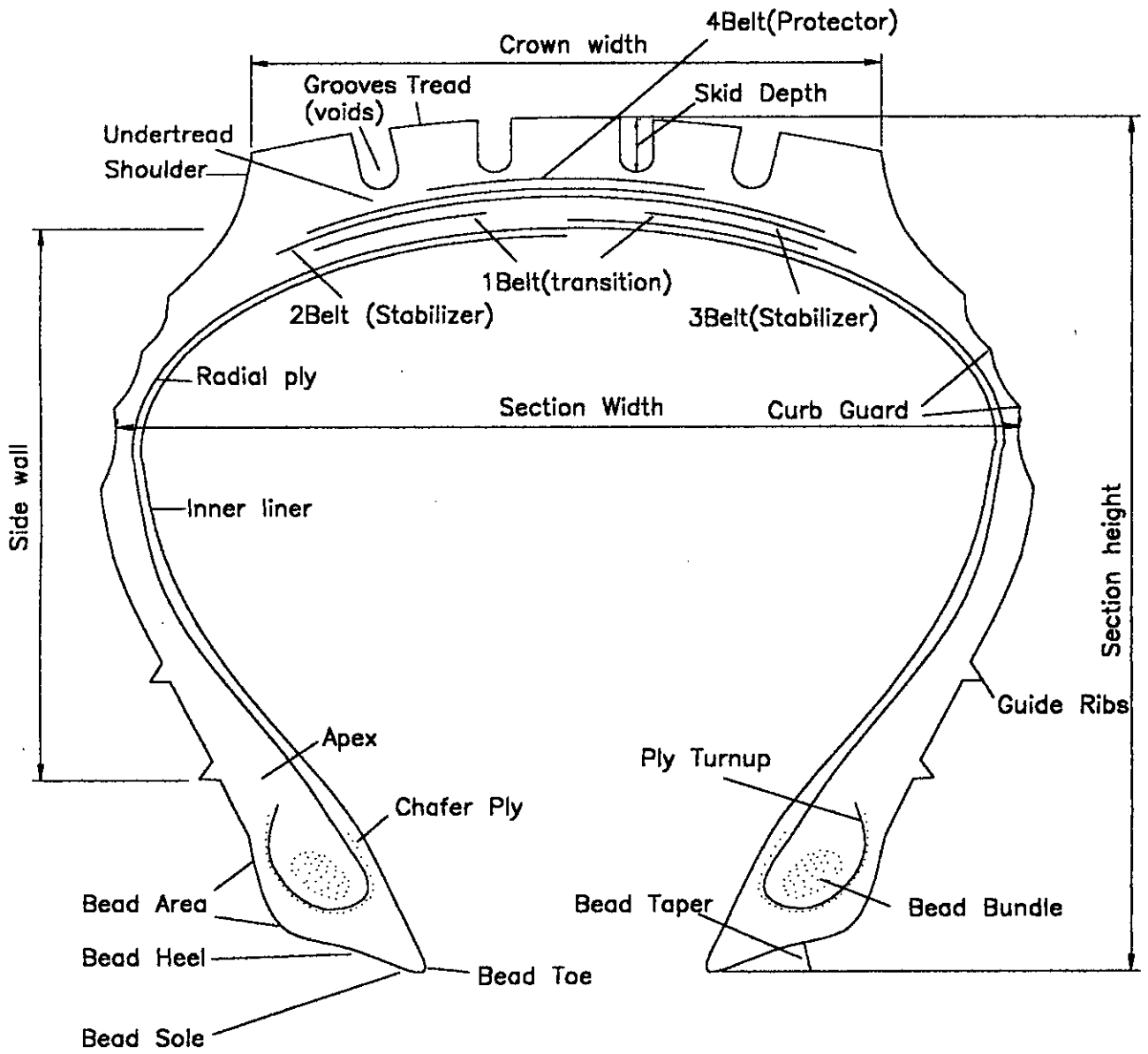
Figure 2.1 Typical Tyre Cross-Section
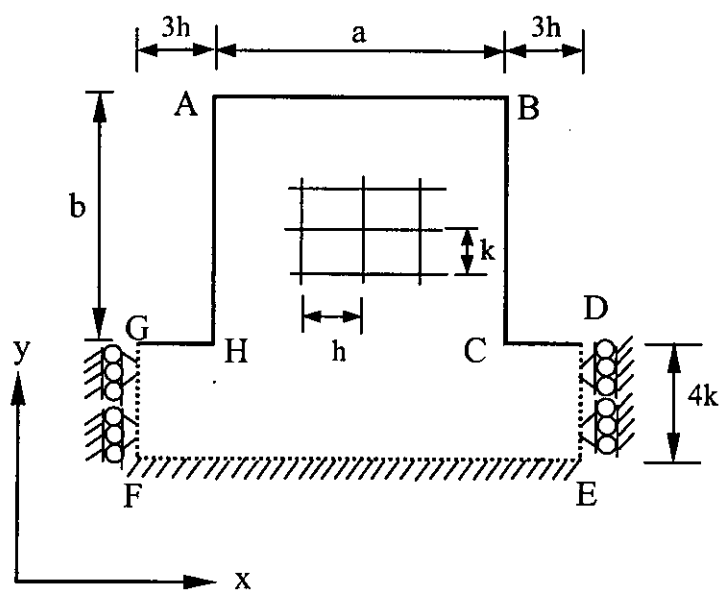
Figure 2. 2 Geometry of the tread section to be considered for the present analysis
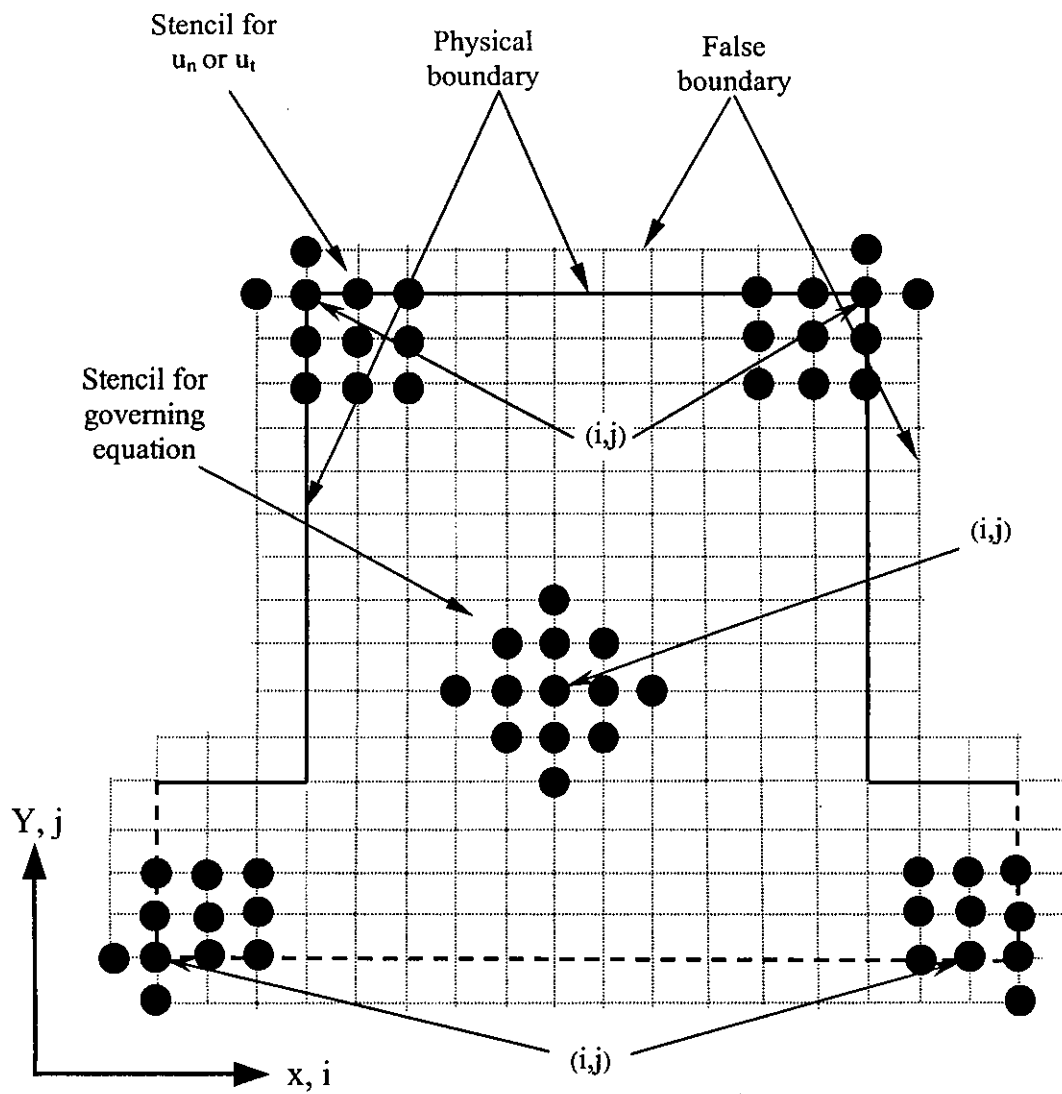
Figure 3.1 Application of the Stencils for the displacement boundary conditions at different corners of the tread section
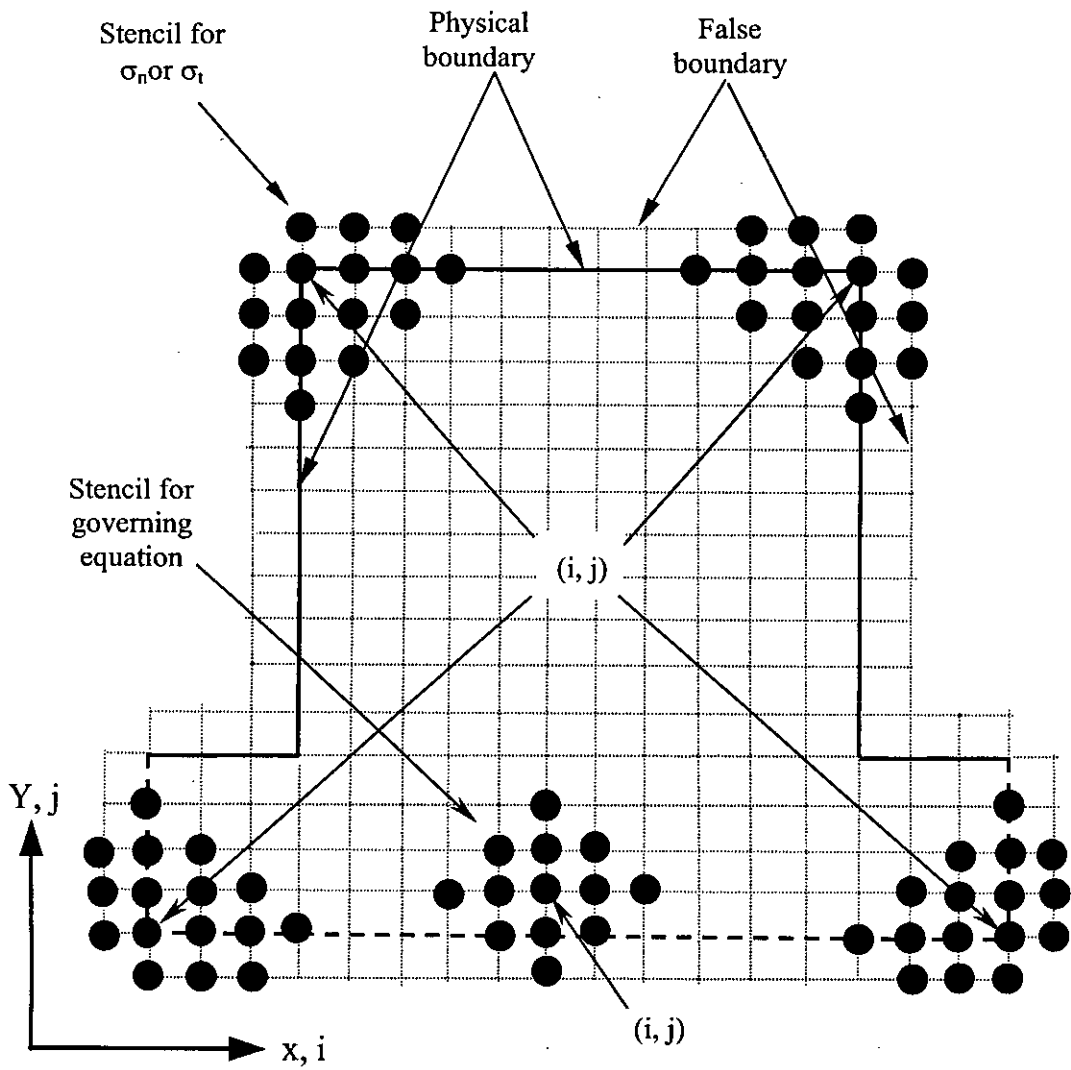
Figure 3.2 Application of the stencils for the stress boundary conditions at different corners of the tread section
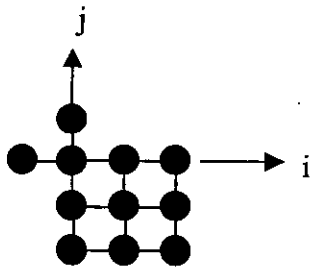
(a) Stencil for top
left boundary
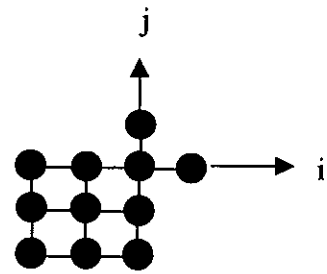
(b) Stencil for top
right boundary
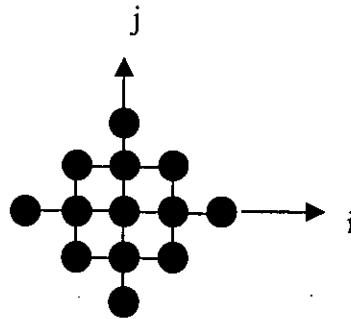
(c) Stencil for governing equation
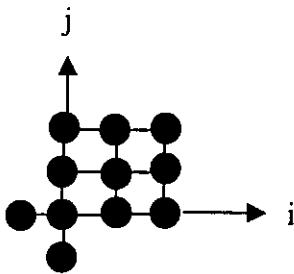
(d) Stencil for bottom
left boundary
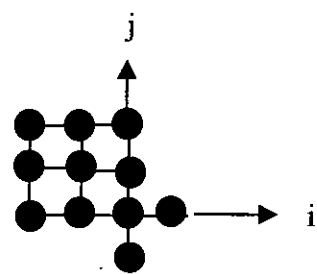
(e) Stencil for bottom
right boundary

Figure 3.3 Different stencils for normal and tangential components of
displacement and governing equation
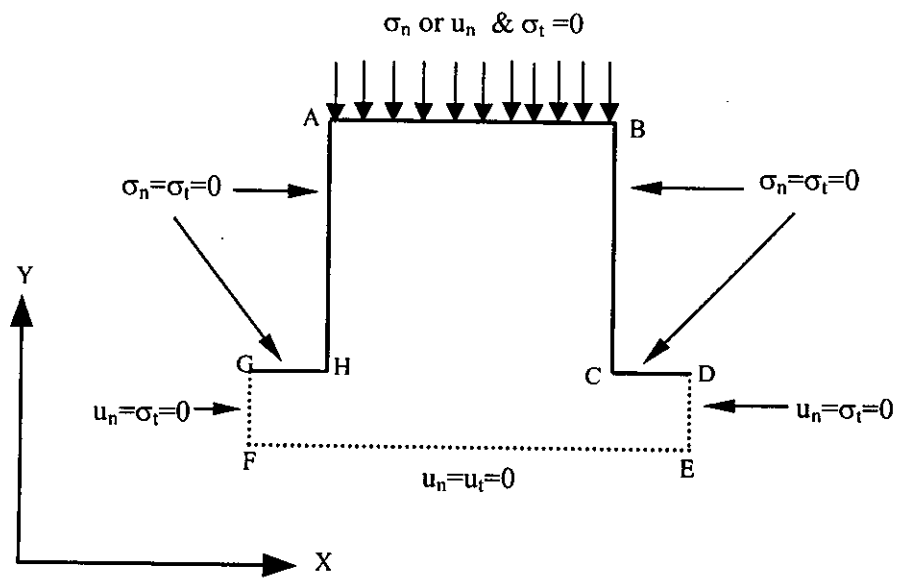
Figure 3.4 Boundary conditions for Tyre tread section neglecting frictional effect on the contact boundary
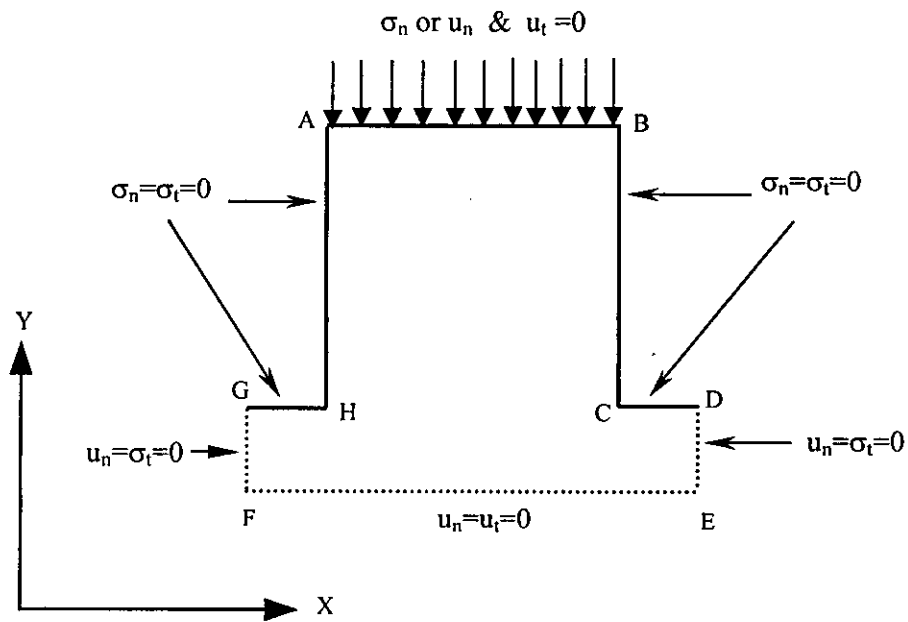
Figure 3.5 Boundary conditions for the tyre tread section simulating the no-slip condition of the contact boundary
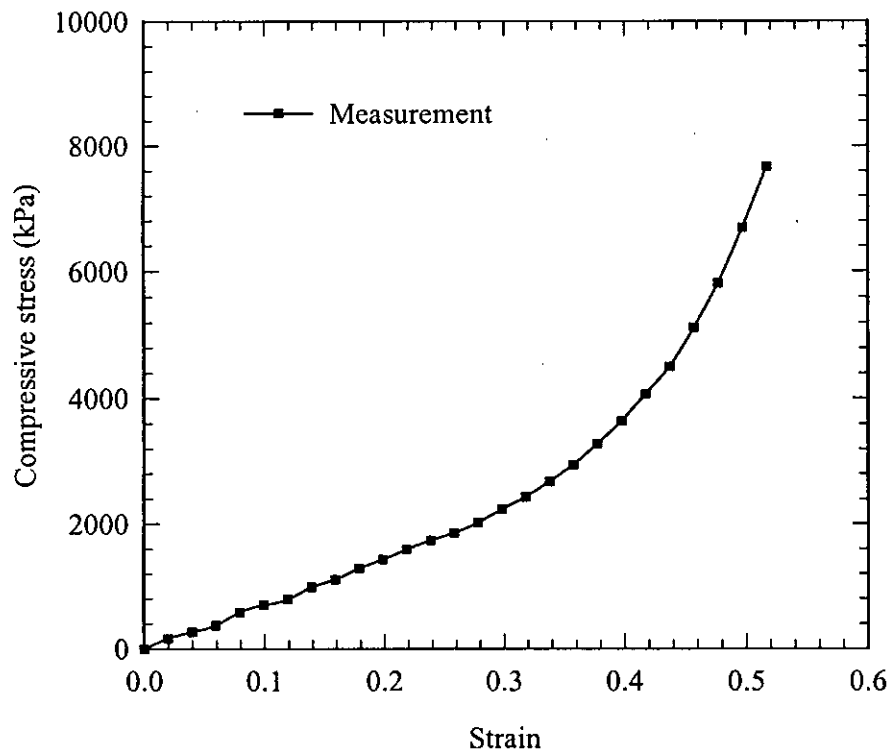
Figure 4.1(a) Measured stress-strain relationship for truck tyre rubber under compression
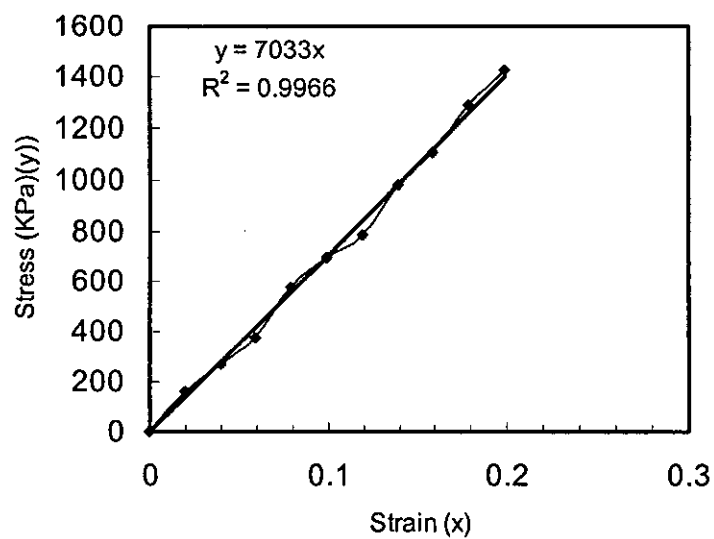
Figure 4.1 (b) Determination of elastic modulus of truck tyre rubber under compression
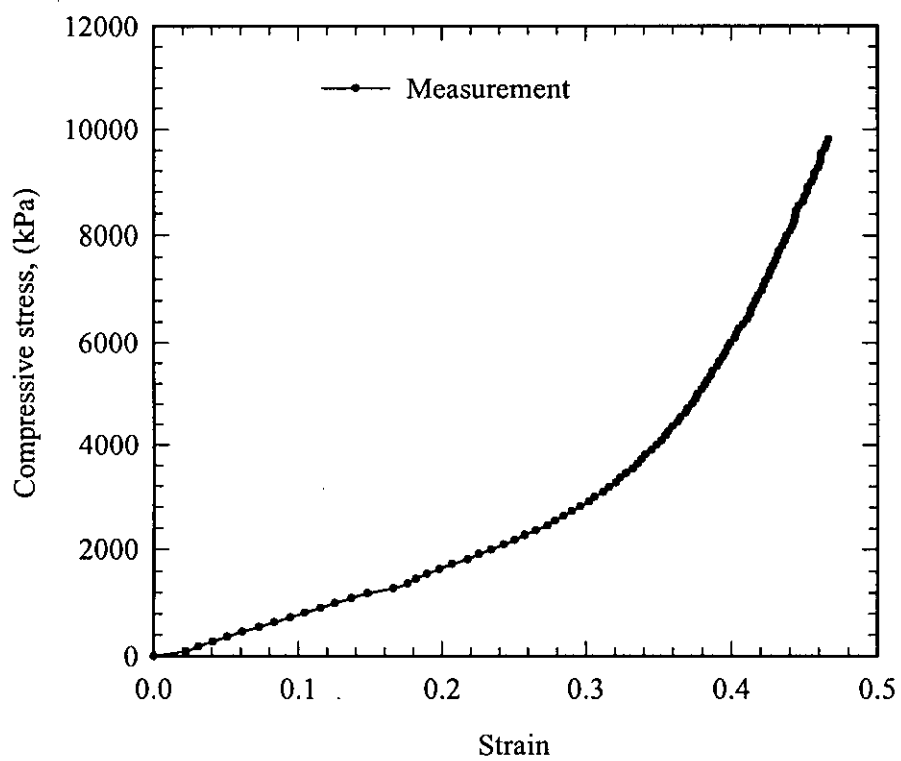
Figure 4.2 Measured stress-strain relationship for retreading tyre rubber under compression
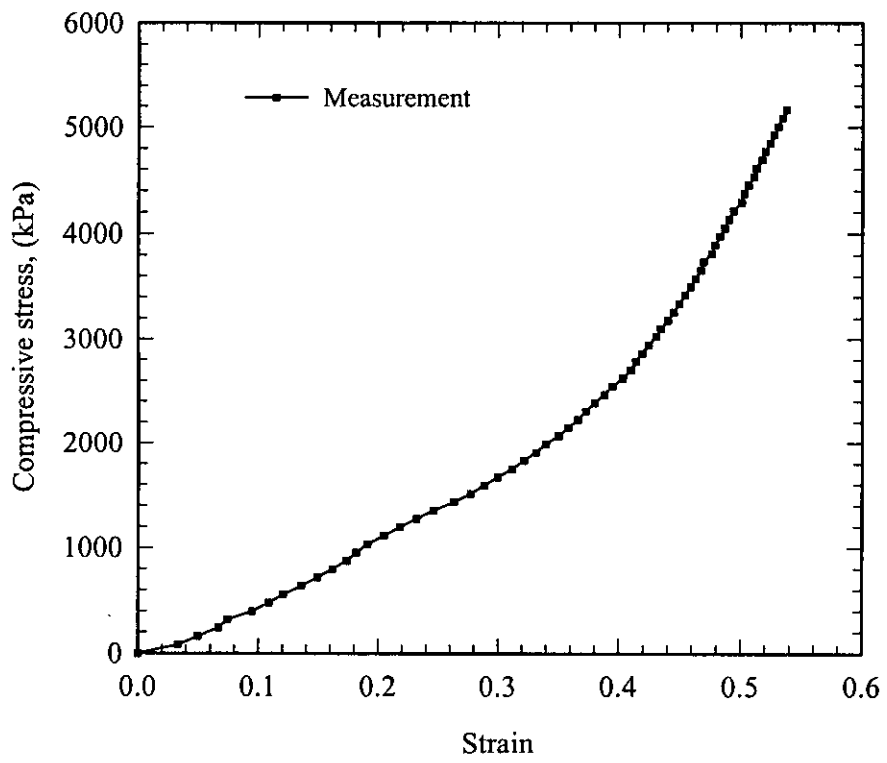
Figure 4.3 Measured stress-strain relationship for natural rubber under compression
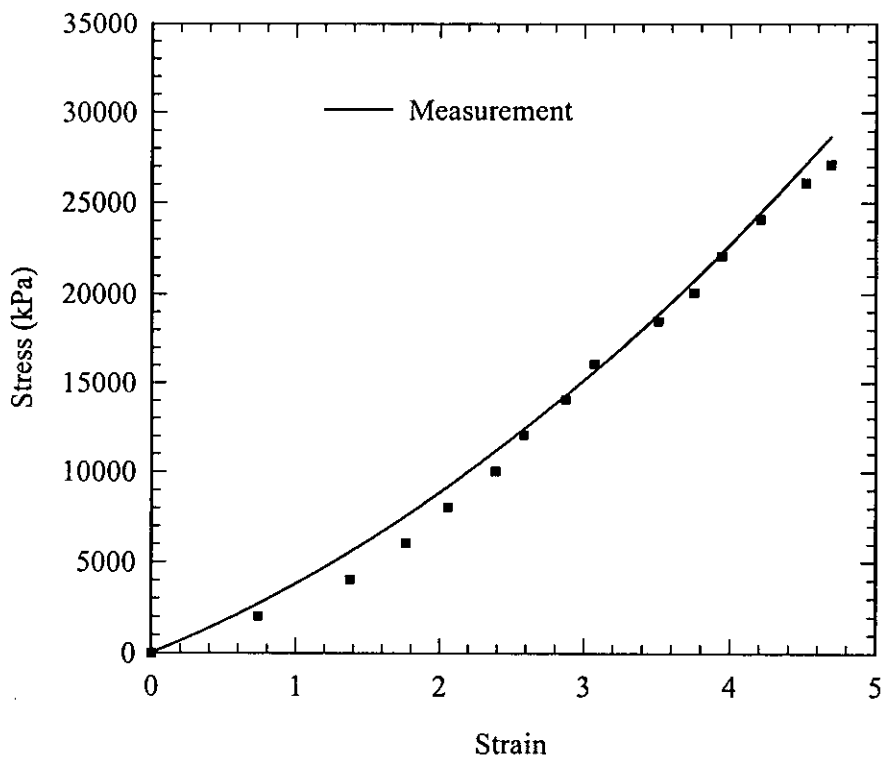
Figure 4.4 (a) Measured stress-strain relationship of truck tyre tread under tension
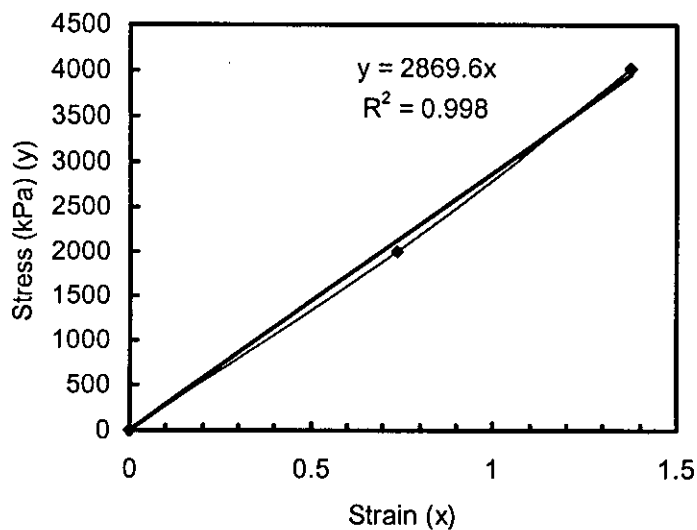
Figure 4. 4 (b) Determination of elastic modulus of truck tire rubber under tension for low strain range
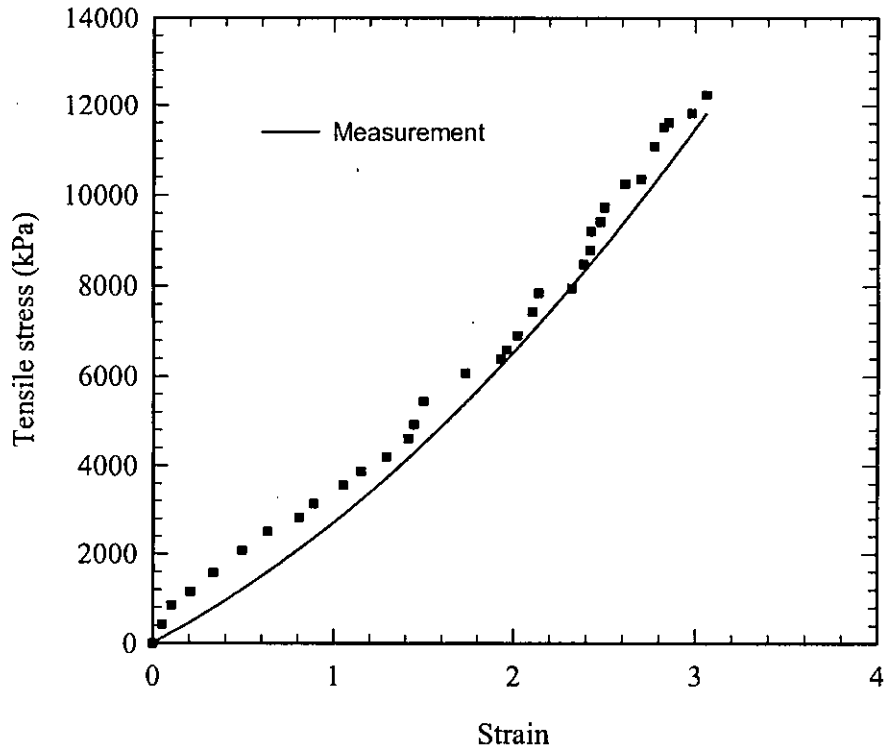
Figure 4.5 Measured stress-strain relationship for retreading tyre rubber under tension
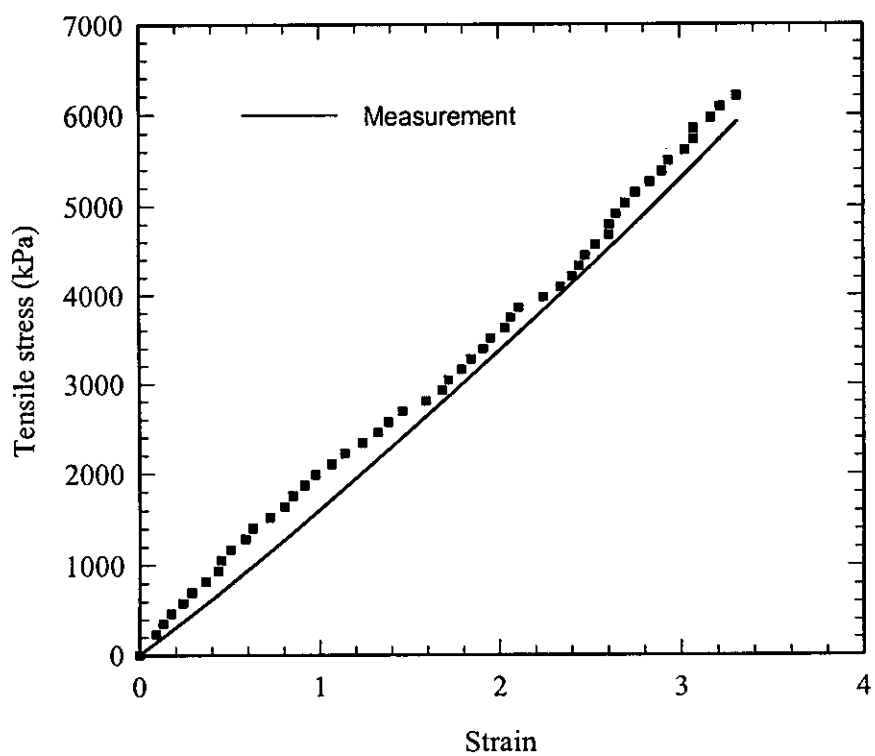
Figure 4.6 Measured stress-strain relationship for neoprene rubber under tension
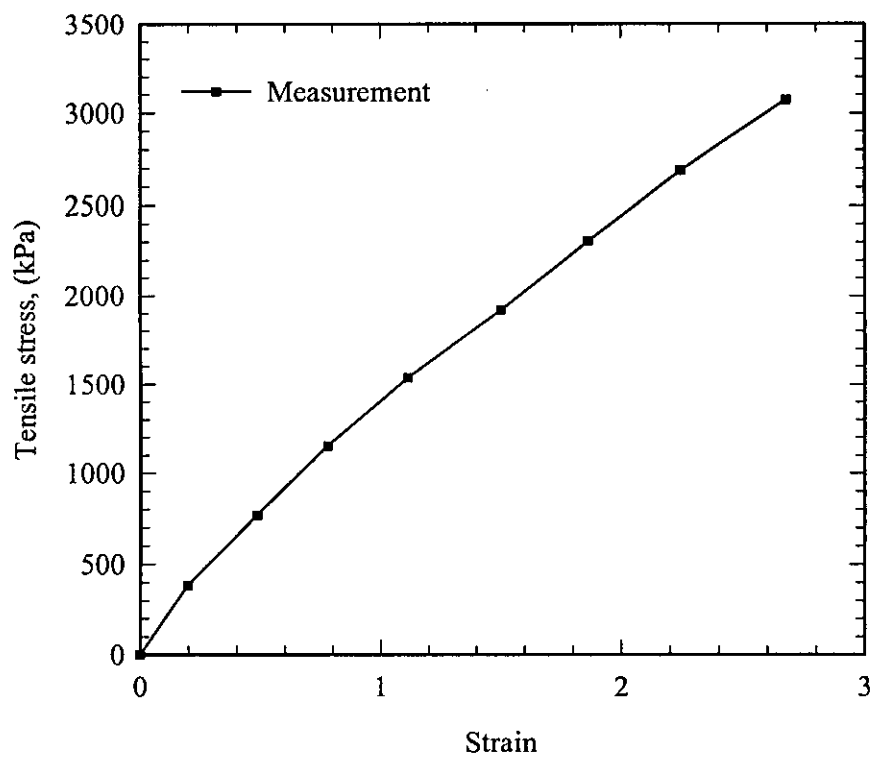
Figure 4.7 Measured stress-strain relationship for natural rubber under tension
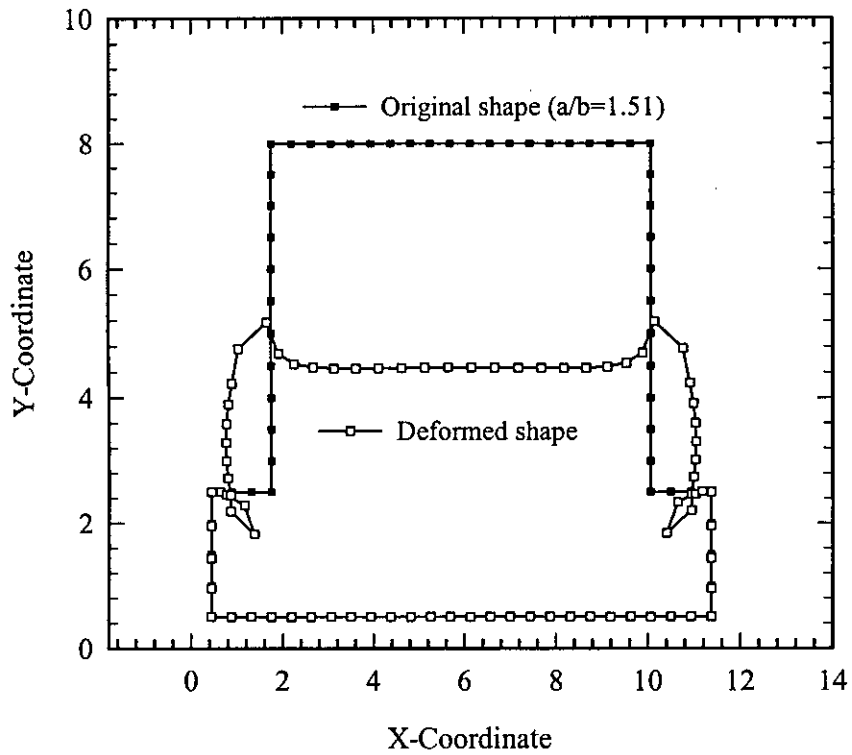
Figure 5.1 Deformation of the truck tyre tread section under the uniform normal contact pressure of 690 kPa (displacements magnified 6 times)
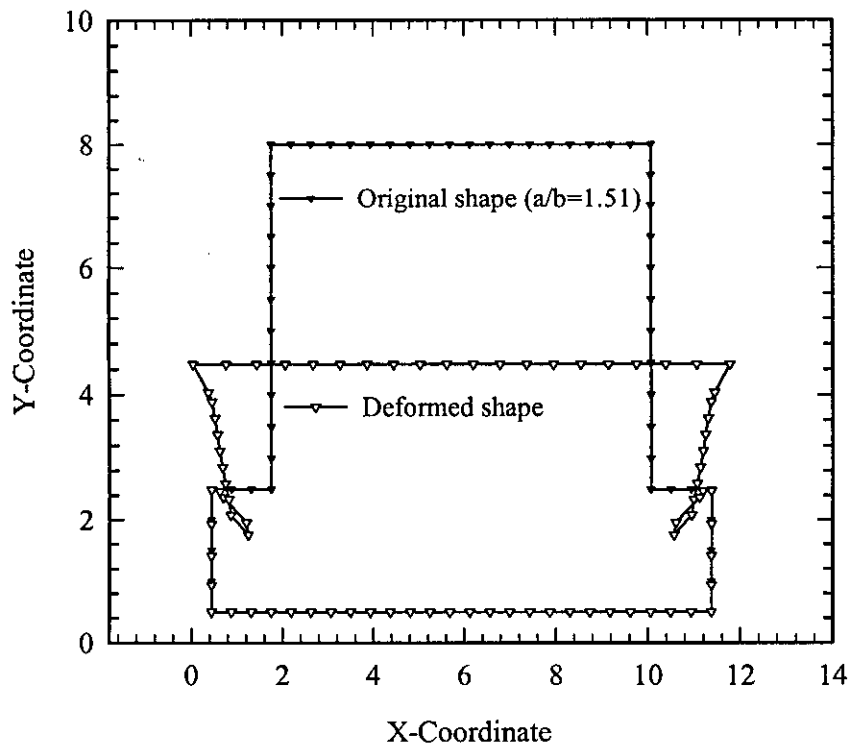
Figure 5.2 Deformation of the truck tyre tread section under un
normal displacement corresponding to 690 kPa (displacements
magnified 6 times)
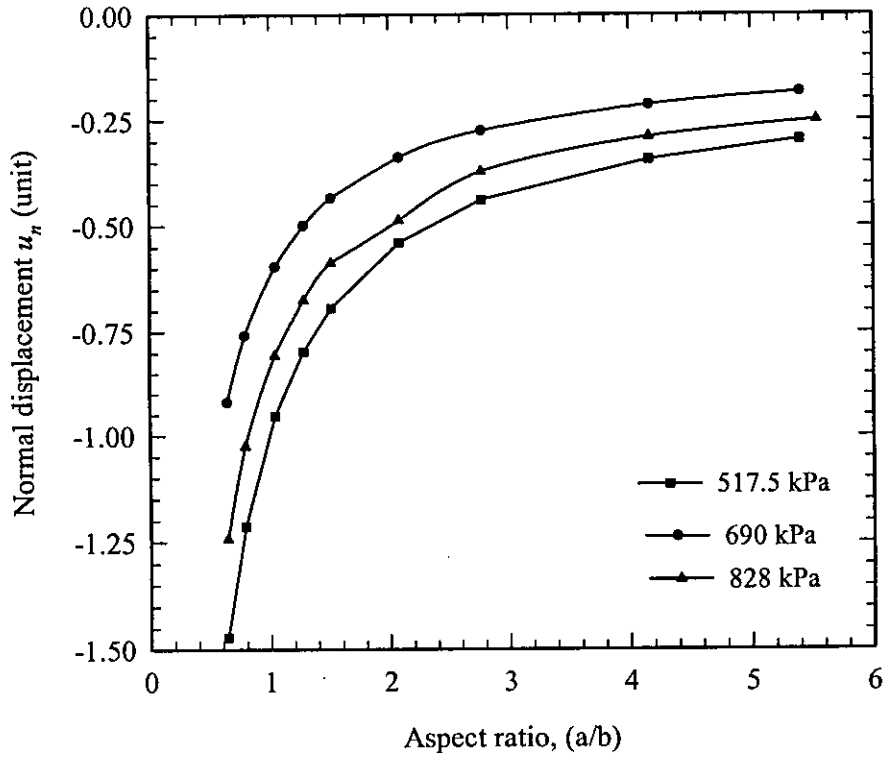
Figure 5.3 Effect of skid depth, b on the normal displacement of the contact boundary (a is kept fixed at 8.31 unit) for different inflation pressure.
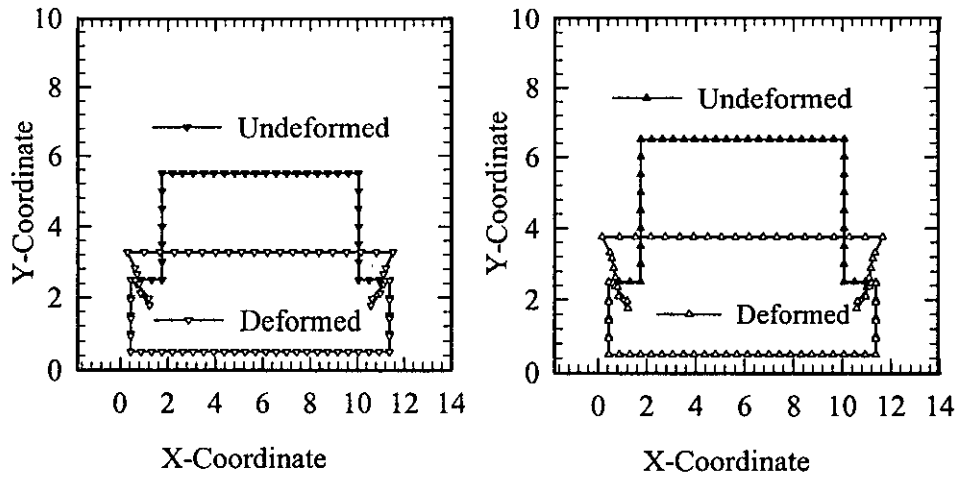
(a) a/b=2.77

(b) a/b=2.08
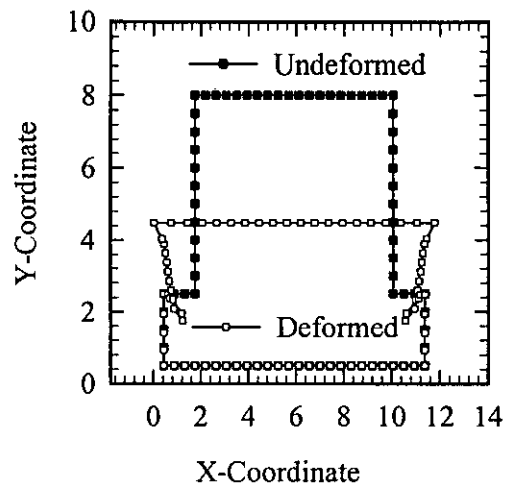
(c) a/b=1.51

Figure 5.4 Effect of skid depth, b on the deformed shape of
the tread section keeping the contact length fixed
(displacements magnified six times)

(d) a/b=1.28

(e) a/b=1.04

(f) a/b=0.79
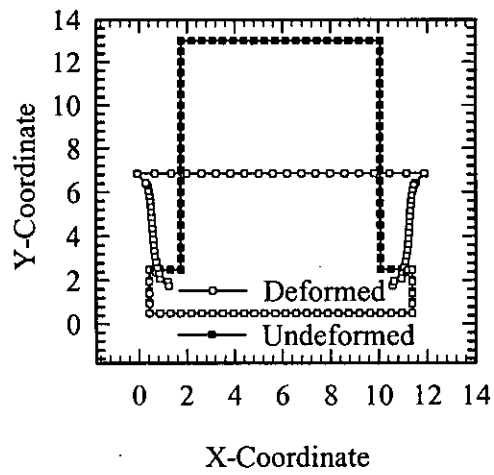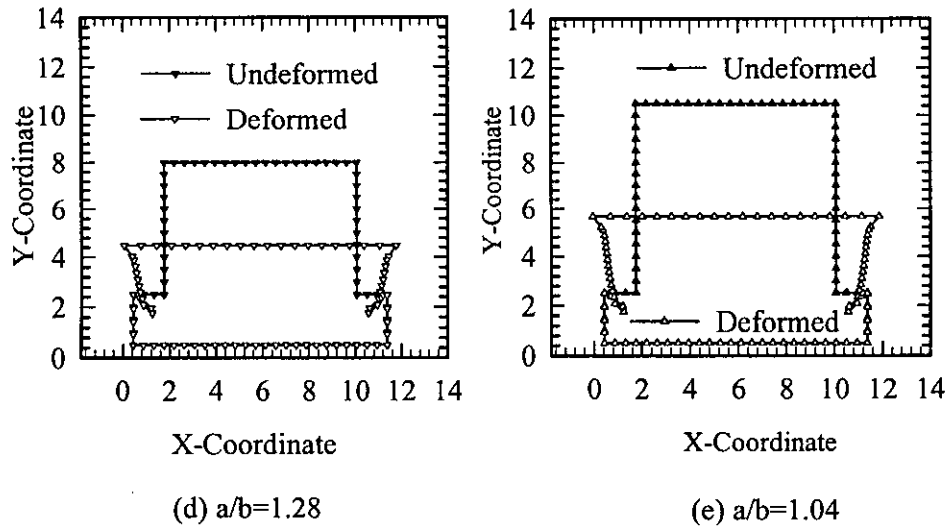
Figure 5.4 Effect of skid depth, b on the deformed shape of
the tread section keeping the contact length fixed
(displacements magnified six times)
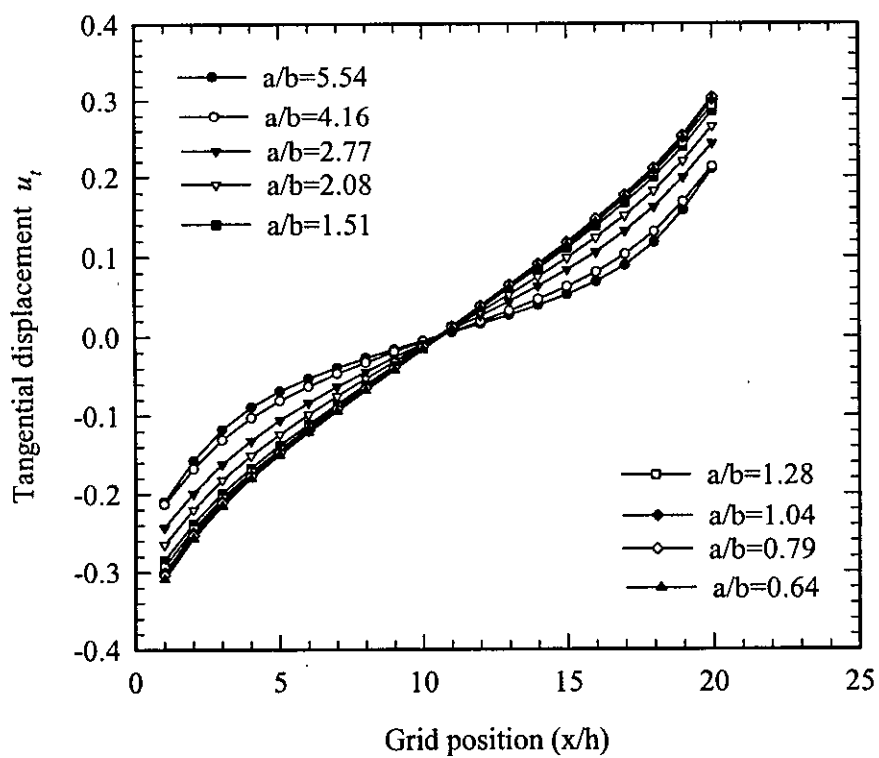
Figure 5.5 Effect of skid depth, b on the tangential displacement of the contact boundary for fixed contact length, a
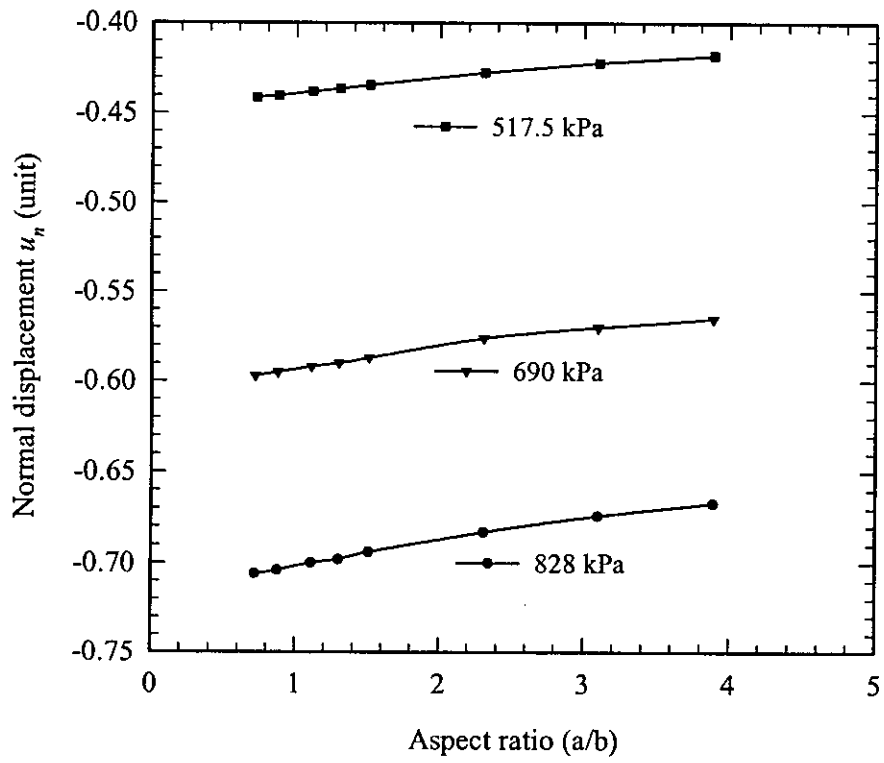
Figure 5.6 Effect of contact length, a on the normal displacement of the contact boundary when skid depth, b is kept fixed.

(a) a/b=0.72

(b) a/b=1.52

(c) a/b=2.31
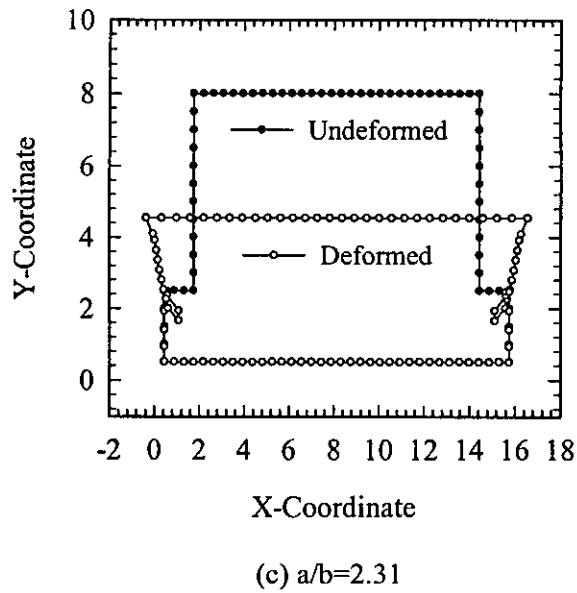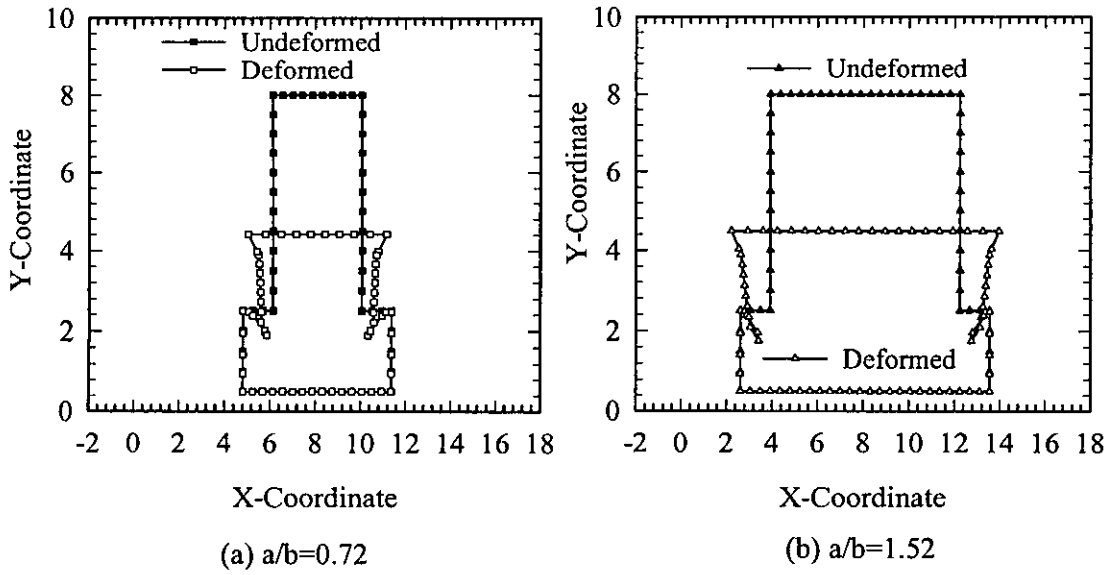
Figure 5.7 Effect of contact length, a on the deformed shape of the tread section keeping the skid depth, b fixed. (displacements magnified six times)
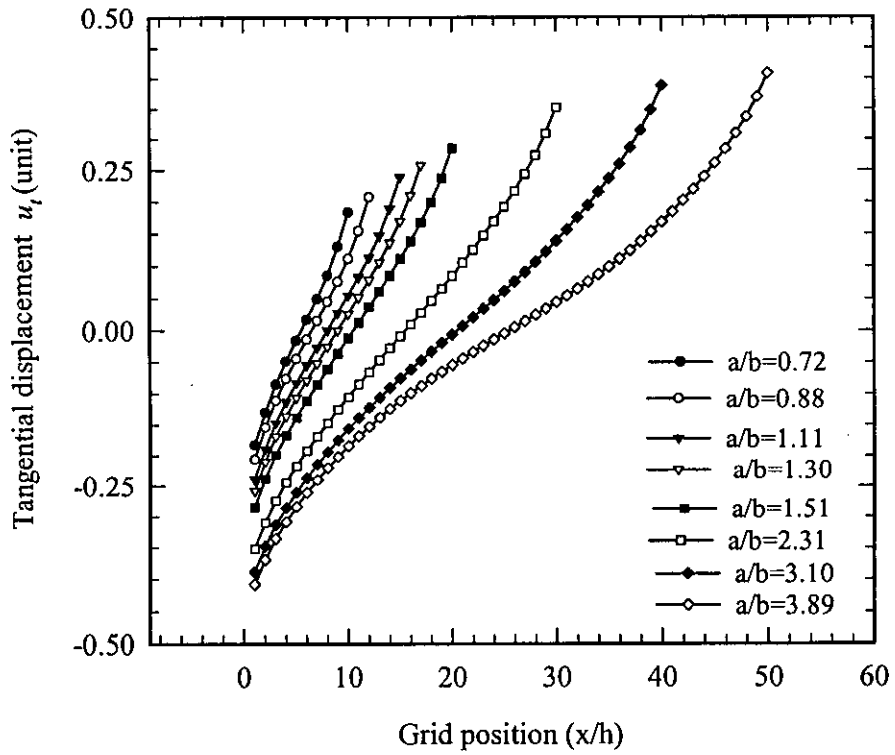
Figure 5.8 Effect of contact length, a on the tangential displacement
of the contact boundary for a fixed skid depth, b
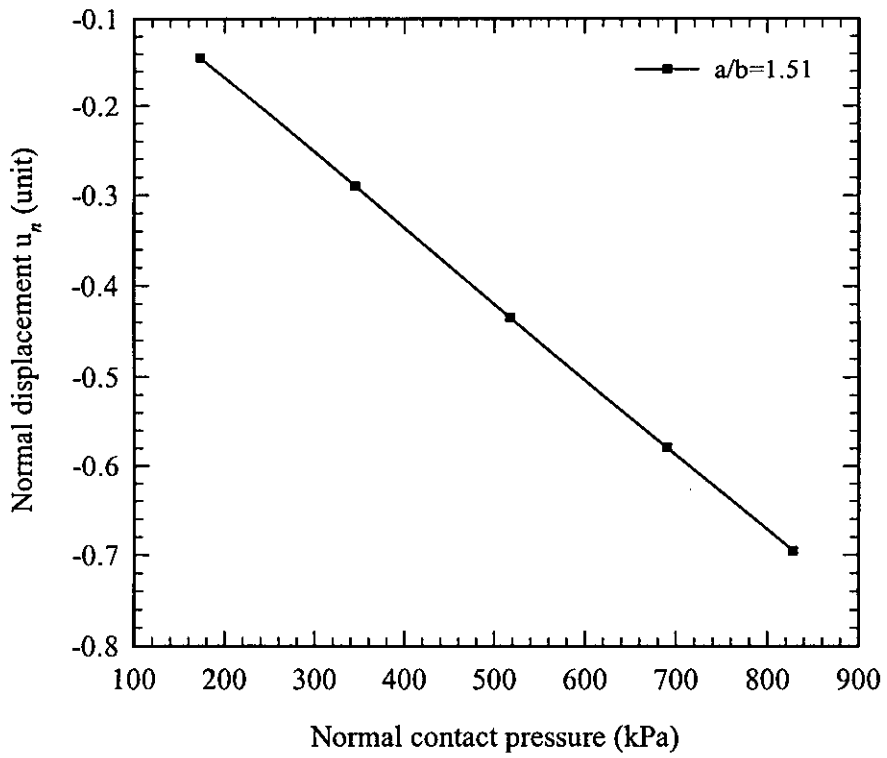
Figure 5.9 Normal displacement of the contact plane as a function of normal contact pressure for a tread section, a/b=1.51
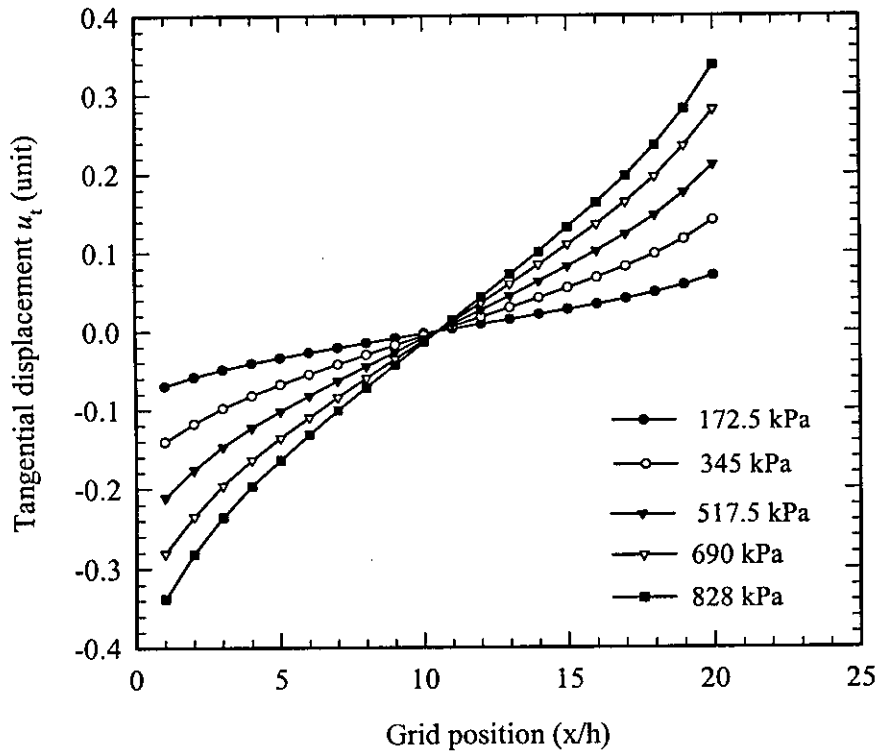
Figure 5.10 Effect of normal contact pressure on the tangential displacement of the contact boundary for a tread section, a/b=1.51
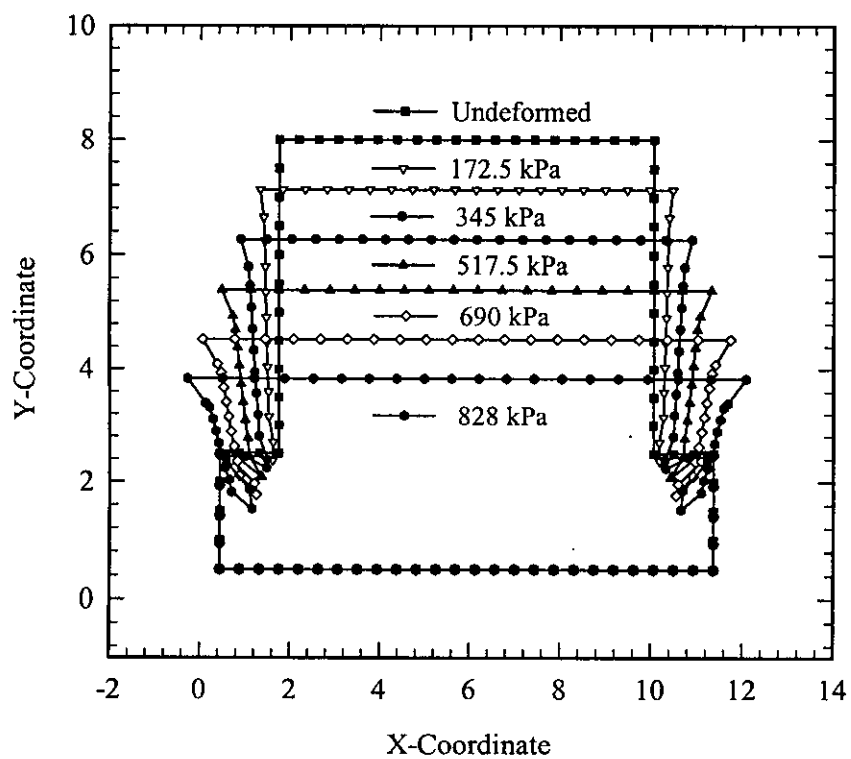
Figure 5.11 Effect of normal contact pressure on the deformed shape of the tread section, a/b=1.51 (displacements magnified 6 times)
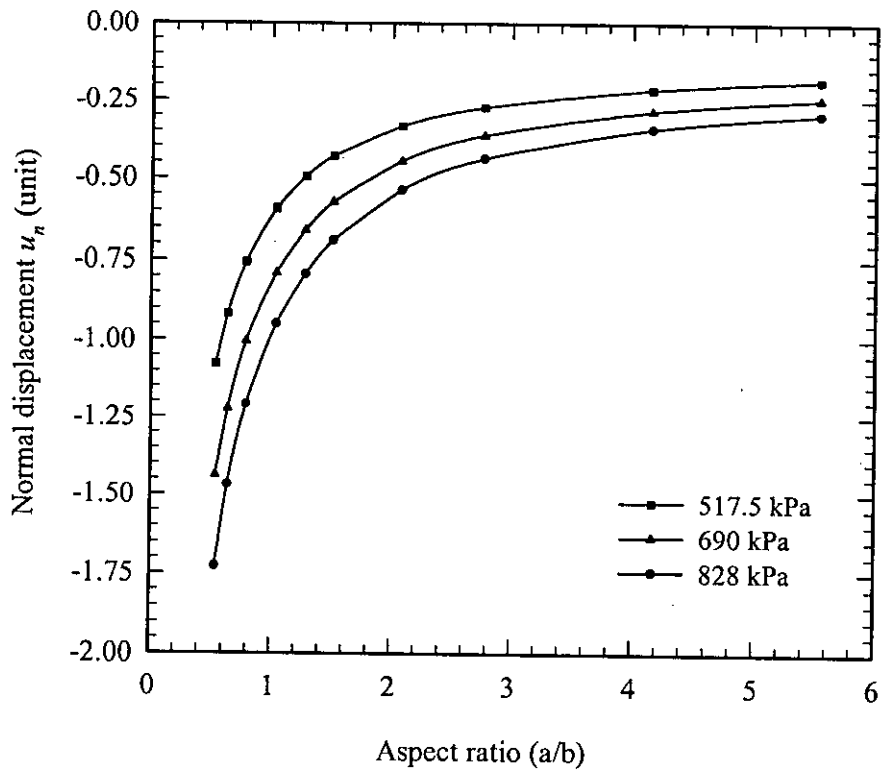
Figure 6.1 Effect of skid depth, b on the normal displacement of the contact boundary under no-slip condition, when the contact length is kept fixed at various inflation pressure
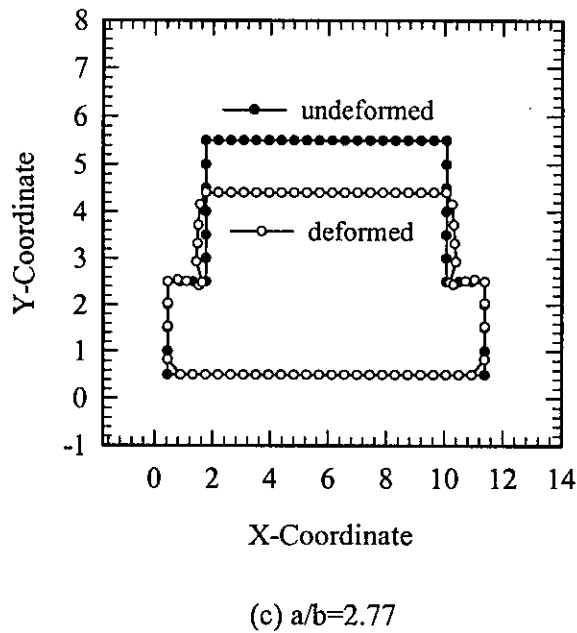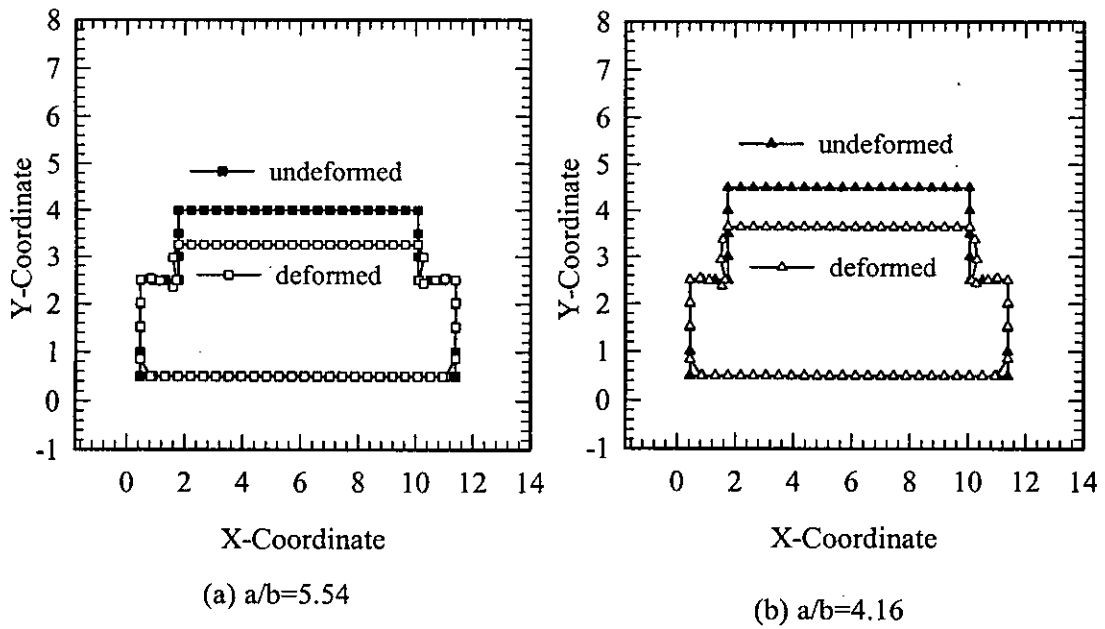
(a) a/b=5.54

(b) a/b=4.16

(c) a/b=2.77

Figure 6.2 Influence of skid depth, b on the deformation of the tread section under no-slip condition, when contact length is kept fixed (displacements magnified 3 times)
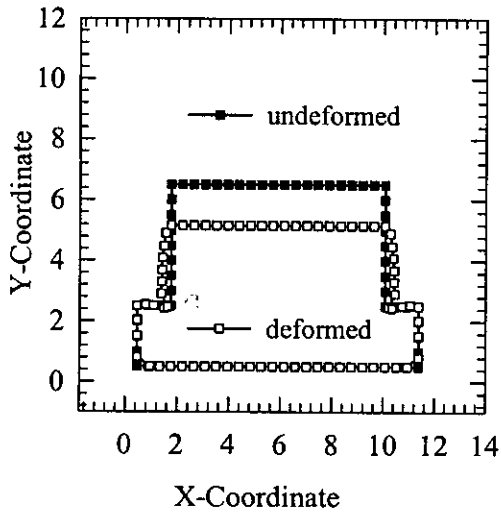
(d) a/b=2.08
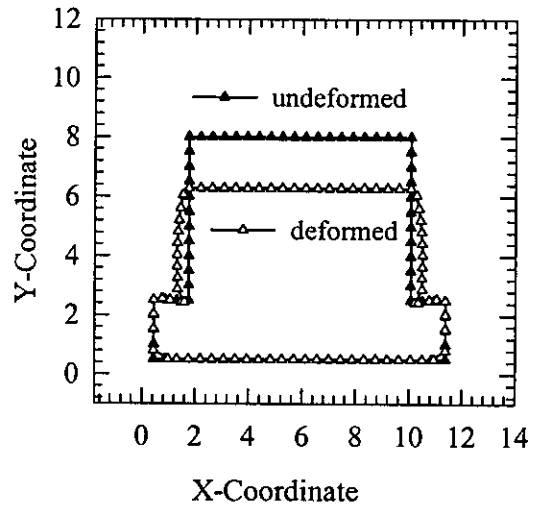
(e) a/b=1.51
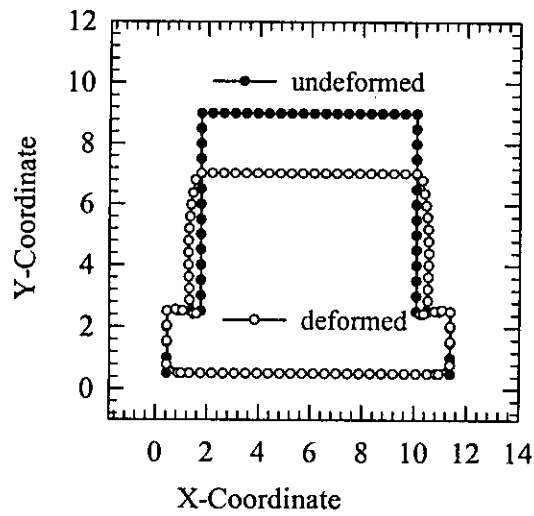
(f) a/b=1.28

Figure 6.2 Influence of skid depth, b on the deformation of the tread
section under no-slip condition, when contact length is kept
fixed (displacements magnified 3 times)
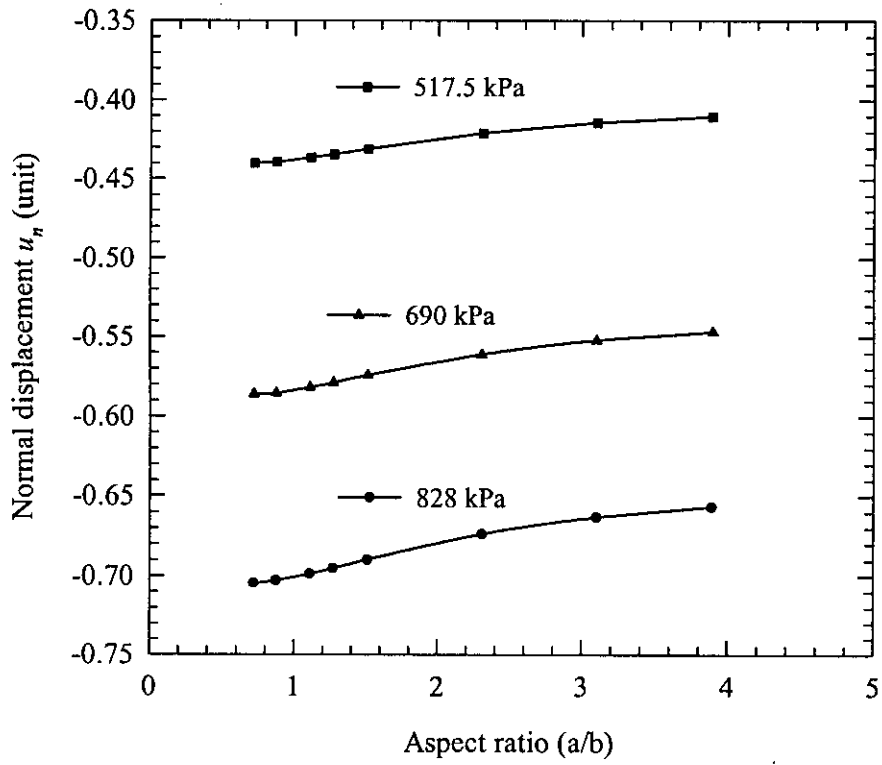
Figure 6.3 Effect of contact length, a on the normal displacement of the contact boundary under no-slip condition, when the skid depth is kept fixed
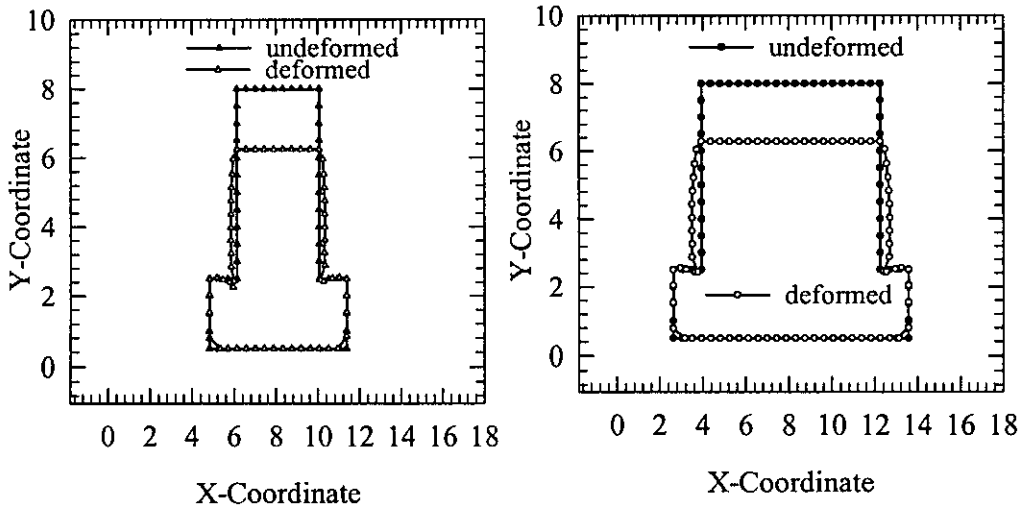
(a) a/b=0.72

(b) a/b=1.27
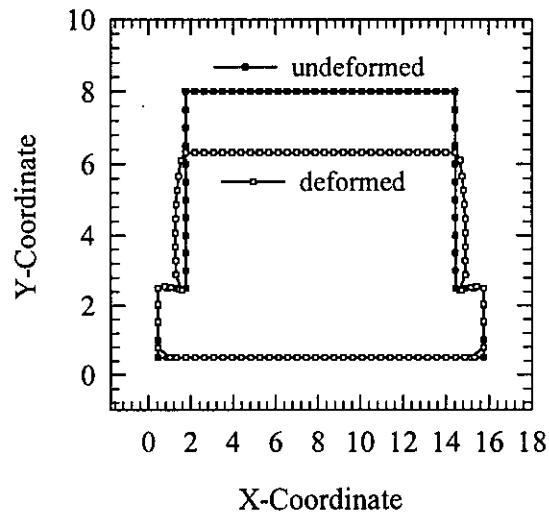
(c) a/b=1.51

Figure 6.4 Influence of contact length, a on the deformation
of the tread section under no-slip condition, when skid
depth b is kept fixed (displacements magnified 3 times)
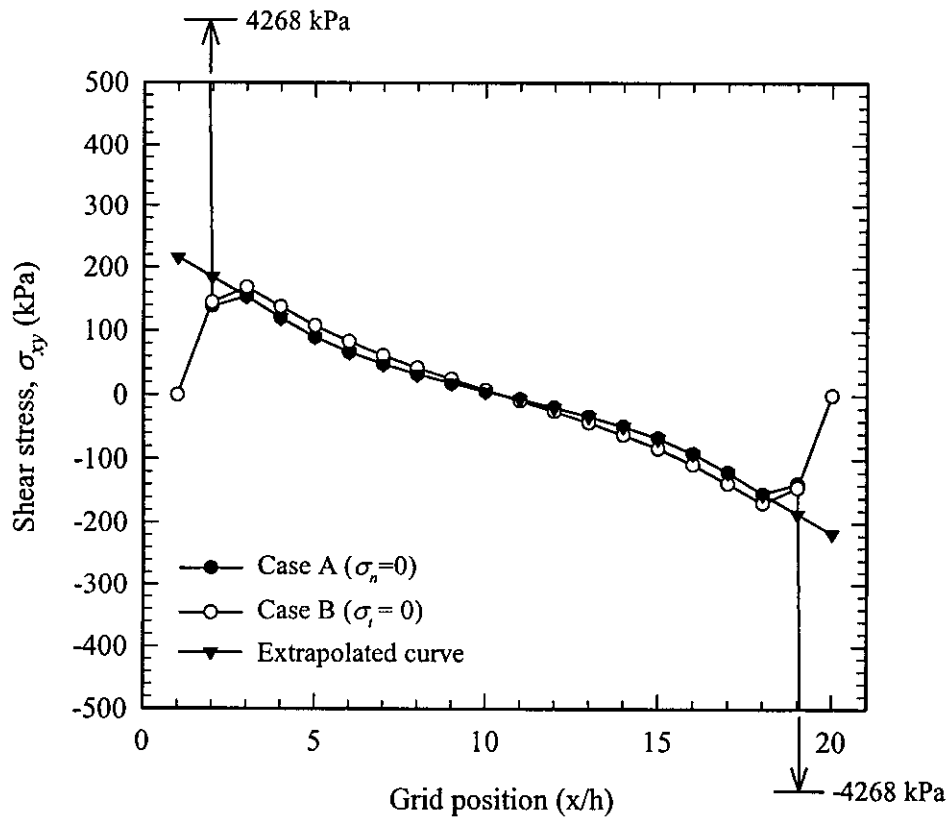
Figure 6.5 Prediction of shearing stresses along the contact boundary of a tread section (a/b=1.51) under no slip condition and an inflation pressure of 690 kPa
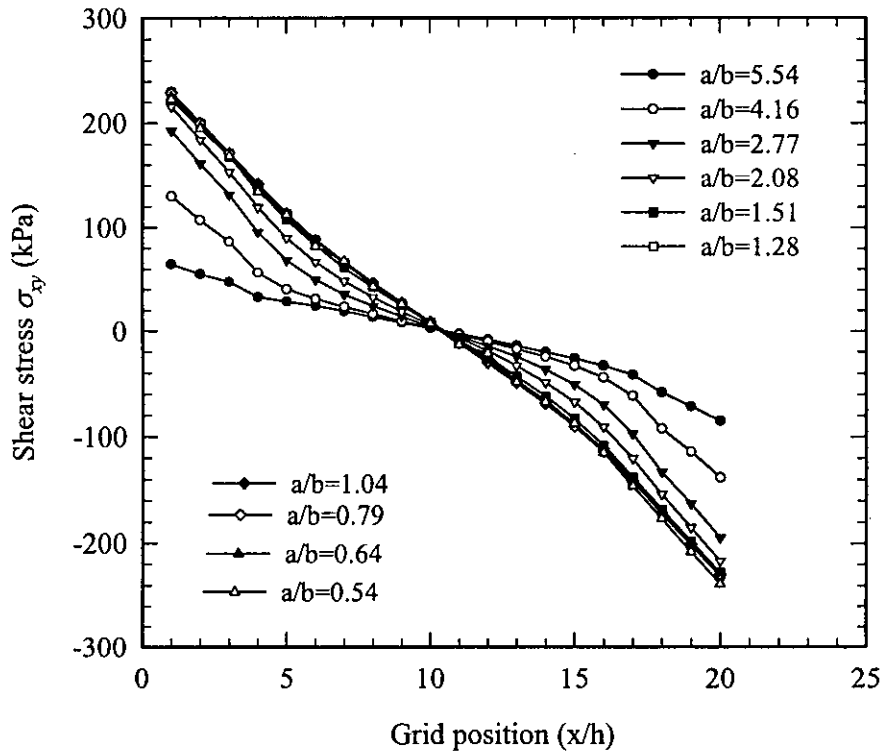
Figure 6.6 Influence of skid depth, b on the developed shear stress along the contact boundary conforming the no-slip condition under normal contact pressure 690 kPa
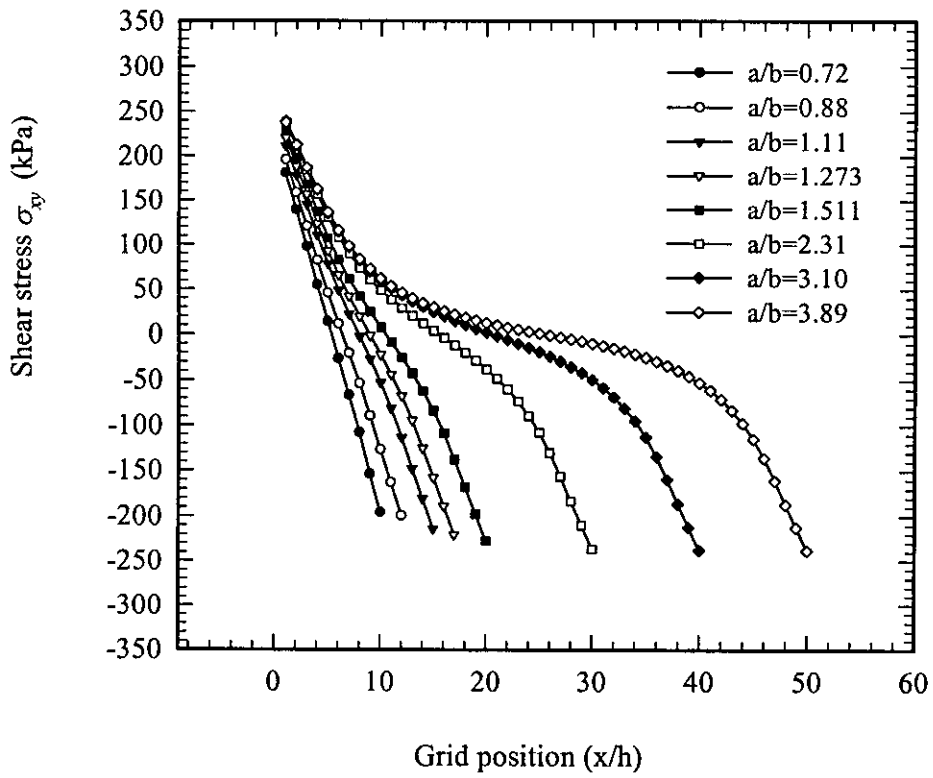
Figure 6.7 Influence of contact length, a on the developed shear stress along the contact boundary conforming the no slip-condition under normal contact pressure 690 kpa
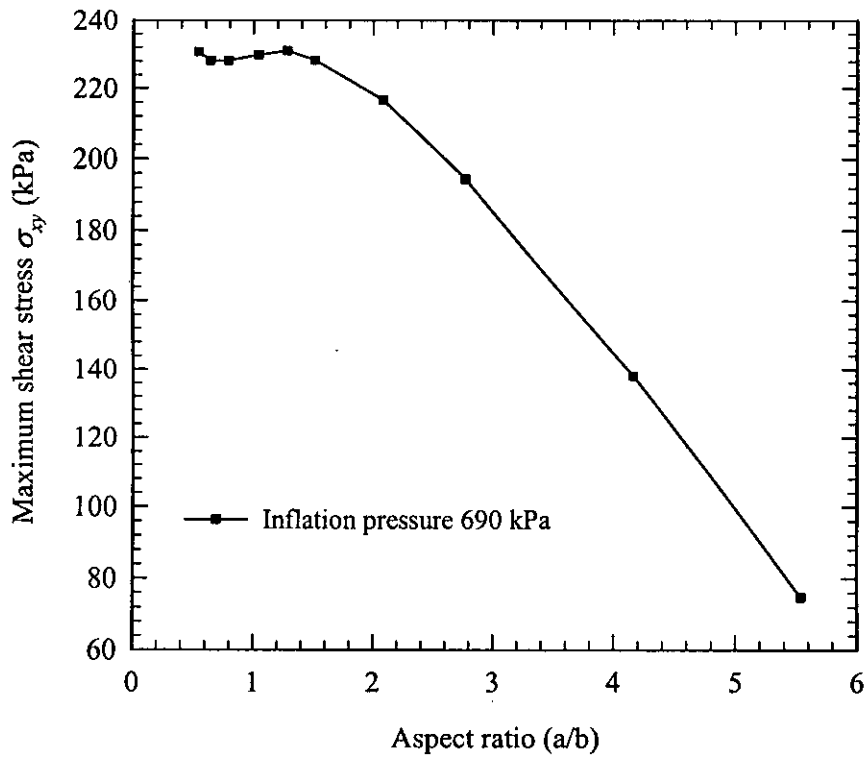
Figure 6.8 Maximum shearing stress on the contact boundary as a function of a tread aspect ratio (a is kept fixed)
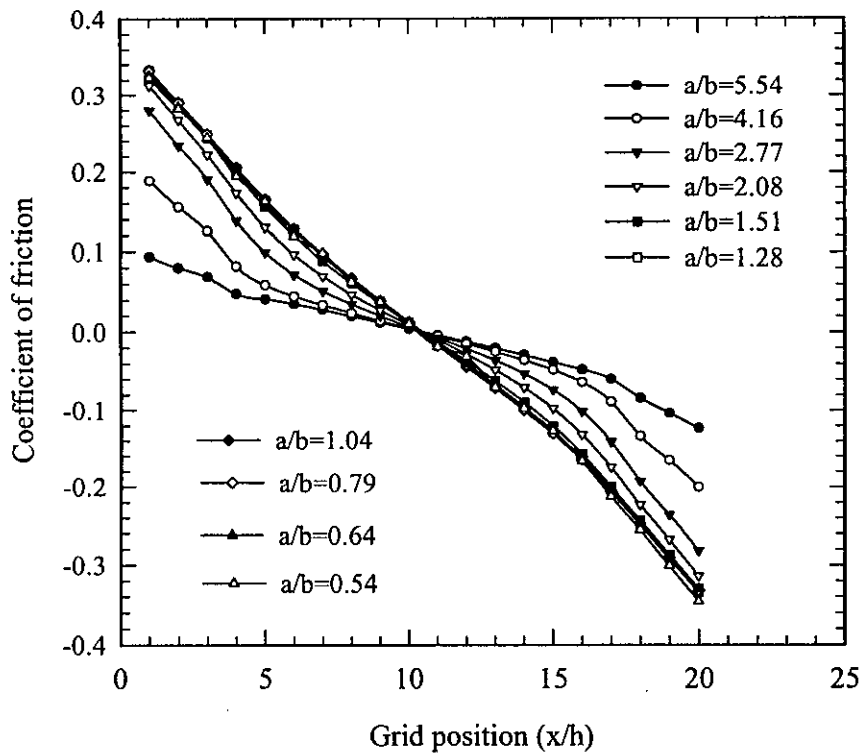
Figure 6.9 Effect of skid depth on the coefficient of friction along the contact surface conforming the no-slip condition under contact pressure 690 kPa
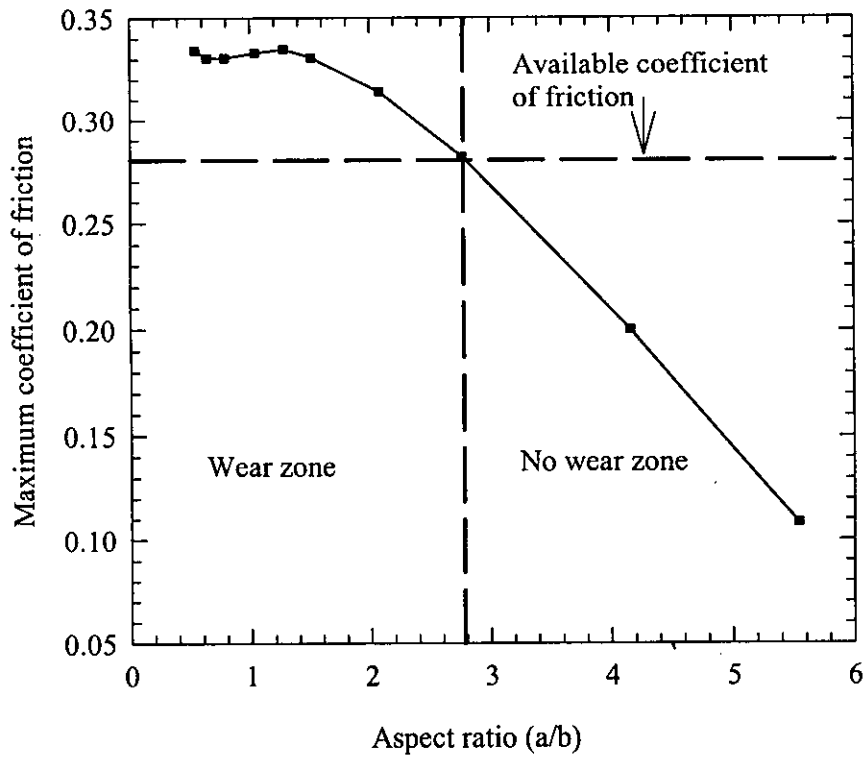
Figure 6.10 Calculated maximum coefficient of friction
as a function under an inflation pressure of 690 kPa
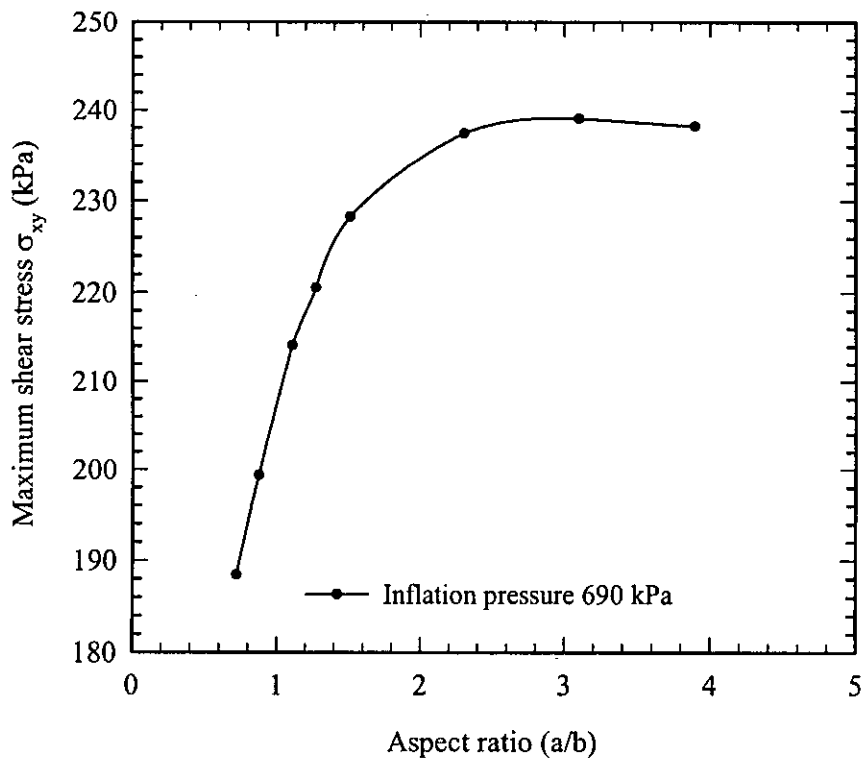
Figure 6.11 Maximum shearing stress on the contact boundary as a function of tread aspect ratio (b is kept fixed)
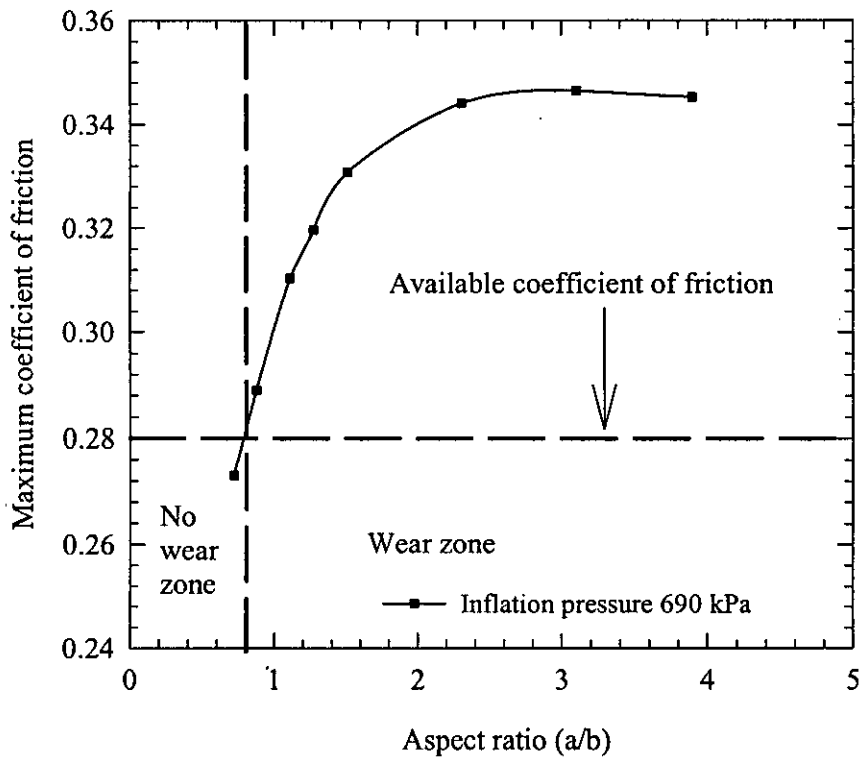
Figure 6.12 Calculated maximum coefficient of friction as a function of tread aspect ratio (b is kept fixed)
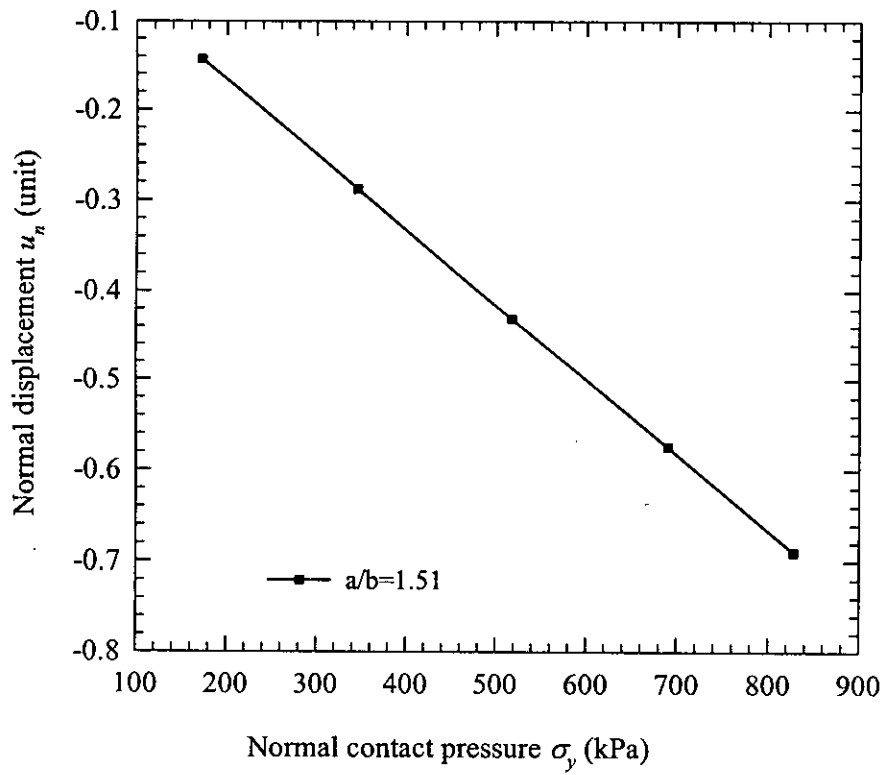
Figure 6.13 Normal displacement as a function of normal contact pressure on the tread contact surface for no-slip condition.
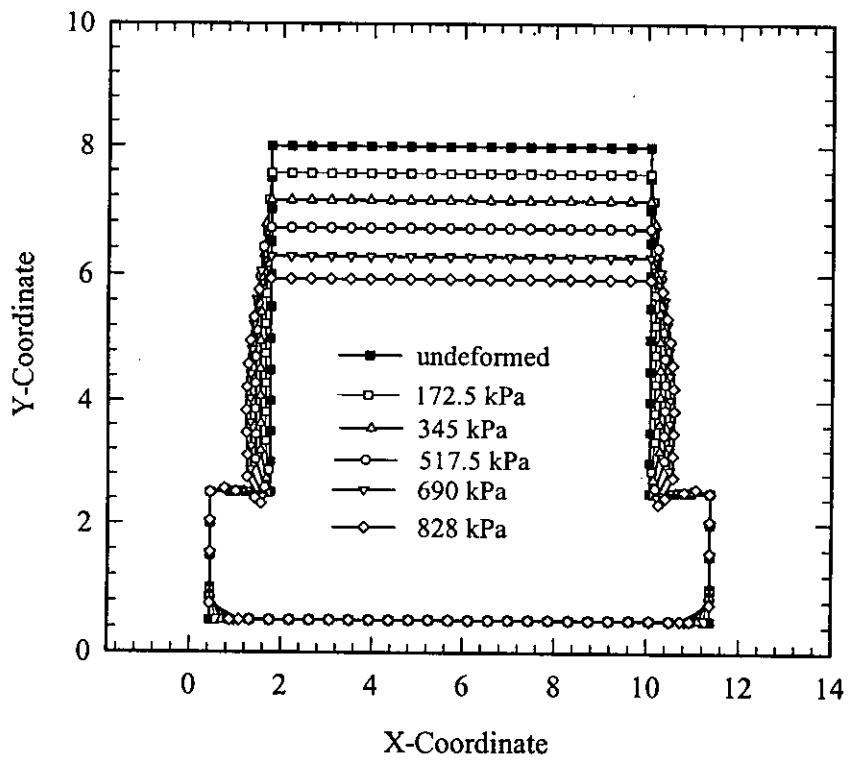
Figure 6.14 Effect of inflation pressure on the deformed shape of the tread section (a/b=1.51) under no-slip condition.
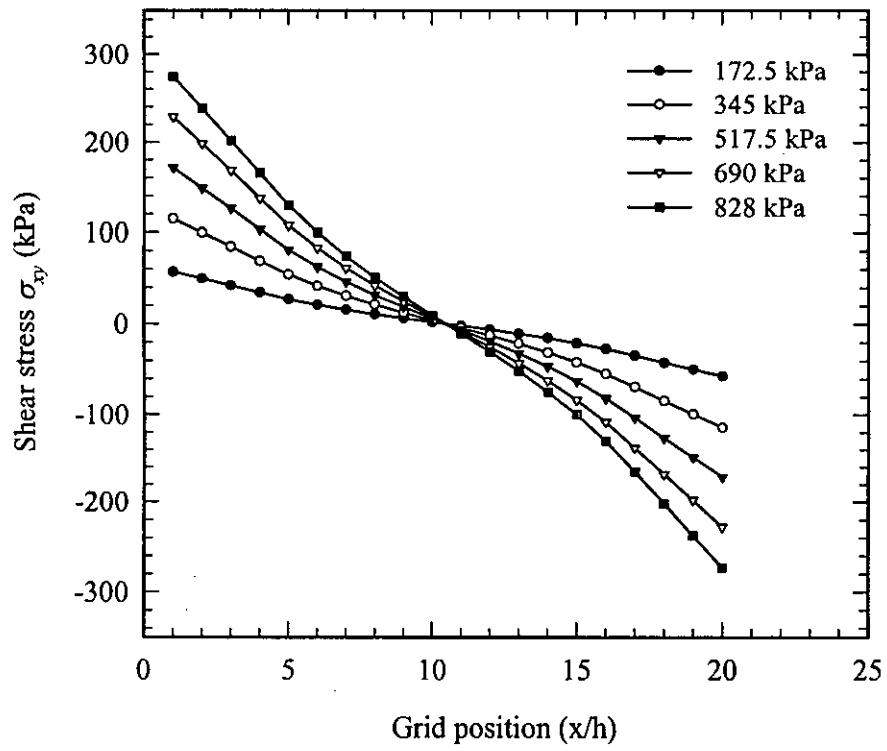
Figure 6.15 Effect of inflation pressure on the shear stress developed along the tread contact surface,under the no-slip condition.
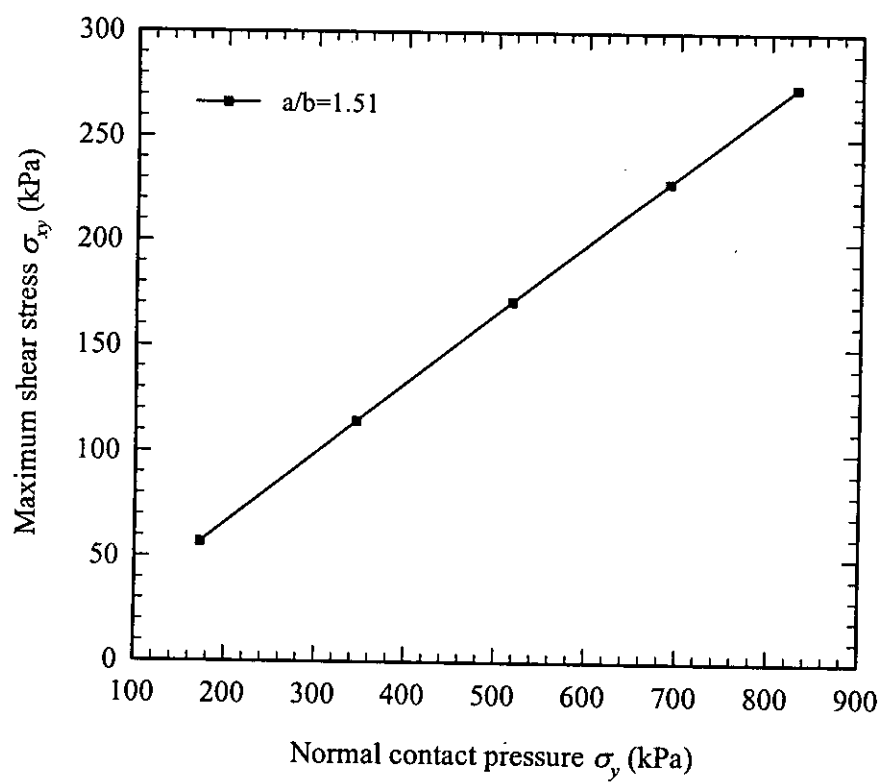
Figure 6.16 Maximum shearing stress (frictional stress) developed on the contact boundary, as a function of inflation pressure, under no slip condition
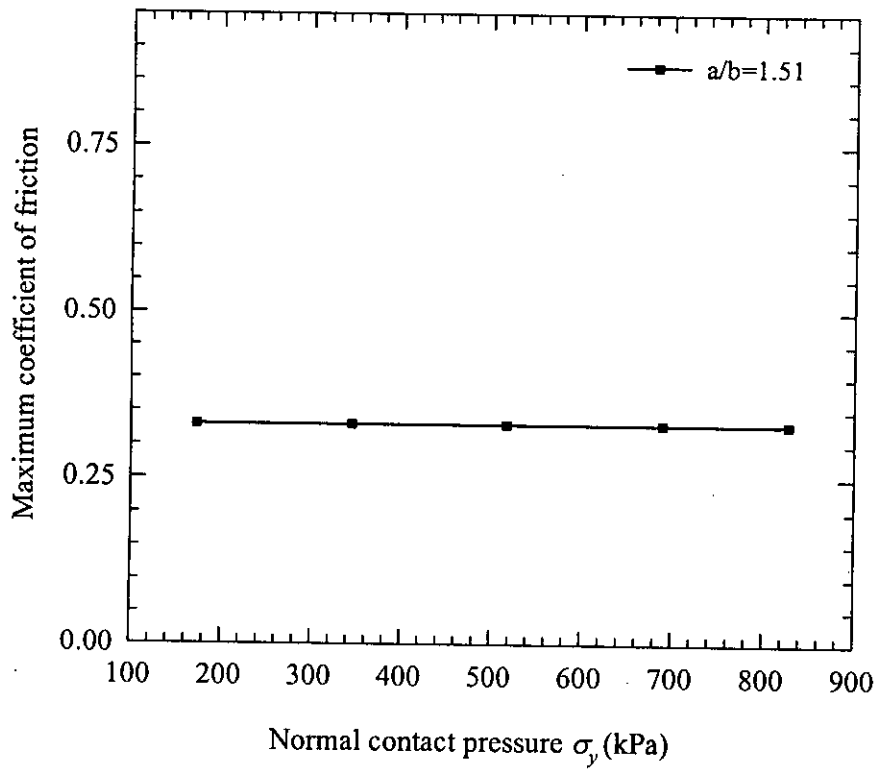
Figure 6.17 Effect of inflation pressure on the calculated maximum coefficient of friction for a tread section under no-slip condition
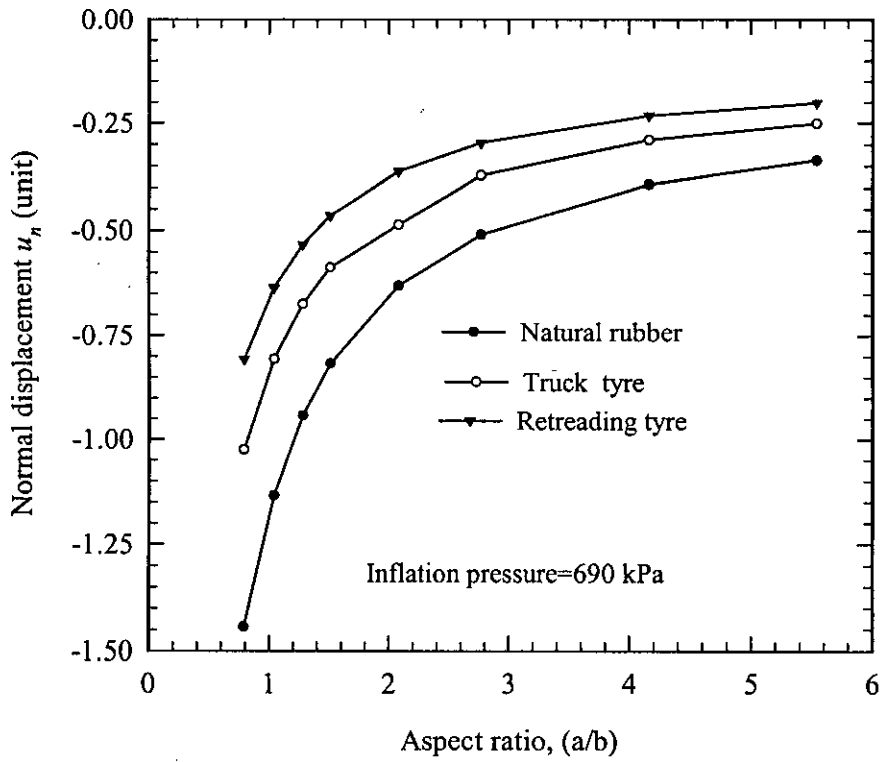
Figure 7.1 Normal displacement as a function of aspect ratio under the frictionless slipping of the tread surfaces (a is kept fixed)
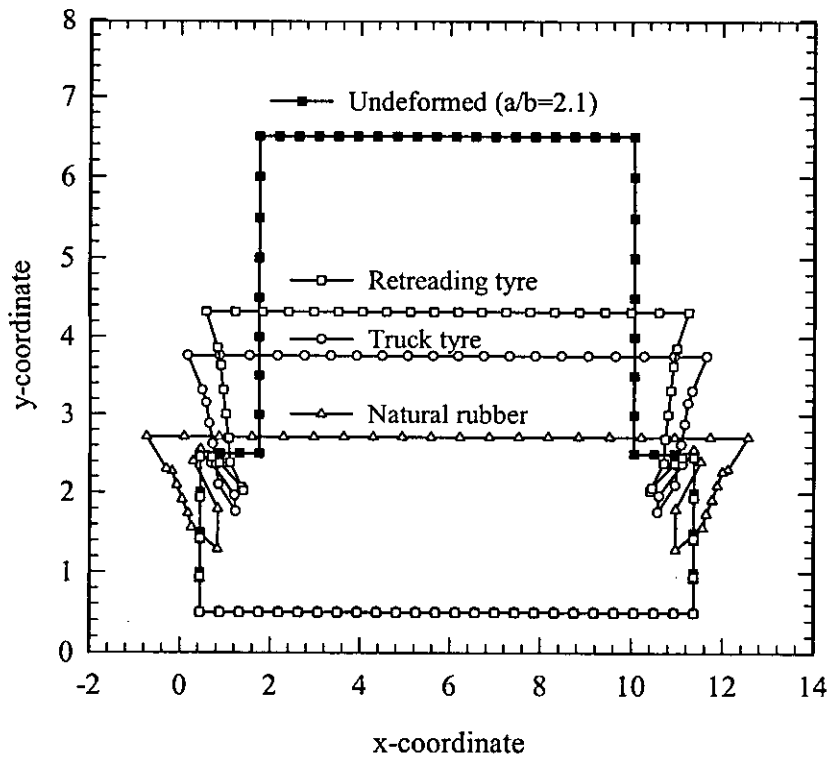
Figure 7.2 Deformed shapes of tyre treads of different materials under the contact pressure of 690 kPa considering frictionless slipping
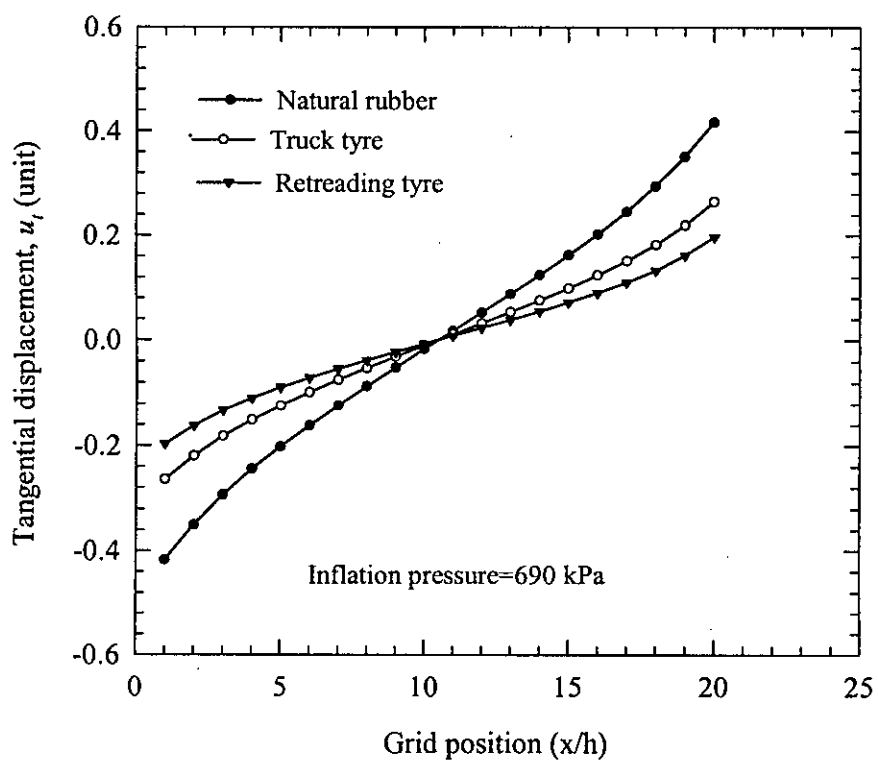
Figure 7.3 Distribution of the tangential displacement along the contact boundary of the treads (a/b=2.1) under frictionless slipping
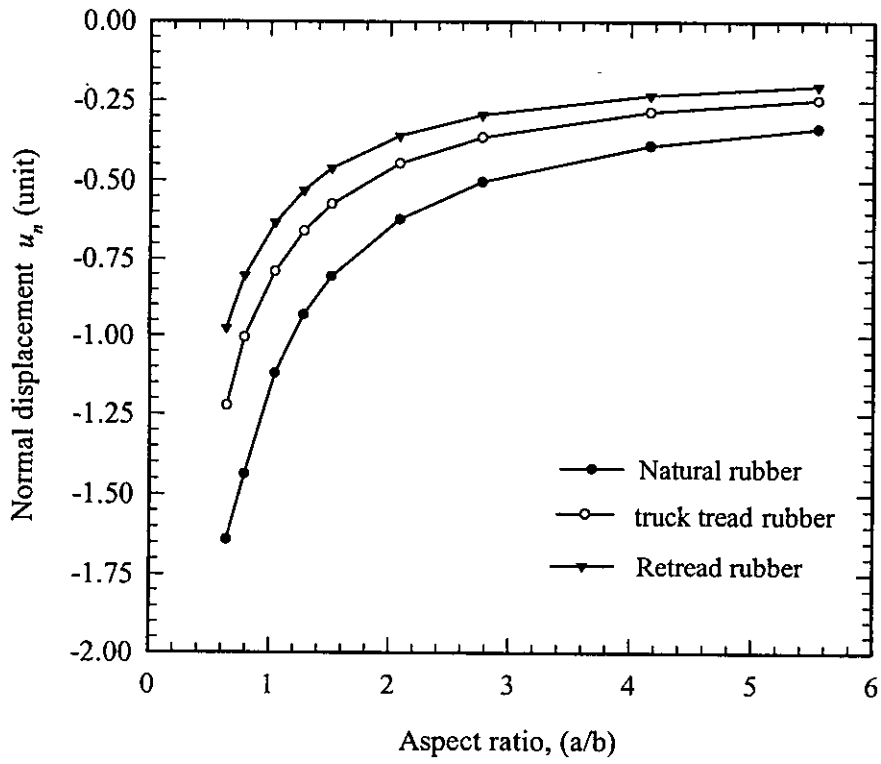
Figure 7.4 Effect of tyre material on the normal displacement of the tread contact surface for varying skid depth under the no slip condition of the contact surface
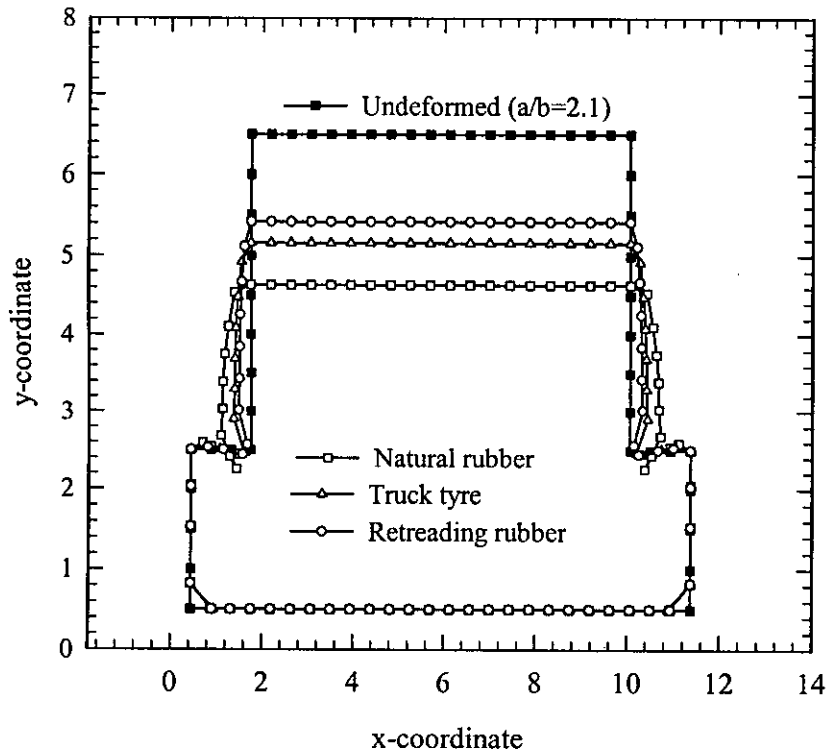
Figure 7.5 Effect of tyre material on the deformed shape of the tread section under the no-slip condition of the contact boundary (displacements magnified 3 times)
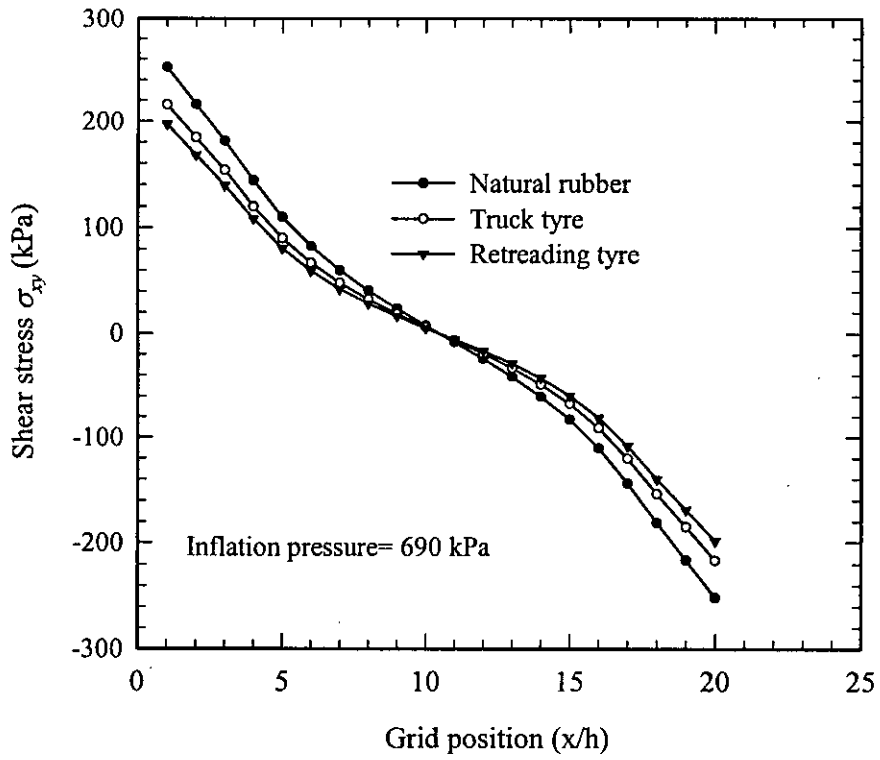
Figure 7.6 Effect of tyre material on the shear stress developed along the tread contact surface under the no-slip condition (a/b=2.1)
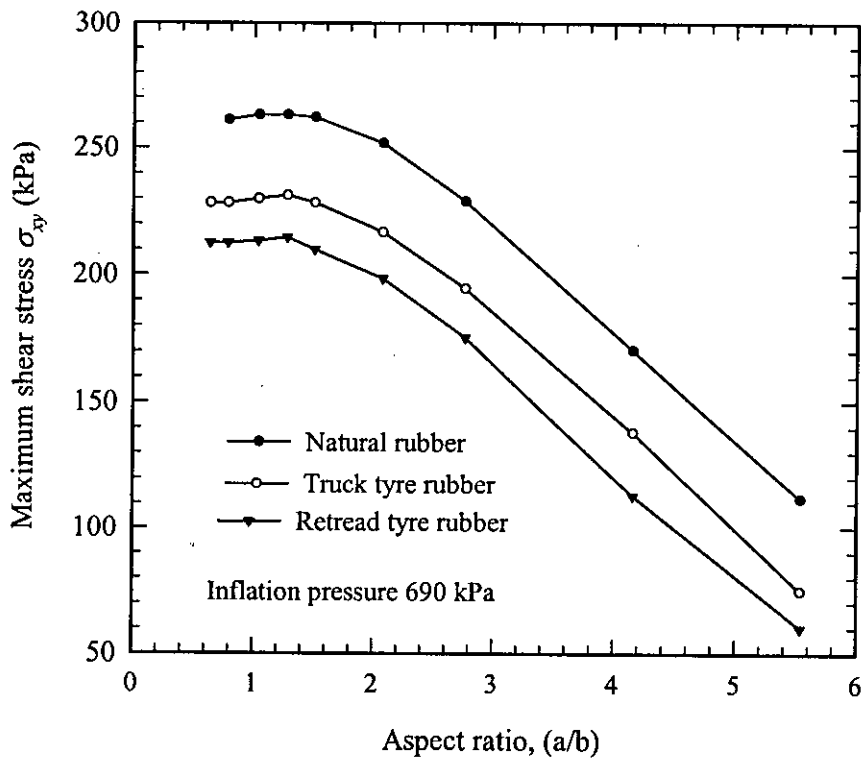
Figure 7.7 Maximum shear stress (frictional stress) as a function of tread sizes for different tire materials (a is kept constant)
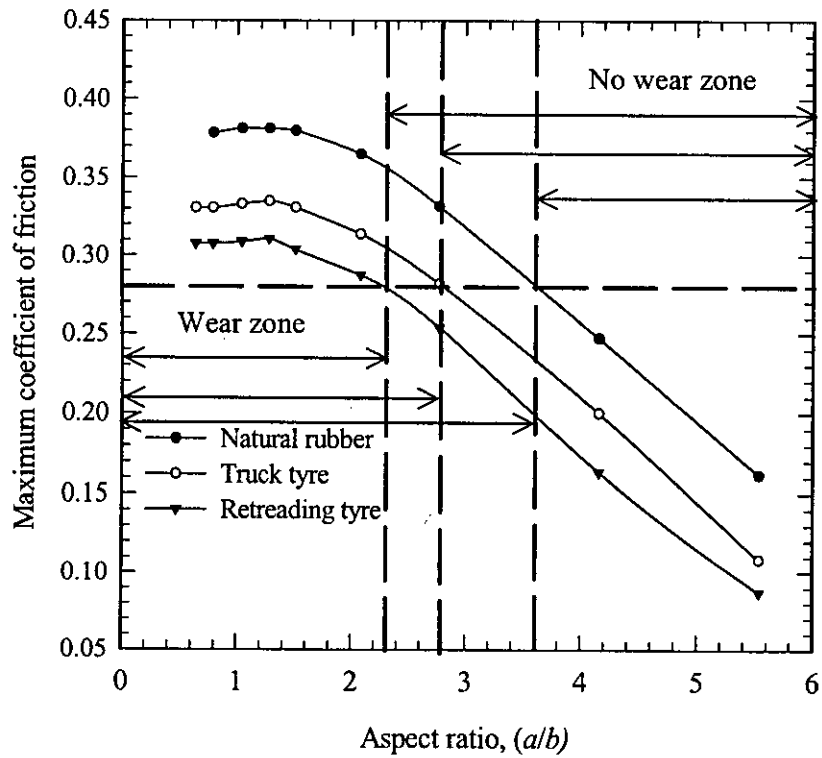
Figure 7.8 Calculated maximum co-efficient of friction as a function of tread size (varying skid depth) for different tyre materials
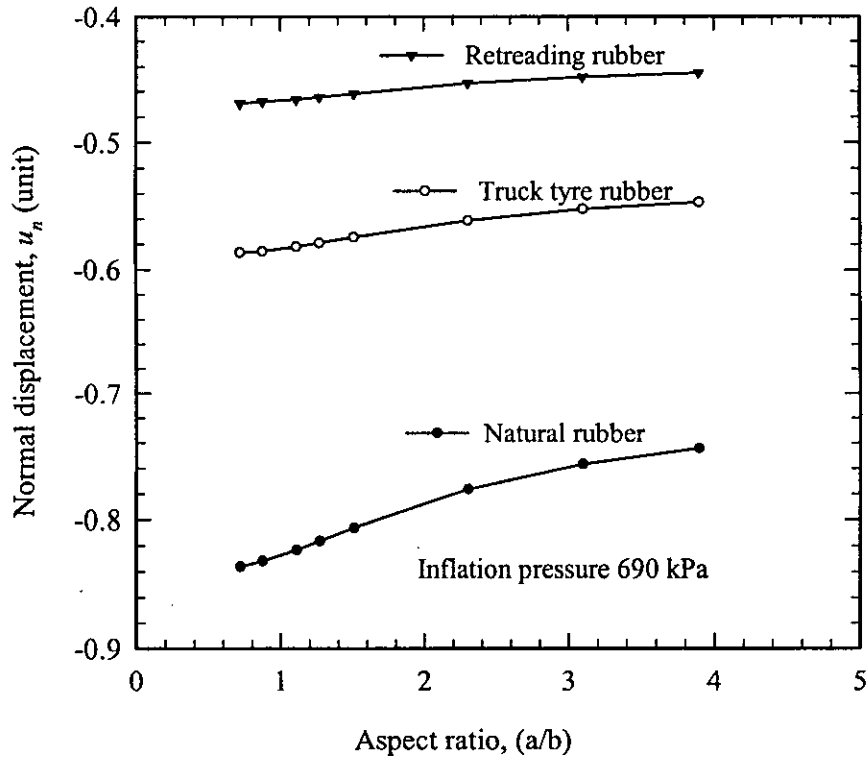
Figure 7.9 Effect of tyre material on the normal displacement of the tread contact surface under the no slip condition, when the skid depth is kept fixed
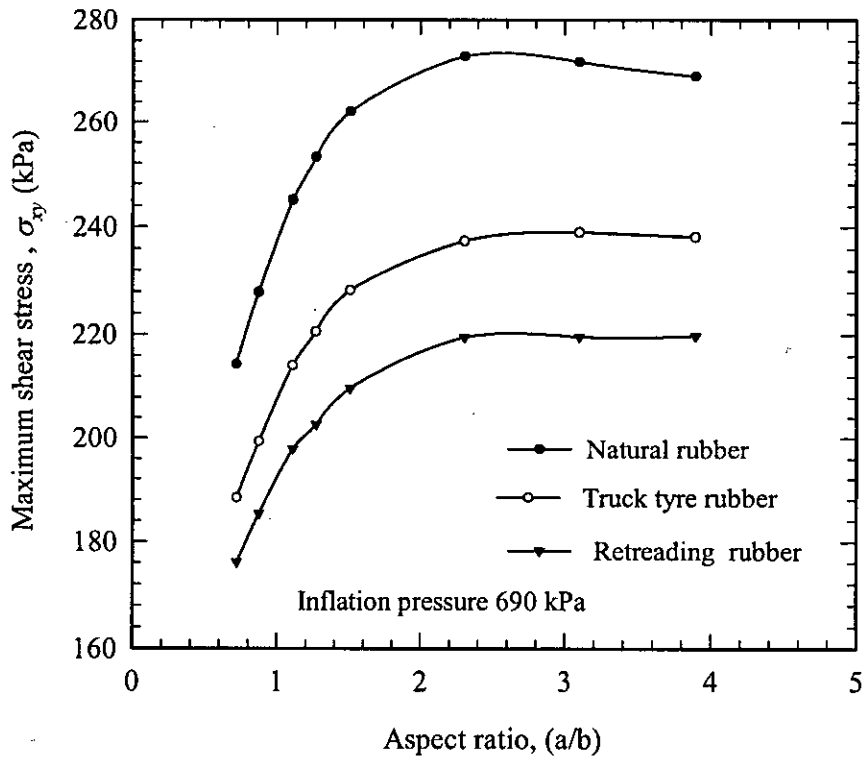
Figure 7.10 Maximum shearing stress (frictional stress) as a function of tread size for different tyre materials when the skid depth is kept fixed
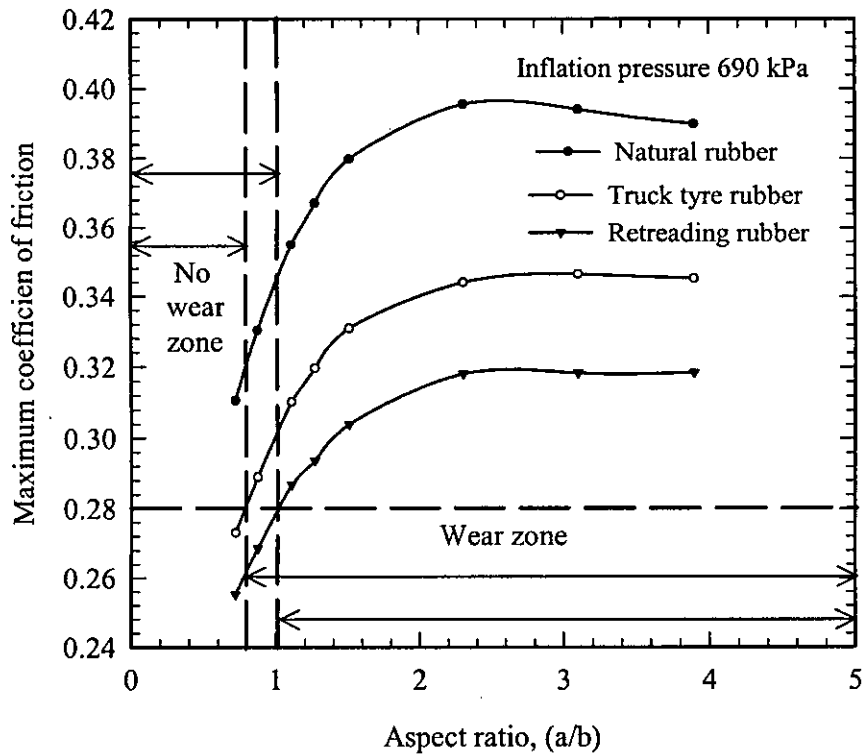
Figure 7.11 Calculated maximum coefficient of friction as a function of tread size (varying contact length) for different tyre materials
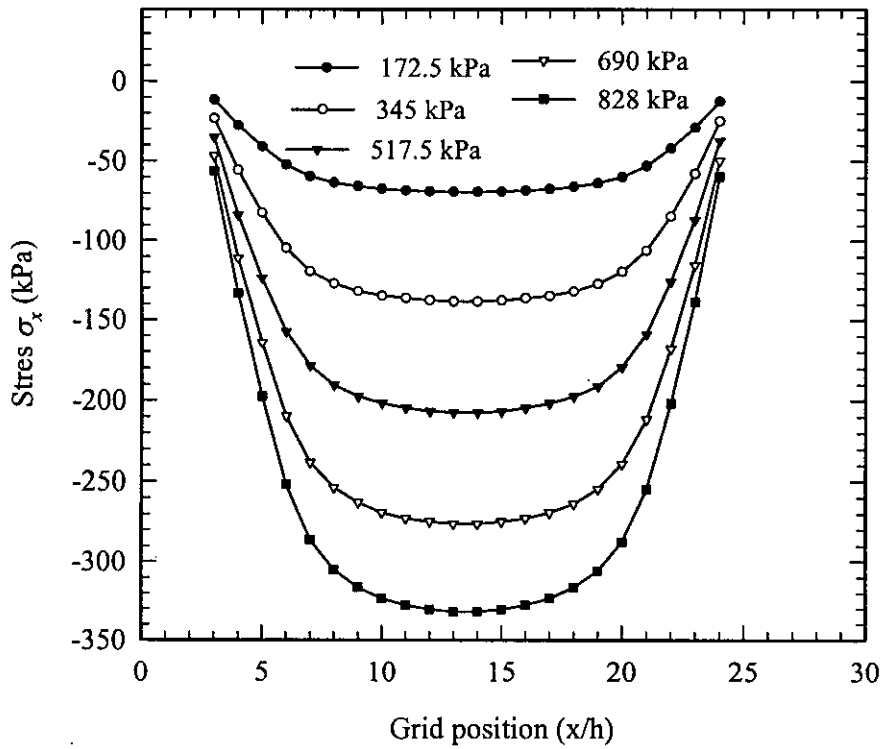
Figure 8.1 Distribution of normal stress component, σ_x along
the bondline of a tread section (a/b=1.51) for different contact pressures
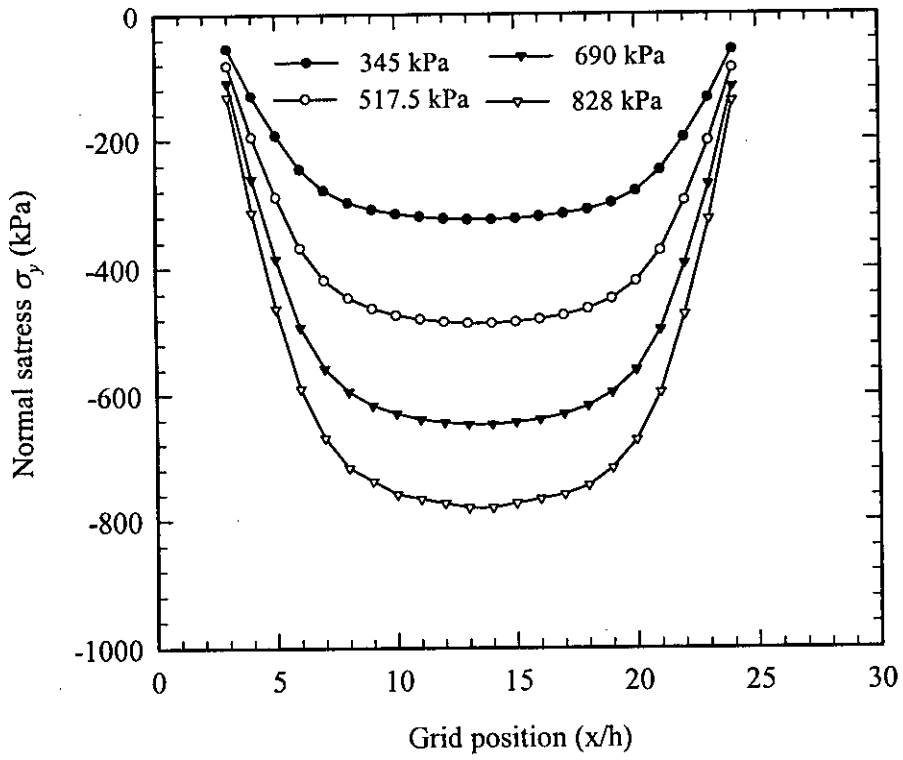
Figure 8.2 Distribution of normal stress component, σ_y along
the bondline of a tread section (a/b=1.51) for different contact pressures
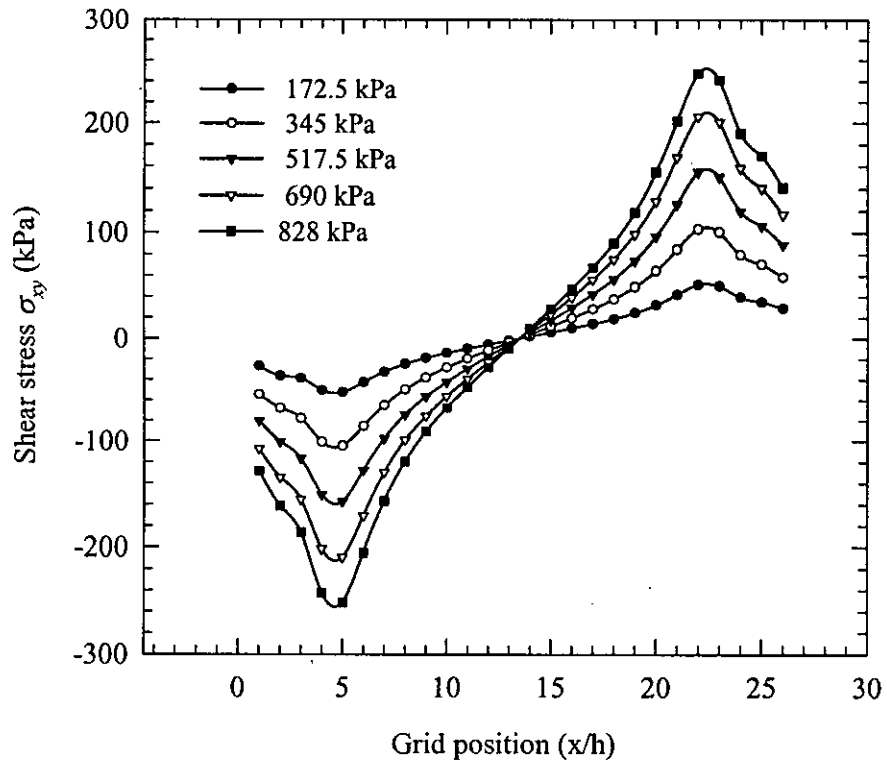
Figure 8.3 Distribution of shearing stress of at the contact
surface with plies at different contact pressure a tread
section of a/b=1.51
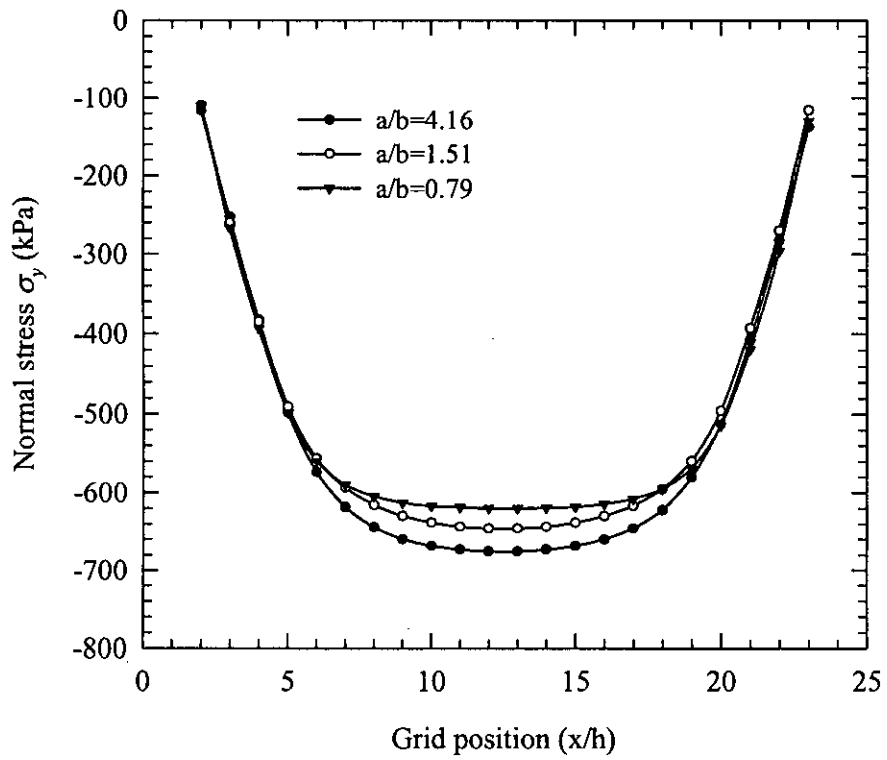
Figure 8.4 Effect of tread size on the prediction
of normal stress component, σ_y along the bondline
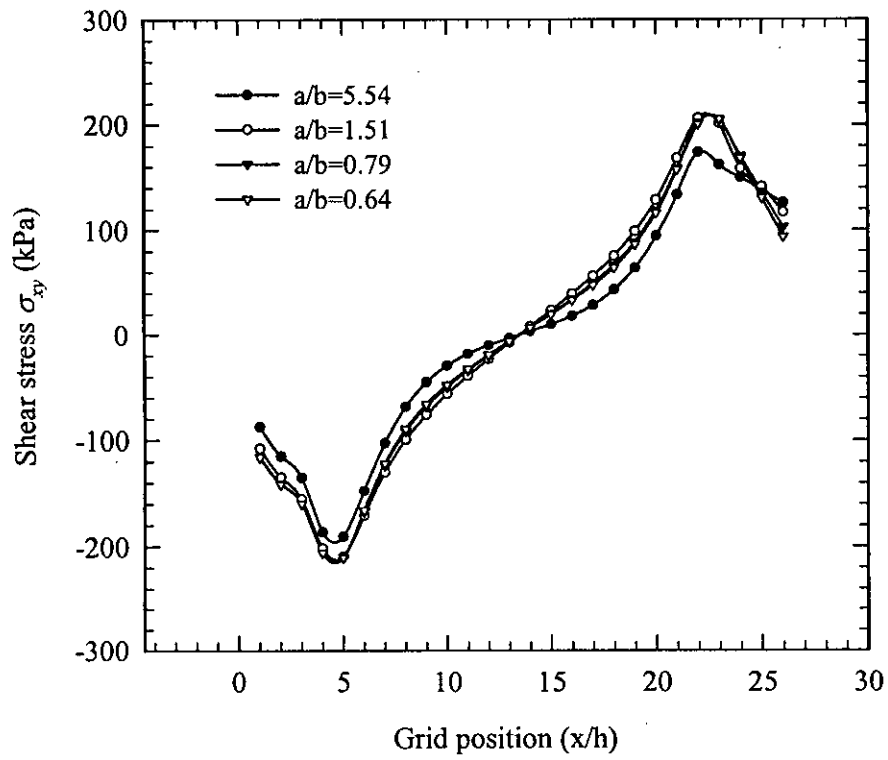
Figure 8.5 Distribution of shearing stress along the bondline region of truck tyre treads when skid depth is varied
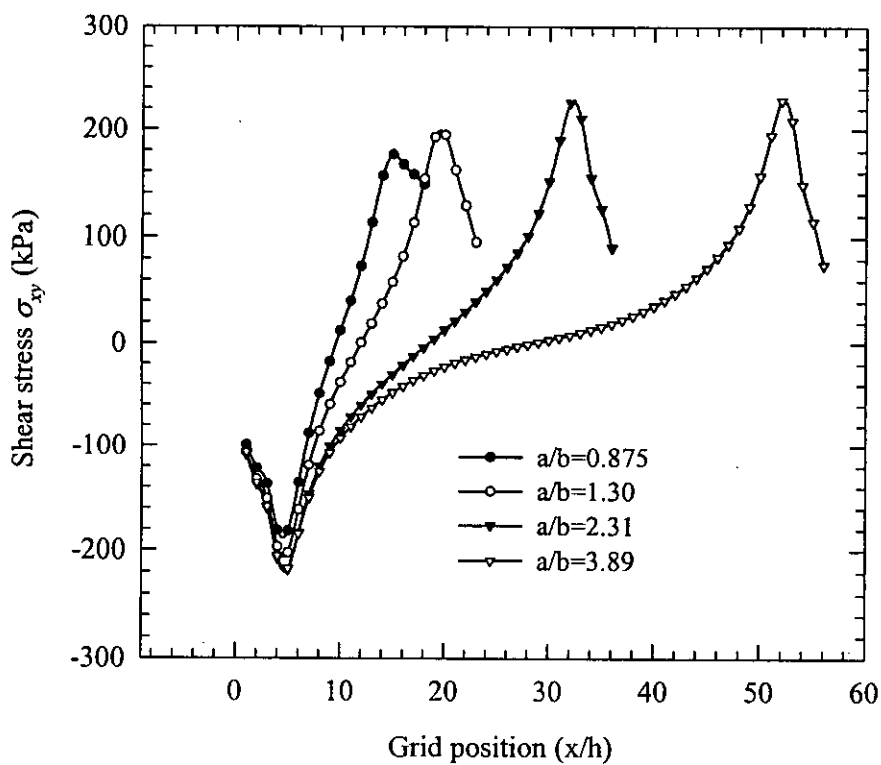
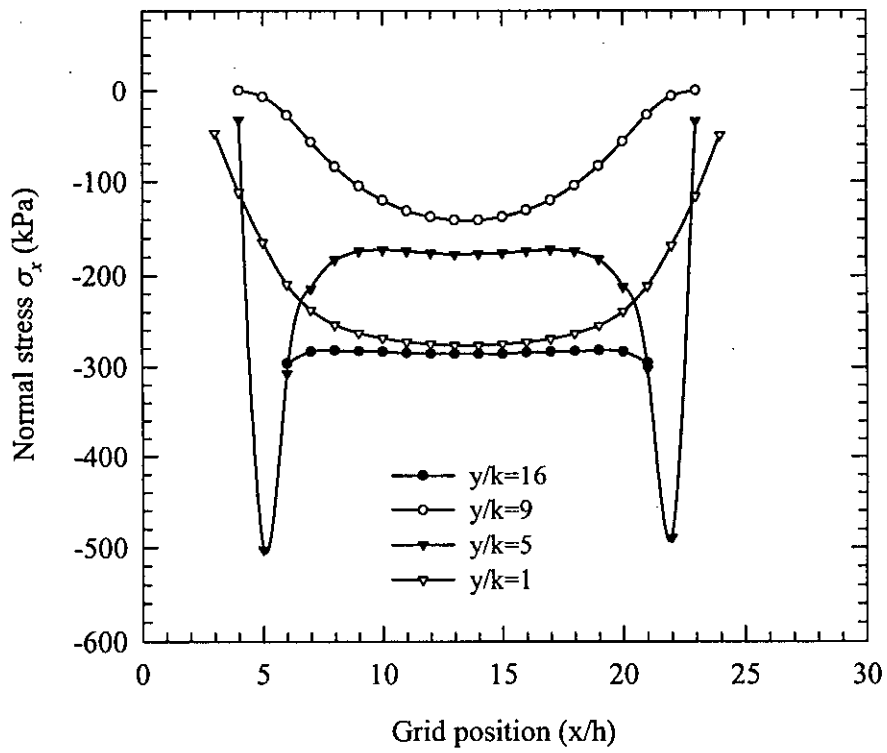Figure 8.6 Distribution of shearing stress along the bondline region of truck tyre treads when the length of the contact boundary is varied

Figure 8.7 Distribution of normal stress σ_x at different sections of tire tread (a/b=1.51) under contact pressure 690 kPa

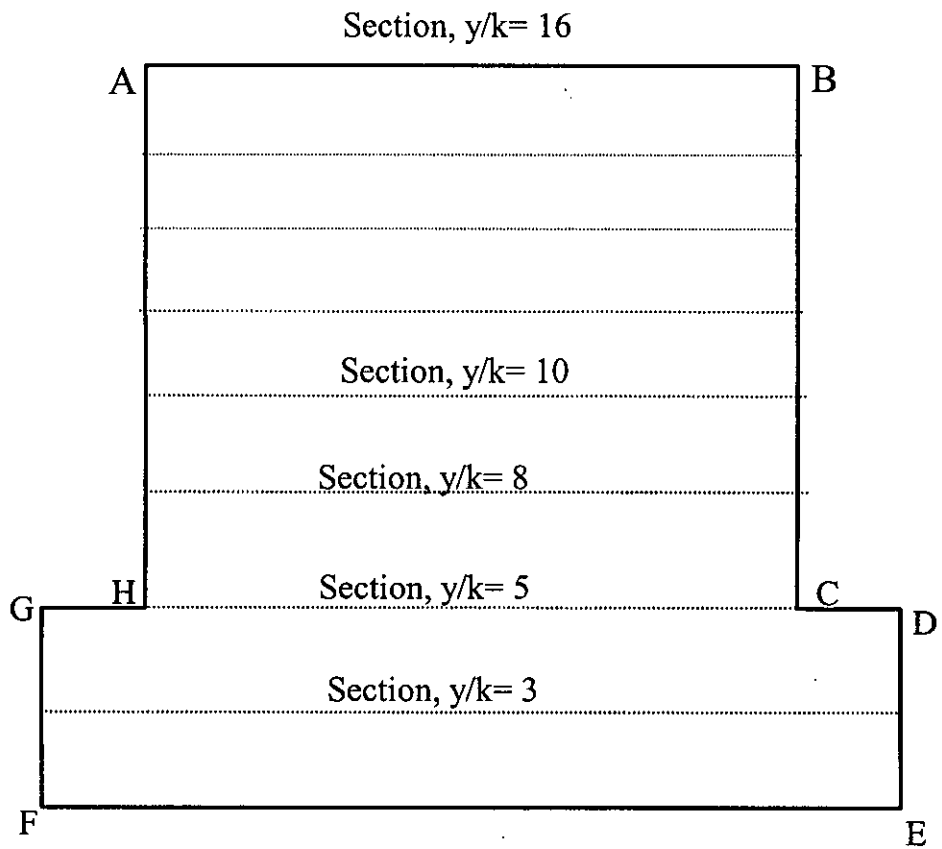Section, y/k= 16

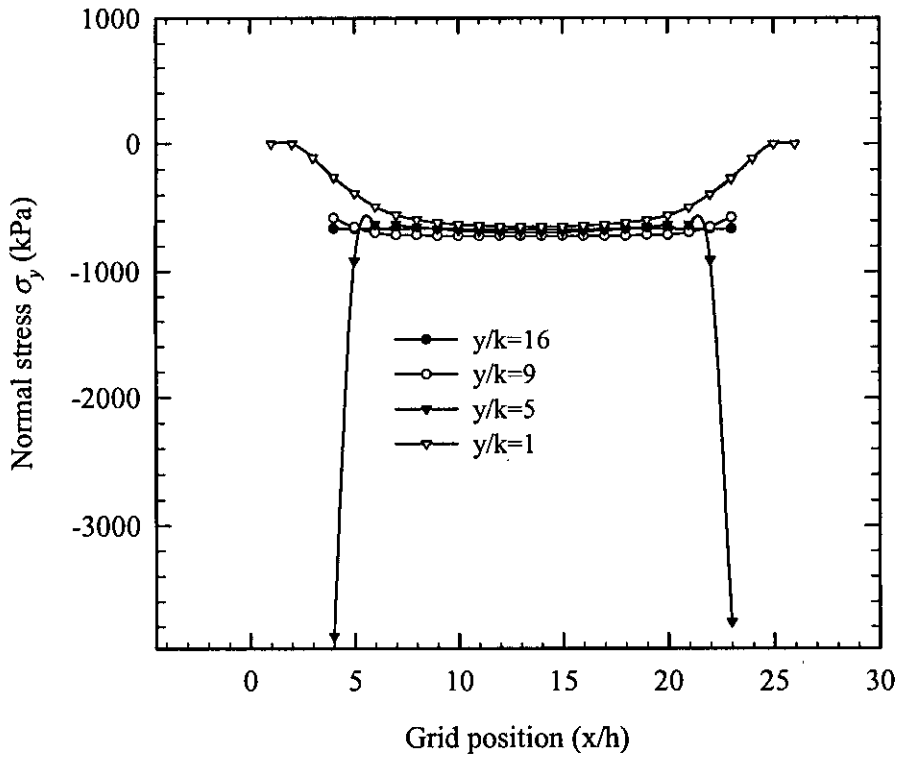Figure 8.7.a Different sections of a tyre tread

Figure 8.8 Distribution of normal stress, σ_y of truck tyre tread of different sections of a tyre tread (a/b=1.51) under contact pressure 690 kPa
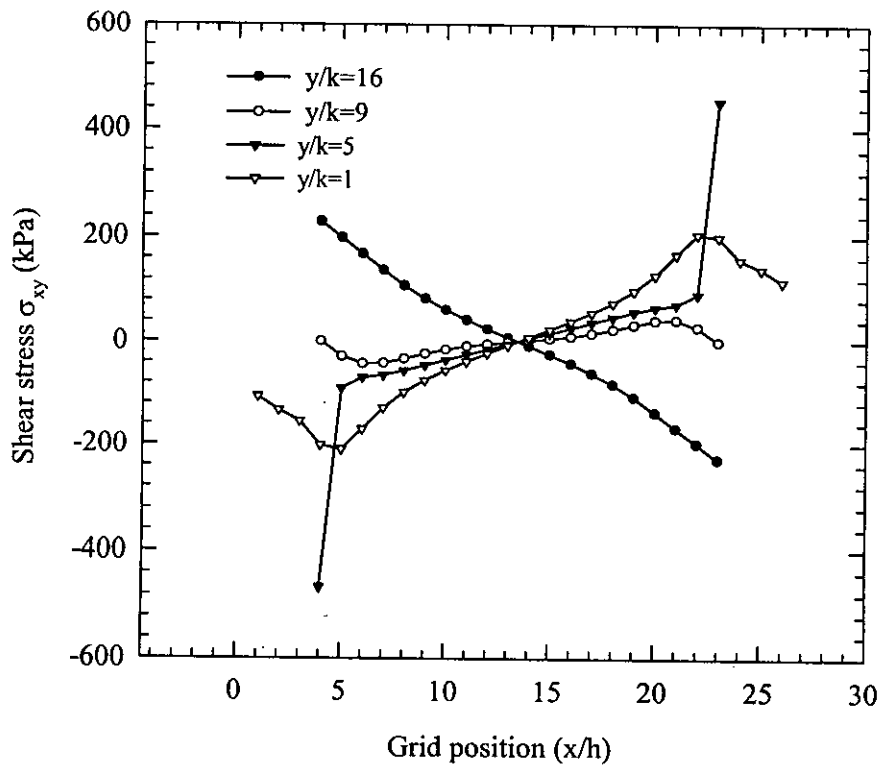
Figure 8.9 Distribution of shearing stress σ_{xy} at different
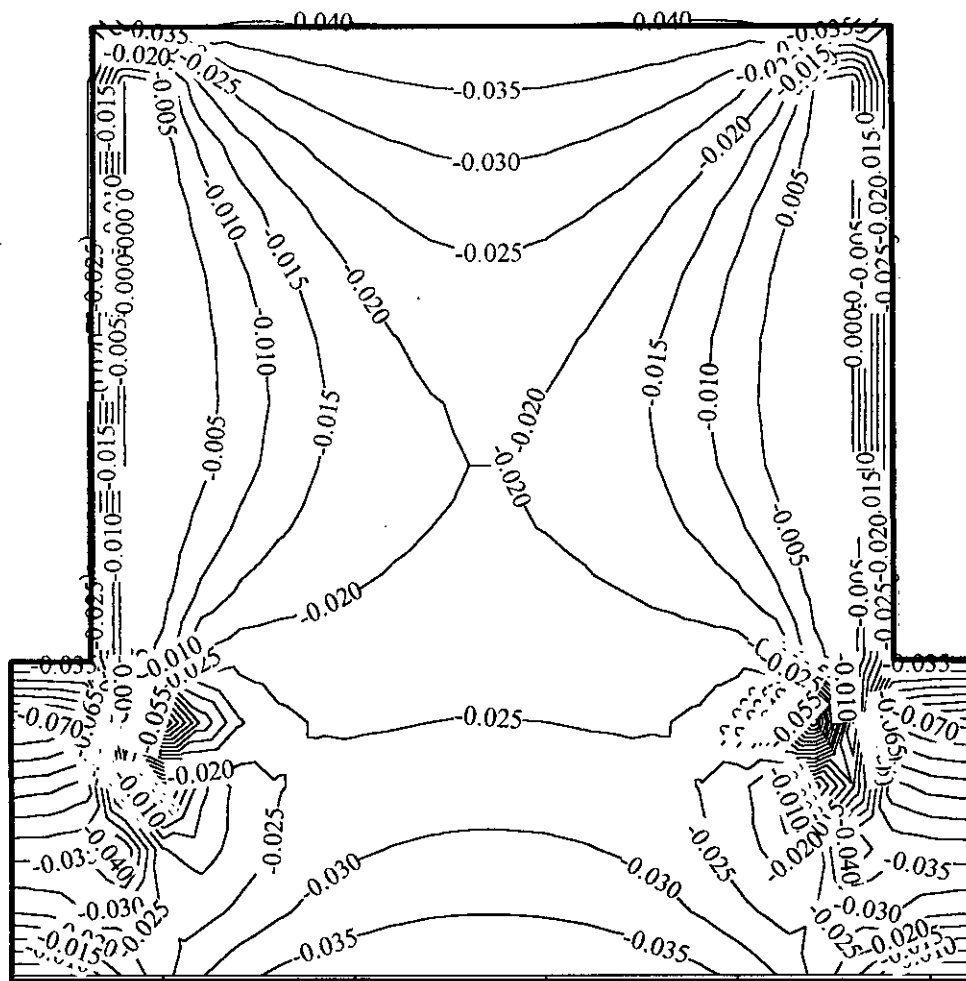sections of a tyre tread (a/b=1.51) contact pressure 690 kPa

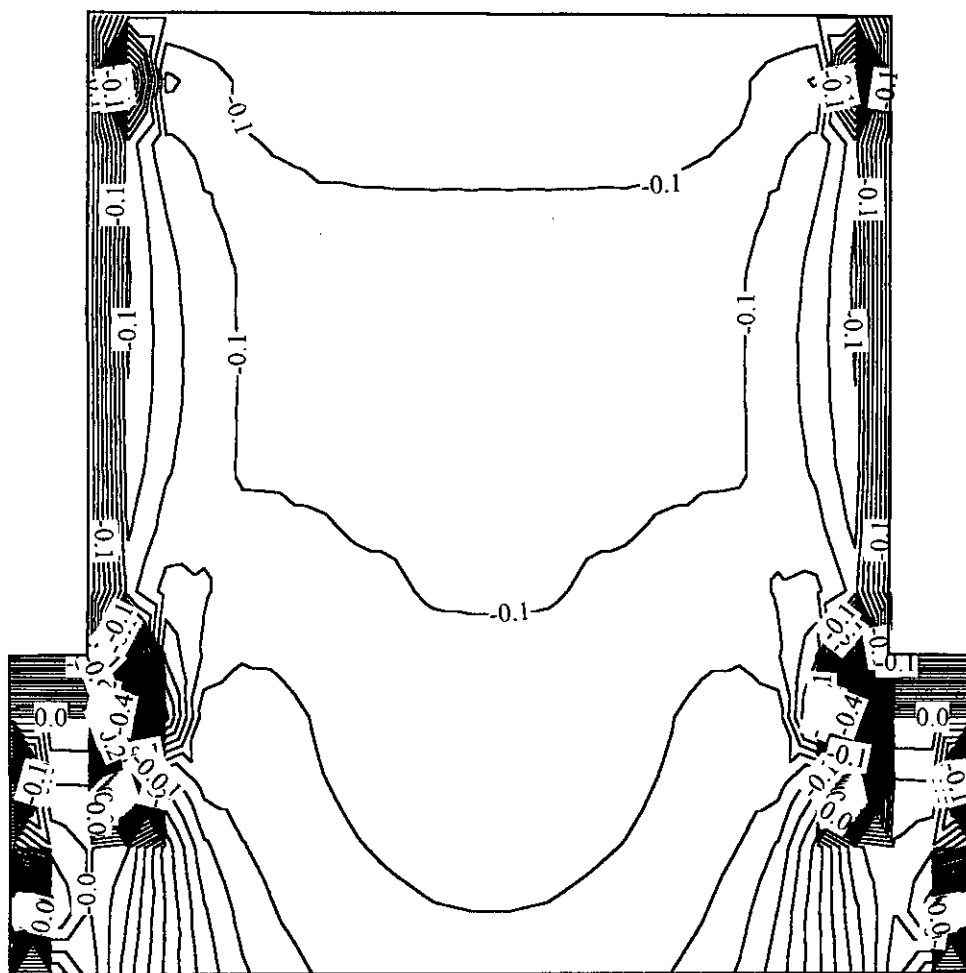Figure 8.10 Contour plot of normalized stress component (σ_x/E) over the whole tyre tread section

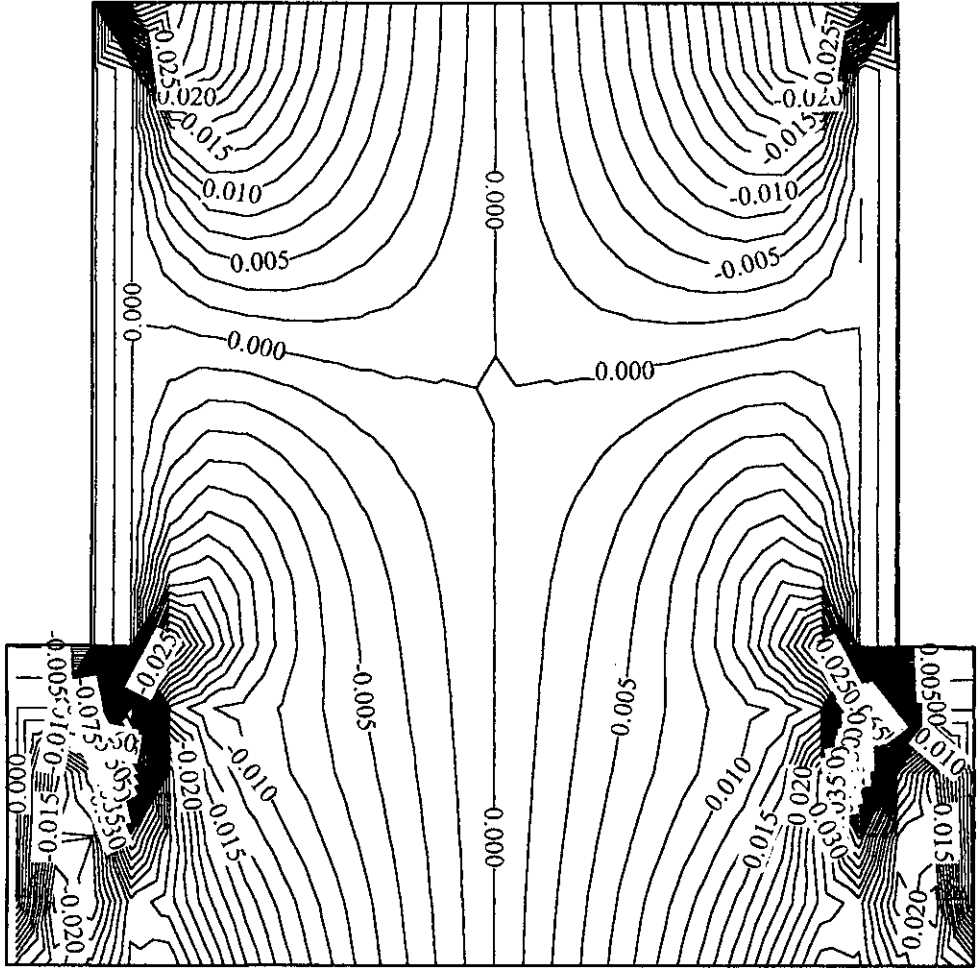Figure 8.11 Contour plot of normalized stress component (σ_y/E) over the whole tyre tread

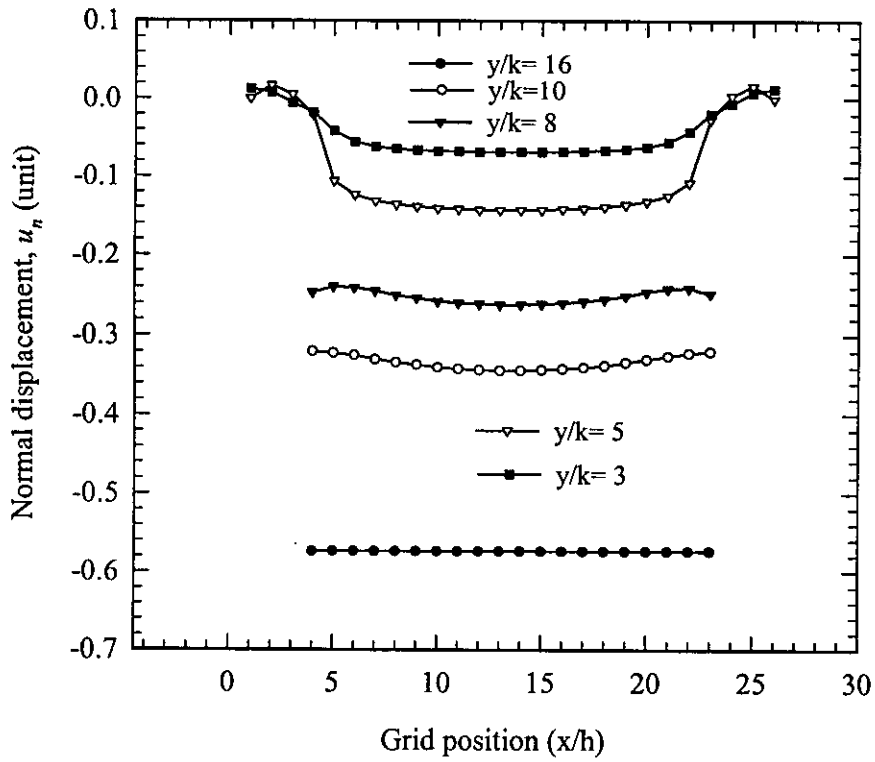Figure 8.12 Contour plot of the normalized shear stress (σ_{xy}/E) for the whole tread section

Figure 8.13 Normal displacement at different sections of a tyre tread
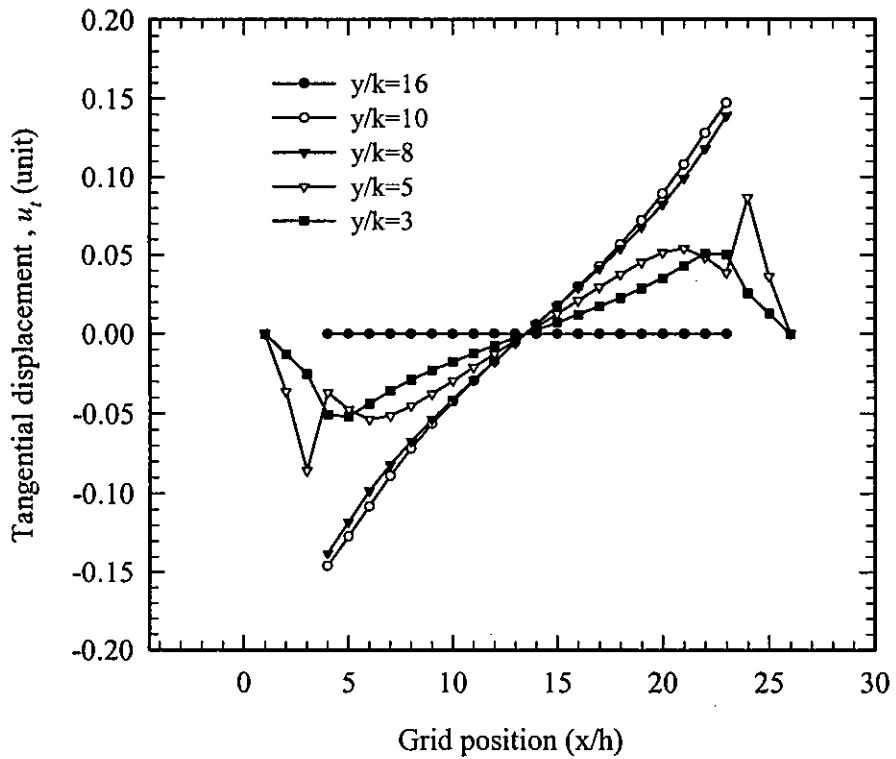(a/b=1.51) under contact pressure 690 kPa

Figure 8.14 Tangential displacement at different sections of a tyre tread (a/b=1.51) under contact pressure 690 kPa

APPENDIX C

PROGRAM OF TREAD GEOMETRY GENERATION

List of variables used in the program of tyre-tread coordinate generation

mn = No of division of the stressed body in x –direction

nn = No of division of the stressed body in y –direction

xl = distance of the left tangent of the stressed body

xr = distance of the right tangent of the stressed body

yb = distance of the top tangent of the stressed body

yt = distance of the bottom tangent of the stressed body

xbr = Left skid depth distance of the tyre tread in the x-direction

xtt = Right skid depth distance of the tyre tread in the x-direction

ytb = Top skid depth distance in the y-direction

m = Initial x-coordinate

n = Initial y-coordinate

dx = mesh length in x-direction

dy = mesh length in y-direction

Program for coordinate generation of the tyre tread boundaries

....

```
dimension bx(800),by(800)
integer mn,nn
real*8  xl, xr, yb, yt, xbr, ytr, ytb, xtt, m, n
open (1,file='infil2.out',status='old')
open (2,file='infil2.xls',status='unknown')
mn=15
nn=65
dx=0.50
dy=dx-0.125/2
yt=(nn+1)*dy
yb=1*dy
xl=dx
xr=(mn+1)*dx
xbr=xl+4*dx
xtt=xl+4*dx
m=xbr
n=yt
ytr=yb+3*dy
ytb=yt-3*dy
bx(1)=m
by(1)=n
do 50 i=1,600
if (bx(i).le.bx(1).and.by(i).eq.by(1).and.bx(i).gt.xl)then
bx(i+1)=bx(i)-dx
by(i+1)=by(i)
```

```
      elseif (bx(i).le.xl.and.by(i).gt.yb)then
      bx(i+1)=bx(i)
      by(i+1)=by(i)-dy
      elseif (bx(i).ge.xl.and. bx(i).lt.xbr.and.by(i).eq.yb)then
      bx(i+1)=bx(i)+dx
      by(i+1)=by(i)
      elseif (bx(i).eq.xbr.and.by(i).ge.yb.and.by(i).lt.ytr)then
      by(i+1)=by(i)+dy
      bx(i+1)=bx(i)
      elseif (bx(i).lt.xr.and.bx(i).ge.xbr.and.by(i).eq.ytr)then
      bx(i+1)=bx(i)+dx
      by(i+1)=by(i)
      elseif (bx(i).eq.xr.and.by(i).lt.ytb.and.by(i).ge.ytr)then
      bx(i+1)=bx(i)
      by(i+1)=by(i)+dy
      elseif (bx(i).le.xr.and.bx(i).gt.xtt.and.by(i).eq.ytb)then
      bx(i+1)=bx(i)-dx
      by(i+1)=by(i)
      elseif (bx(i).eq.xtt.and.by(i).lt.yt.and.by(i).ge.ytb)then
      bx(i+1)=bx(i)
      by(i+1)=by(i)+dy
      elseif (bx(i).ge.(xl+2*dx).and.bx(i).le.xtt.and.by(i).eq.yt)then
      bx(i+1)=bx(i)-dx
      by(i+1)=by(i)
      else
      endif
50    continue
      do 100 i=1,(mn+nn+2)*2
      write(2,18) bx(i),by(i)
      write(1,17) bx(i),by(i),i-2
```

```
100      continue
17       format(1x 2f12.4,i7)
18       format(1x 2f12.4,i7 )
         stop
         end
```